AIR FORCE INSTITUTE OF TECHNOLOGY

AIR UNIVERSITY
UNITED STATES AIR FORCE

AN INVESTIGATION OF THE EFFECTS OF GRAVITY ON CRATER FORMATION IN A COHESIONLESS MEDIUM

by

Leon K. Moraski
Capt USA

David J. Teal
Capt USA

Mech/GSP-65-35

SCHOOL OF ENGINEERING

WRIGHT-PATTERSON AIR FORCE BASE, OHIO

AN INVESTIGATION OF THE EFFECTS OF GRAVITY ON CRATER FORMATION IN A COHESIONLESS MEDIUM

THESIS

Presented to the Faculty of the School of Engineering

of the Air Force Institute of Technology

Air University

in Partial Fulfillment of the

Requirements for the Degree of

Master of Science

by

Leon Karol Moraski B.S. in M.S. & E.
Capt USA

David Jens Teal B.S. in M.S. & E.
Capt USA

Graduate Space Facilities

July 1965

Preface

In order to make our two year association with the Air Force a memorable one, it was decided that any thesis we did would involve the zero gravity aircraft located at Wright-Patterson AFB. With this as a personal goal, we set out in search of a worthy topic. Based upon the guidance of Captain S. W. Johnson, the topic contained in this report was chosen. For his patience and assistance in our time of decision we are most grateful.

The idea of detonating an explosive on board an aircraft in flight was admittedly not an easy one to propose to the Air Force. Through the efforts of Mr. Donald Griggs of the Zero Gravity Section, the obstacles involving the flight portion of the investigation were overcome. Without his persistence and ability to overcome the seemingly impossible, this thesis would literally not have gotten off the ground.

The report attempts to present a complex phenomenon in a fundamental manner. This was done in order to make the principles developed applicable to a wide range of explosives and mediums even though the experiment dealt with small scale explosives and a single medium. Since this was, to our knowledge, the first experiment ever attempted on cratering in varied gravity fields, we feel that it marks an important step into an hitherto unexplored area.

The assistance that various individuals gave us throughout the different phases of the investigation was outstanding. We are indebted

to Messrs. Jim Taylor, Jack Warwick, and Robert Price for their enthusiastic support in helping us solve our photography problems. The assistance given to us by Lieutenant Larry Pierce of the Zero Gravity Section was an important factor in the successful completion of the flight phase of our investigation. We would also like to thank Captain S. Alexander and Dr. D. O. Norris for their assistance, interest, and support during the analysis phase of the investigation. Finally, we wish to thank our wives for the encouragement and assistance we received throughout the investigation.

Leon K. Moraski

David J. Teal

Contents

Contents (Contd)

List of Figures

List of Figures (Contd)

List of Figures (Contd)

List of Figures (Contd)

List of Tables

Abstract

An experimental investigation was conducted on the effects of gravity on explosion crater formation. Accompanying the presentation of the experimental results is a discussion of gravity effects on the cratering processes of compaction, scouring, spalling, and gas acceleration. The discussion suggests that gravity influences the shear resistance of the medium and the range of the particle throwout and hence should influence the crater formation.

To test this hypothesis, an experiment was conducted in a medium of dry silica sand using a six-grain electrically initiated squib as the explosive source. Craters were formed under 0.17 g, 0.38 g, 1.0 g, and 2.5 g conditions and at depths of burst ranging from surface to five inches. The statistical t-test was used to determine if the crater depth and diameter were affected by the gravity field. Crater dimensions versus depth of burst (DOB) were compared for the different gravity fields to study the effect on the optimum and maximum DOB. An equation expressing crater dimensions as a decreasing exponential function of increasing gravity was assumed. Parameters of the exponential function were adjusted to achieve the best fit in the least-squares sense.

The conclusions arrived at during the investigation are that (1) crater depth, diameter, optimum DOB for depth, and maximum DOB vary inversely with gravity, (2) the optimum DOB for diameter is not a function of gravity, and (3) the sensitivity of changes in crater dimensions to changes in gravity is a function of DOB.

AN INVESTIGATION OF THE EFFECTS OF GRAVITY ON CRATER FORMATION IN A COHESIONLESS MEDIUM

I. Introduction

Statement of Purpose and Scope

The objective of this investigation was to determine the effect of gravity on the formation of explosion craters in a cohesionless medium. A discussion based on principles of soil and explosion mechanics is given. An experiment was performed in a cohesionless medium to test the validity of the hypotheses formulated in the discussion. In the experiment, explosion craters were formed by the detonation of identical sources of chemical energy at various depths of burst and at four different levels of gravity.

Background

The subject of cratering as a means of large scale soil and rock excavation has been of interest to engineers for many years. Numerous studies have been made in order to obtain a better understanding of the complex phenomenon of crater formation. These studies have revealed that terrestrial craters produced by subsurface explosions have dimensions which depend upon numerous factors, the most important being (1) the energy of the explosion, (2) the depth of the explosion, and (3) the physical properties of the medium in which the explosion takes place.

Permanent manned bases may be established on the Moon in the near future. If these bases include subsurface installations, there will

be a need for a reliable and efficient means of excavation for the placement of the installation (Ref 36:113). Once a primitive base is established, dependence upon local resources might require that some type of crude mining and quarrying operations be initiated. Explosives, either chemical or nuclear, can be used for these operations.

If explosives are used in an extraterrestrial environment, the effects of environmental factors such as gravity and atmosphere on the performance of the explosives must be known in order that the efficiency of the explosive as a means of excavation can be properly evaluated. It is the purpose of this report to present the results of an investigation of the effects of gravity on crater formation.

Current knowledge on crater formation in other than a terrestrial (1 g)* field is very limited. A few authorities have discussed in a qualitative manner portions of the problem and have arrived at differing conclusions concerning the probable effect of gravity (Ref 39:325; 21:12).

Two quantitative studies have been made where the lunar environment of 0.17 g and the absence of an atmosphere were considered. These studies also resulted in conflicting conclusions (Ref 27:77; 25:3412). No experimental work appears to have been done on the problem of gravity effects on crater formation.

Discussion of Explosion Crater Formation

After an investigation into current theories of crater formation

---

* 1 g is the gravity field on earth and is equal to 32.2 feet per second per second. Throughout this paper, the varying gravity fields are expressed in terms of the terrestrial gravity field.

and size prediction, it was decided that a discussion of the cratering processes based on soil and explosion mechanics principles would be the most feasible. One of the reasons for this decision was that the processes considered are operative during the formation of craters of any size explosion in any medium. The other reason was that the soil mechanics approach considers the shear strength of the medium which the commonly used hydrodynamic model does not consider. As is shown in this paper, shear strength is an important property in the consideration of gravity effects. After the discussion of the processes of crater formation under terrestrial conditions, certain hypotheses are offered as to the likely effect of gravity on each of these processes and the resultant effect on the final formation of the crater.

Experimental Procedure

In order to test the hypotheses offered as to the effect of gravity on crater formation, an experimental phase was conducted. Small explosive charges were detonated in Ottawa sand and crater depths and diameters were measured. Tests were conducted at 1.0 g in the laboratory and at 0.17, 0.38, and 2.5 g on a C-131B aircraft. A statistical comparison was made between crater data taken from the same DOB# out at different gravity conditions to determine whether varying the gravity field caused a significant change in the crater dimensions. In addition, a relationship between crater dimensions and gravity was assumed and the parameters in the relationship were adjusted to achieve the best fit to the data in the least-squares sense.

DOB refers to the depth of burst of the explosive beneath the medium-air interface.

Organization

This paper is organized to place emphasis on the discussion of crater formation and the results from the experiment. The detailed experimental procedure, raw data, methods of statistical analyses, and drawings of crater profiles can be found in the appendices.

II. A Discussion of Gravity Effects on Cratering

The purpose of this section is to discuss the effects of gravity on crater formation in a cohesionless medium. Throughout the discussion, a homogeneous medium and identical explosive sources are assumed. A typical crater is described and the terminology used in cratering is defined. The formation of a crater is then traced from the detonation of the explosive to the final depression. The sources of mechanical energy released by the detonation and the ensuing cratering processes are analyzed to determine the effect of gravity on the crater depth and diameter. Finally, the relative importance of the cratering processes is considered.

Description of a Crater

In order to discuss the cratering process, it is first necessary to define the terminology associated with a crater. Figure 1 is a cross-sectional profile of a typical crater. The material on the surface of the crater is called the fallback. This is the portion of the medium that was initially ejected from the crater but because of the high angle and/or low velocity of ejection, the medium particles were not thrown clear of the final formed crater. The original ground material in contact with the fallback is called the rupture zone. The medium in the rupture zone is completely fragmented and broken due to shear and compressive failure. The next zone of interest is the plastic zone. In this zone, the medium is permanently displaced but fractures are not commonly found here. The region

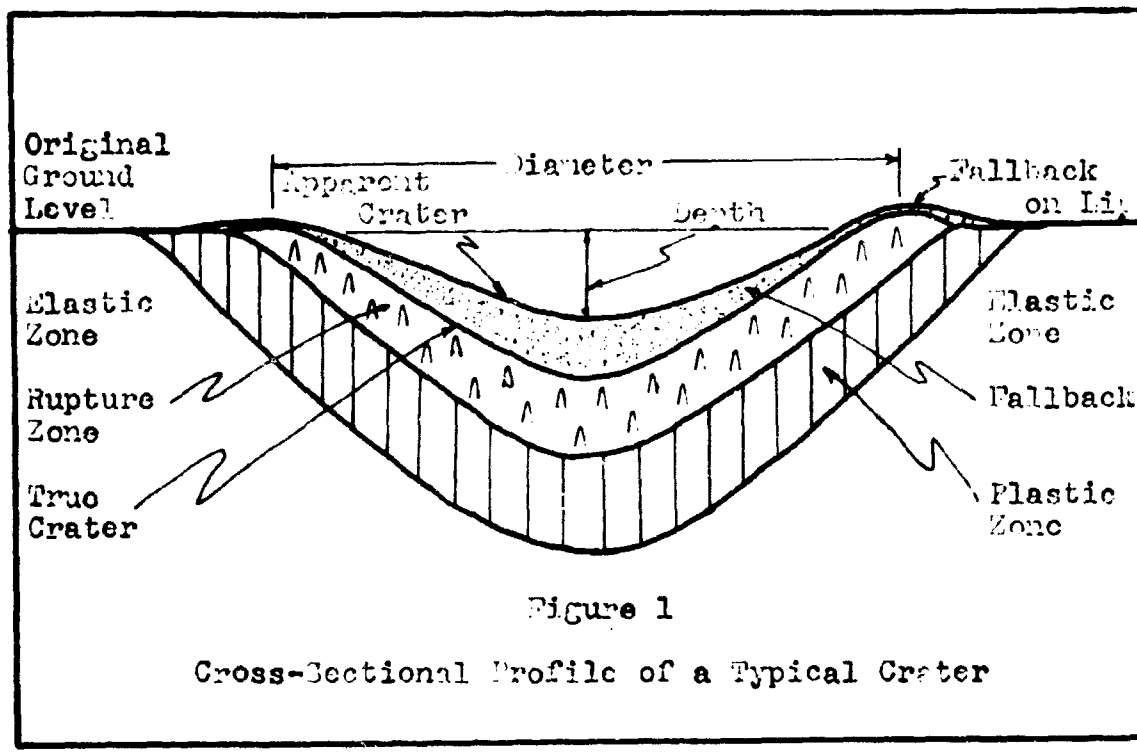

Figure 1

Cross-Sectional Profile of a Typical Crater

beyond the plastic zone is called the elastic zone. In this zone, the medium has not been permanently deformed by the cratering process (Ref 42:3447; 34:15). The crater depth and diameter are defined in this paper as shown in Fig. 1.

Sources of Mechanical Energy

Craters of the type shown in Fig. 1 are formed by the detonation of an explosive or the hypervelocity impact of a projectile. In this discussion, only craters formed by the detonation of a chemical explosive source are considered.

The ignition of the explosive is accompanied by a great release of energy which is manifested by high pressures on the order of hundreds of thousands of atmospheres. The detonation process provides two sources of mechanical energy, the first of which is a compressive shock wave which causes a sharp discontinuity in the physical state

of the medium. This shock wave initially travels faster than the highest elastic wave velocity. As its energy density decreases, the shock wave slows down and approaches the compressional elastic wave velocity. The second source of mechanical energy is provided by the pressure produced by the adiabatically expanding gases near the source of the explosion. These gases are composed of (1) the air in the voids of the medium, (2) the gaseous products of the detonation, and (3) the gases produced by vaporization of any moisture in the medium. These gases expand at a lower velocity than the shock wave.

Cratering Processes

The sources of mechanical energy contribute to four cratering processes that result in the formation of a crater. These processes are (1) compaction, (2) scouring, (3) spalling, and (4) gas acceleration. Figure 2 is a cross-section of the medium surrounding the

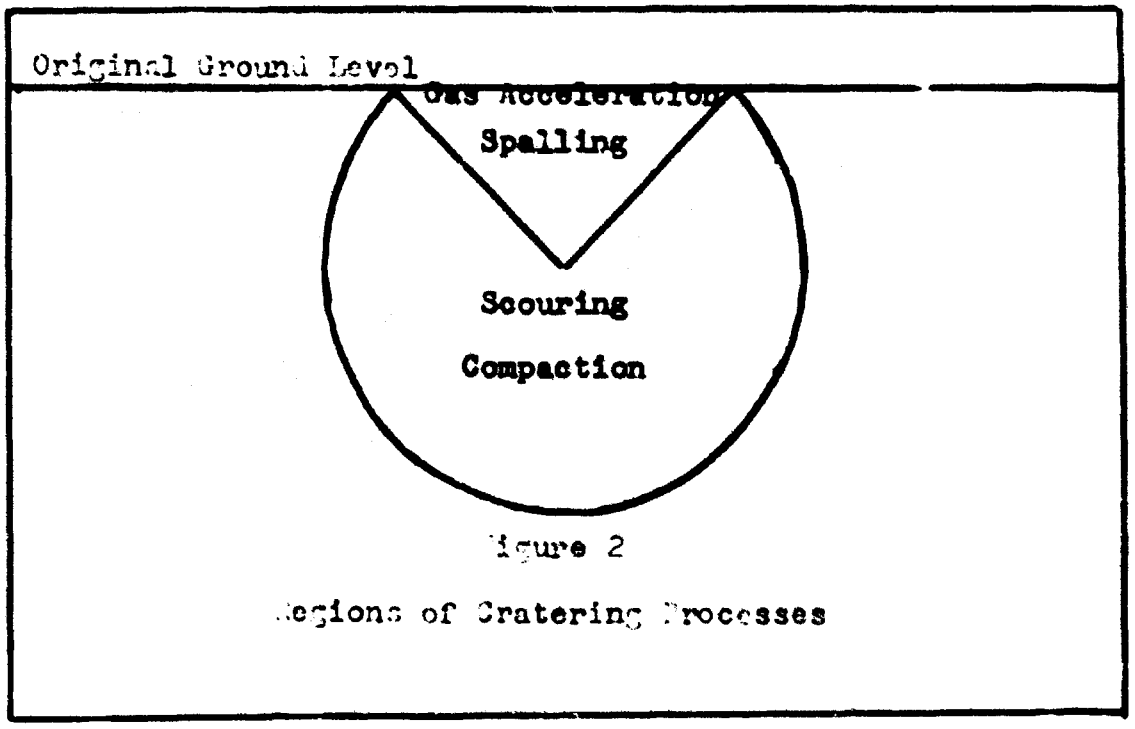

Figure 2

Regions of Cratering Processes

explosion. It schematically illustrates the regions in which these processes act during the formation of the crater. Gas acceleration and spalling take place primarily in a cone-shaped volume above the charge while compaction and scouring occur in the remaining spherical volume surrounding the charge.

Compaction. The action of the shock wave as it passes through the medium is the primary cause of compaction. The high compressive stress characteristic of the shock wave and the pressure discontinuity associated with the shock front cause the medium to be violently deformed as the shock propagates in a spherically diverging shell from the source of the explosion (Ref 42:3450). Because of the high initial stress, the medium near the point of detonation behaves hydrodynamically. This high stress level is several orders of magnitude higher than any restoring forces within the medium (Ref 10:4). As the initial stress level in the medium caused by the explosive is not a function of gravity, the hydrodynamic behavior in a cohesionless medium is independent of gravity.

Due to energy dissipation resulting from the spherical expansion of the shock wave and the work being done on the medium, the stress level of the shock wave falls below the value necessary for hydrodynamic behavior of the medium. At this level of stress, the compressive strength of the medium is exceeded and the medium is crushed. This is the start of what has been described as the rupture zone. Because the compressive strength of the medium is a function primarily of molecular bonding, it is not affected by gravity. Therefore, in the first portion of the non-hydrodynamic region where the medium fails because its compressive strength is exceeded, a varying gravity

field has no effect.

As the stress level further decreases, the medium in the rupture zone undergoes shear failure. The shear resistance of a dry cohesionless medium can be expressed by the equation

$$s = p \tan \phi \qquad (1)$$

where s = shear resistance

p = effective stress normal to the plane of failure

ϕ = angle of internal friction

The shear resistance of a cohesionless medium depends on the weight of the overburden. Since weight is gravity dependent, Eq. (1) can be expressed as

$$S = \rho g H \cos i \tan \phi \qquad (2)$$

where ρ = mass density of the medium

g = acceleration due to gravity

H = depth of overburden

i = angle shear plane makes with the horizontal

This last equation shows that (1) the shear resistance is directly proportional to the gravity field and (2) the amount of overburden required to develop a certain value of shear resistance is inversely proportional to the gravity field.

In the rupture zone, shear failure results from (1) the dynamic compaction of the medium in the region beneath the detonation and (2) the pressure on the medium in a lateral direction from the detonation. In considering the dynamic compaction of the medium, an analogy of

the mode of failure can be made to static compaction because the strength of the medium under consideration is not appreciably altered by differing load rates (Ref 61:67). When a compressive load acts on a dry cohesionless medium, an inverted triangular prism of the medium is forced downward. As the prism moves, the medium at the sides is forced laterally outward as shear failure occurs along surfaces of sliding (Ref 50:355). This type of failure is shown in Fig. 3. Although the spherical loading of the medium by the shock front results in more complicated interactions than depicted in Fig. 3, it has been

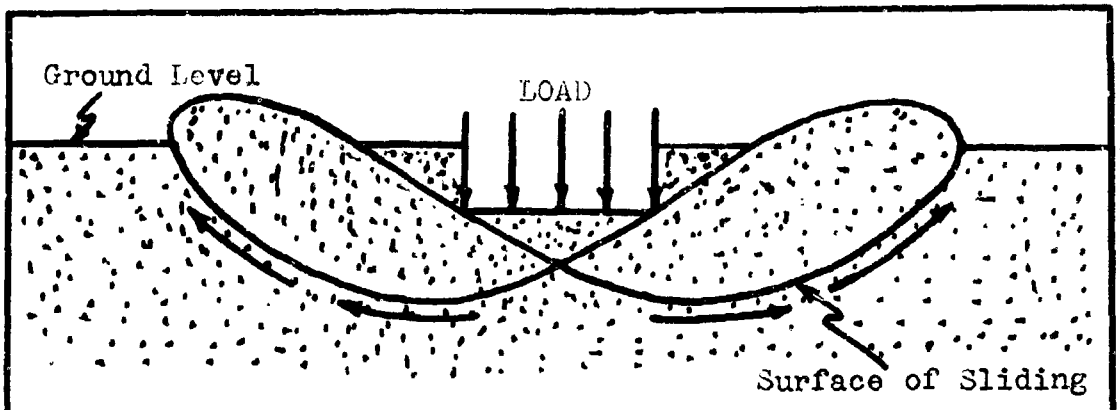

Figure 3

Downward Shear Failure for Compacted Cohesionless Sand

established that similar medium failure does occur and is instrumental in the formation of a crater. In a series of small scale tests conducted at shallow depths of burst, Baldwin noticed that the crater rims were produced mainly by compressional effects which squeezed the lower portions of the medium up to the surface (Ref 5:121).

In bearing capacity tests, a dense cohesionless soil fails in the manner depicted in Fig. 3 (Ref 53:168). By means of a series of these tests conducted in various gravity fields, Halajian showed that the bearing capacity of a dry cohesionless soil varies directly with gravity. This result was attributed to the shear resistance of the soil which varies inversely with gravity. Based upon Eq. (2) and the above experimental result, it is suggested that the depth and extent of the surface of sliding shown in Fig. 3 varies inversely with gravity. This, in turn, implies that the crater depth and diameter should vary inversely with the gravity field.

The effect of the lateral pressure of the shock wave is schematically represented in Fig. 4. As the lateral pressure acts on the

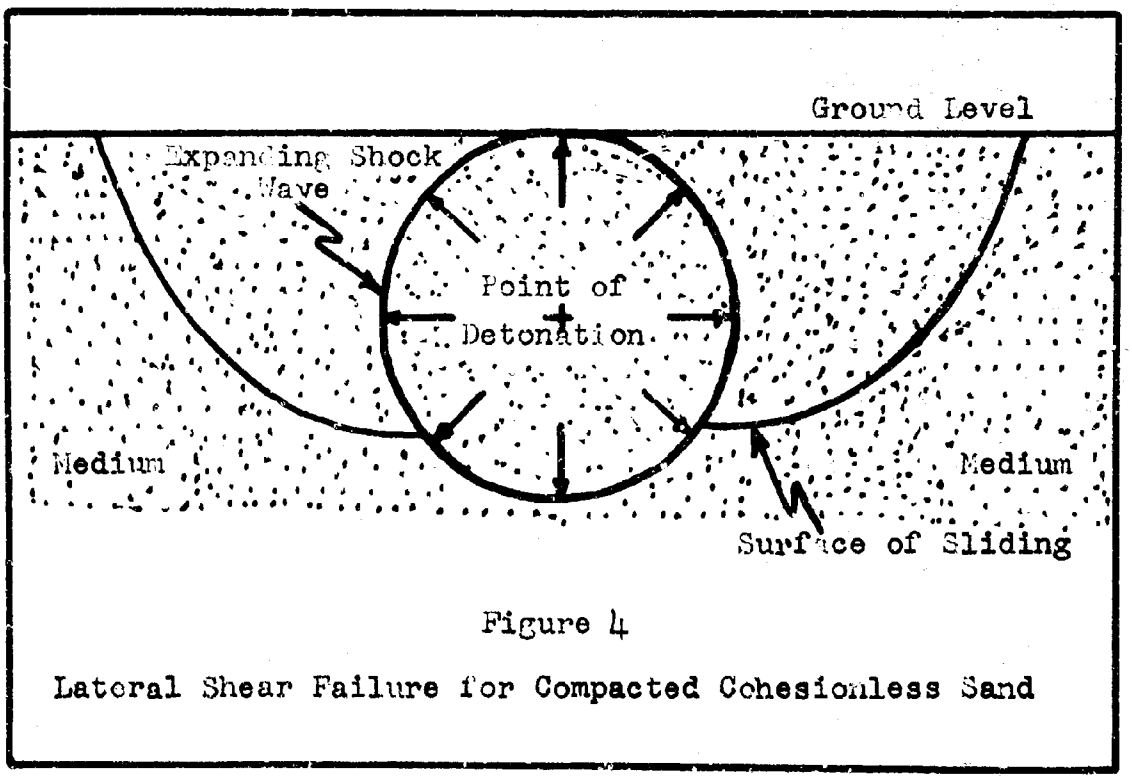

Figure 4

Lateral Shear Failure for Compacted Cohesionless Sand

medium, a portion of the medium is displaced along a surface of sliding on which the shear resistance developed in the medium resists the movement. The shape of the surface of sliding is determined by the shear resistance developed in the medium. Equation (2) has shown the shear resistance to be directly proportional to gravity while the amount of overburden required to develop a certain value of shear resistance to be inversely proportional to gravity. Therefore, the depth and extent of the surfaces of sliding vary inversely with gravity. This should result in the crater depth and diameter varying inversely with gravity.

In the remainder of the zones formed by the process of compaction, the medium responds plastically or elastically depending on the state of stress to which it is subjected. Because of the negligible amount of particle displacement in the plastic and elastic zones, the contribution from these zones to the final crater dimensions is insignificant compared to the contribution from the rupture and fallback zones. For this reason, gravity effects on these zones are not considered.

In certain types of explosives known as deflagrating compounds, the energy of the explosive is released by means of the rapid burning of the explosive material instead of a nearly instantaneous decomposition. This results in a slower buildup of pressure in the detonation of a deflagration compound. As a result, only a weak shock wave is formed. In this case, compaction is also caused by the stress generated by the expanding gases. The main differences in the compaction process are that the deflagration process has (1) a lower stress level acting on the medium and (2) a longer period of time in which the mechanical energy is active.

Based on the above paragraphs, it is hypothesized that the process of compaction is affected by a change in the gravity field. Although not all portions of the process are influenced by the gravity field, those that are affected should result in the crater depth and diameter varying inversely with the gravity field.

Scouring. The process of scouring is caused by the turbulent action of the gases as they expand from the source of the explosion. These gases propagate at a slower velocity than the shock wave. By means of an erosive type of action, the gases remove the material from the crater cavity and push it up and over the edge of the forming crater. Some of the material remains on the edge of the crater and forms the lower portion of the crater rim. Scouring is normally of minor importance compared to the other cratering processes. However, in cases when the energy is released by the burning of a deflagrating explosive, a weak shock is formed and scouring becomes more important in crater formation.

During scouring, the medium fails in shear because the gas pressures exceed the shear resistance of the medium. Since the effectiveness of scouring is related to the shear resistance, which, in turn, is a function of the gravity field, the effectiveness of scouring at any given DOB varies inversely with the gravity field. This implies that the crater depth and diameter vary inversely with the gravity field.

Spalling. The process of spalling is caused by the interaction of the shock wave with the medium-air interface. To determine the effect of gravity on this process, it is necessary to trace the

propagation of the shock wave through the medium. The vertical line in Fig. 5 represents a plane shock front traveling with velocity U in the x-direction through the medium. The undisturbed medium in front of the shock is in a state described by density ρ_o, particle velocity u_o, stress σ_o, and internal energy E_o. The shocked medium is described by ρ_1, u_1, σ_1, and E_1. The equations that describe the medium under the influence of a shock wave are the Rankine-Hugoniot jump conditions

$$\rho_o(U - u_o) = \rho_1(U - u_1) \tag{3}$$

$$\sigma_1 - \sigma_o = \rho_o(U - u_o)(u_1 - u_o) \tag{4}$$

$$E_1 - E_o = \frac{1}{2}(\sigma_1 - \sigma_o)\left(\frac{1}{\rho_o} - \frac{1}{\rho_1}\right) \tag{5}$$

These equations express the conservation of mass, momentum, and energy across the shock front. They relate the state of the shocked material to the state of the undisturbed material. None of the variables described in the Rankine-Hugoniot jump conditions depend on the weight of the material concerned. The variables are described in terms of mass and consequently gravity has no effect on them. This means that a shock wave is independent of gravity when traveling through a medium and transfers the same amount of energy to a given particle in a cohesionless medium regardless of the gravity value.

When the shock wave reaches the medium-air interface, the boundary condition that the normal stress on the medium is zero at all times must be satisfied. To satisfy this condition, a negative stress wave, or rarefaction wave, must be reflected back into the medium. This reflected wave counteracts the stress produced by the incident compressive wave. This action is shown graphically in Fig. 6. In this figure, σ_d is an exponential stress wave which represents stress as a function of distance from the point of detonation. The vertical portion of the stress wave is the shock front. The wave reaches the surface and is then reflected as shown in Fig. 6, a, b, and c. The stress level of the rarefaction is opposite in sign and equal in magnitude to the stress level of the incident compressive wave at the interface. This keeps the normal stress equal to zero. As is indicated by the line AB in Fig. 6, c, the algebraic sum of the stresses results in a net tensile stress in the medium as the rarefaction propagates back toward the point of detonation. Since a cohesionless medium exhibits no tensile strength, spalling occurs when the tensile stress exceeds the restoring force of gravity which acts on the cohesionless particles. The particles are then separated from the

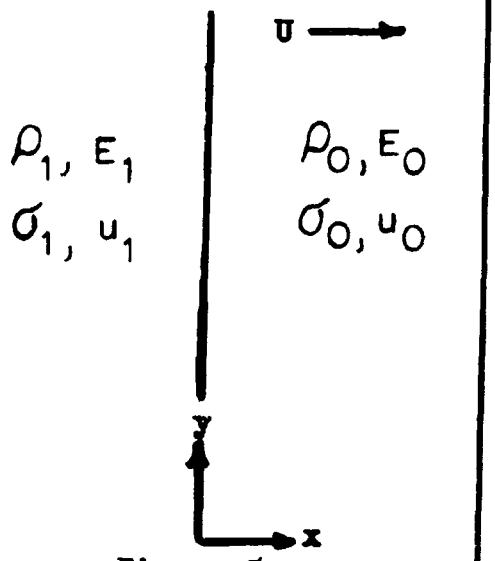

Figure 5

Plane Shock Front

(From Ref 26:66)

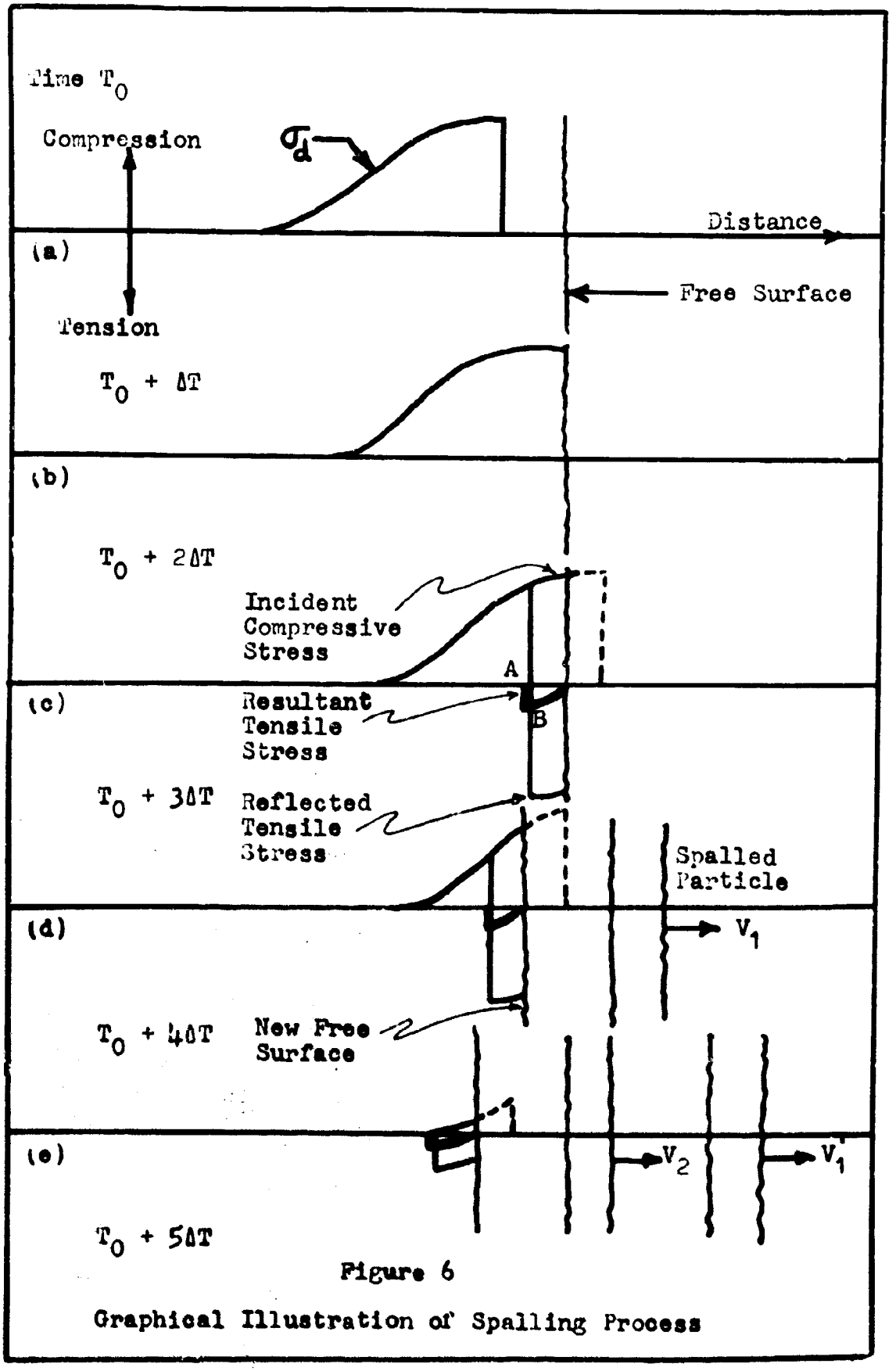

Figure 6

Graphical Illustration of Spalling Process

remainder of the medium as shown in Fig. 6, d. The velocity of the particles, V_1, depends on the energy transferred to it by the tensile wave and the magnitude of the restoring force. This process can repeat itself whenever a new surface is created if the tensile stress, or force, exceeds the restoring force of gravity. The Rankine-Hugoniot jump conditions have shown that the energy transfer to the medium is independent of gravity. Therefore, a change in the gravity field and the consequent change in the restoring force should result in (1) a change in the initial velocity of the particles which were originally spalled and (2) a change in the amount of spalled particles. In each case, the change will vary inversely with the change in gravity.

Some of the spalled particles are thrown clear of the final crater while others return to the depression as fallback. As seen in Fig. 1, the amount of fallback significantly affects the depth of the crater but not the diameter. The amount of material that becomes fallback depends on the range of the spalled particles which is expressed by

$$R = \frac{V_o^2 \sin 2\theta_o}{g} \tag{6}$$

where R = range of particle in free flight

V_o = initial particle velocity

θ_o = angle of initial particle heading as measured from the horizontal

g = acceleration due to gravity

From Eq. (6) it is evident that the range of a particle in free flight is inversely proportional to gravity if the remaining terms are assumed to be unchanged. However, it has been stated that the initial

velocity of the spalled particles should vary inversely with a change in gravity. This would also result in an additional change in the particle range in the same manner (increase or decrease) as a change in the gravity field. As gravity is reduced, the resulting increase in range results in a decrease in the amount of fallback. Less fallback results in a greater crater depth. In addition, the increase in the amount of spalled particles that result from a decrease in the gravity field also tends to increase the crater depth. Therefore, it is expected that the crater depth varies inversely with gravity when spalling is considered. Furthermore, the crater diameter is not appreciably changed during the spalling process when gravity is varied as fallback does not influence the crater diameter to a significant degree.

Gas Acceleration. Gas acceleration is caused by the escape of the expanding gases through the medium into the air. These gases impart a force to the particles of the medium and accelerate them in accordance with Newton's second law. The particles accelerated by the gases are of two types. First, certain spalled particles, because of their low initial velocity, go through a period of free fall in the vicinity of the forming crater. As the gases escape from the crater cavity, they impart a second positive acceleration to the particles (Ref 42:3455). The final range of these particles is affected by changes in the gravity term in Eq. (6) and results in the depth of the crater being inversely proportional to gravity.

The second types of particles accelerated by expanding gases are those that have not been spalled but have had a motion imparted to

them by the passage of the shock wave. In this instance the medium moves as one mass and the particles remain in contact with each other after the passage of the shock wave (Ref 42:3455). The vertical shear resistance of the medium now comes into consideration as this resistance must be overcome before the particles can be accelerated by the expanding gases.

Mediums have shear resistance on vertical planes because of the lateral pressures within the material. In a cohesionless medium, the lateral pressure acts parallel to the plane on which the vertical stress acts. This vertical stress is caused by the unit weight of the soil. Figure 7 shows a stress diagram of vertical and lateral stresses acting on a small element of the cohesionless medium.

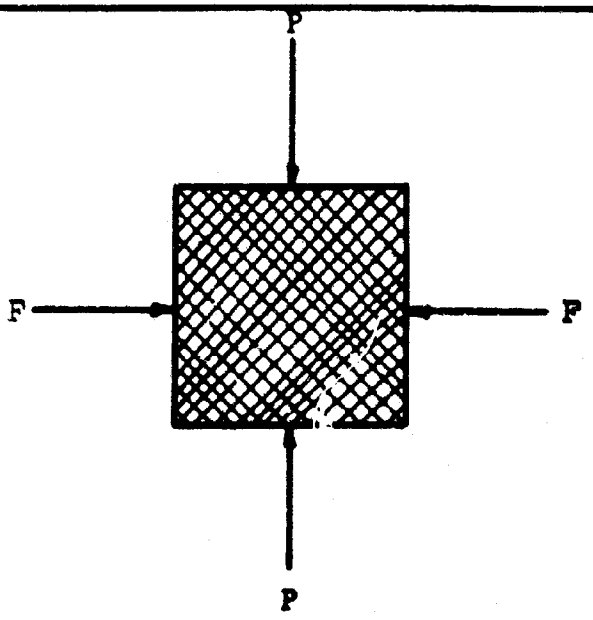

Figure 7

Forces Acting on a Small Element of Cohesionless Soil

The arrangement of the stresses satisfies the definition that "if the stress on a given plane at a given point is parallel to a second plane, the stress on the second plane at the same point must be parallel to the first plane" (Ref 50:290). Rankine has shown that these conjugate stresses are related to each other by the formula

$$\frac{F}{P} = K = \frac{1 - \sqrt{1 - \cos^2\phi}}{1 + \sqrt{1 - \cos^2\phi}} \tag{7}$$

where F = lateral stress parallel to slope

P = vertical stress on plane parallel to slope

ϕ = angle of internal friction of soil

K = conjugate ratio

Since the vertical stress P is due to the weight of the medium overburden, a gravity dependency for the lateral stress F can be expressed by

$$F = \rho g H K \tag{8}$$

where ρ = mass density of the medium

g = acceleration due to gravity

H = depth of plane below surface

The vertical shearing resistance is a function of the lateral stress through the relation

$$V = \mu F \tag{9}$$

where V = vertical shear resistance

μ = coefficient of friction

Therefore, the vertical shear resistance, which must be overcome in order to accelerate the particles, is directly proportional to gravity. The constant force of the expanding gases generated by the detonation of identical explosives at the same DOB must overcome the restoring force of gravity and the vertical shear resistance. For a decrease in gravity there is a decrease in the shear resistance on vertical planes which allows the expanding gases to accelerate the particles to higher velocities during the time that the particles are in contact. The higher velocities attained result in higher initial velocities of the particles when they begin free flight as ejected particles.

On the basis of the above explanation it is hypothesized that crater depths are inversely proportional to gravity when the fallback due to gas acceleration is considered.

Relative Importance of Processes as a Function of DOB

The final size of a terrestrial crater is usually considered to be a function of the type and energy of the explosive, the medium in which the explosion takes place, and the depth of burst of the explosion. Since an explosive source, constant in type and energy, and a homogeneous cohesionless cratering medium are assumed, only the DOB is discussed.

The DOB at which the explosion takes place is probably the most important factor in determining crater size. The reason for this is that the four cratering processes previously discussed are very sensitive to the DOB. This sensitivity is in turn reflected in any comparison between crater dimensions and DOB such as is illustrated in Fig. 8. As is shown in this figure, the depth and diameter of a

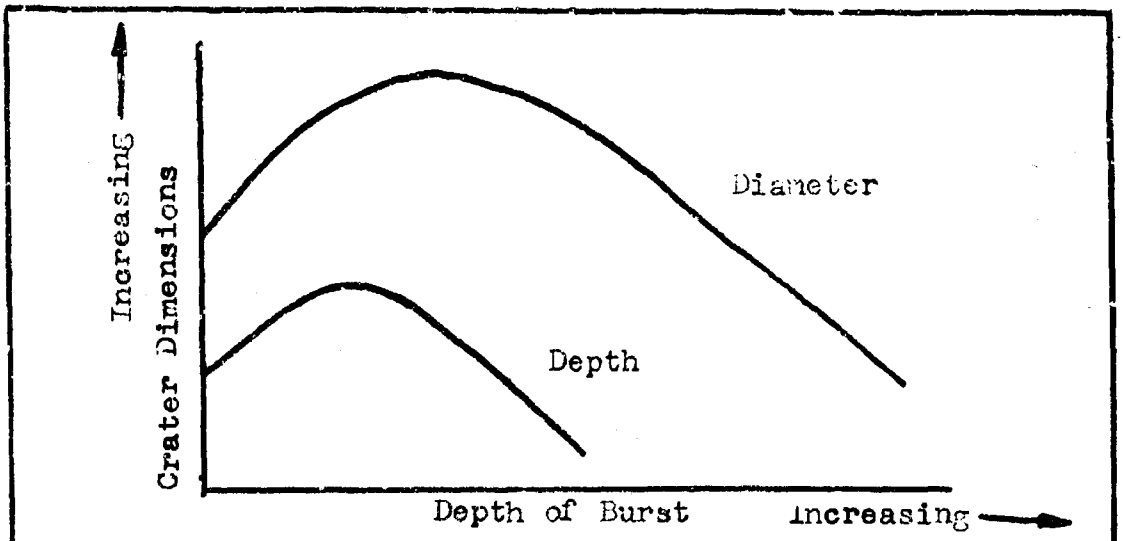

Figure 8

Crater Dimensions as a Function of Depth of Burst

crater increase as the DOB is increased. After some optimum DOB is reached for each dimension, the dimensions begin to decrease. The peaks of these representative curves are influenced by the type of medium in which the crater is formed and the explosive used. However, the concave downward shape of these curves is characteristic of all mediums and explosives.

When the charge is detonated on the surface of the medium, compaction and scouring are the only processes available to form the crater. Because no portion of the medium is located above the charge, spalling and gas acceleration have no influence on crater formation. For a shallow DOB, spalling becomes the dominant process in the formation of a crater (Ref 41:3395). Because of the high velocities imparted to the medium by spalling, the expanding gases escape into the atmosphere without having to expend their energy on the medium above the detonated charge. Compaction, and to a lesser extent, scouring, are still involved in the crater formation. As the DOB is increased,

an optimum DOB is achieved. At optimum DOB, all processes except scouring play an important role. Gas acceleration tends to be the dominant factor, followed by spalling and then compaction. As the DOB is further increased, the relative importance of gas acceleration increases. Spalling continues to decrease because the shock wave intensity is reduced by the time it reaches the surface from a deeply buried charge. The role of compaction also continues to decrease since the shear strength of the medium increases with the amount of medium overburden. The overall effect is that the crater dimensions decrease. When the charge is buried deeply enough, the cratering processes are so ineffective that all of the disturbed medium subsides back into the depression, leaving no crater at all. Eventually, the medium attenuates the entire explosion to such an extent that no motion is observed on the surface of the medium. Figure 9, modified from

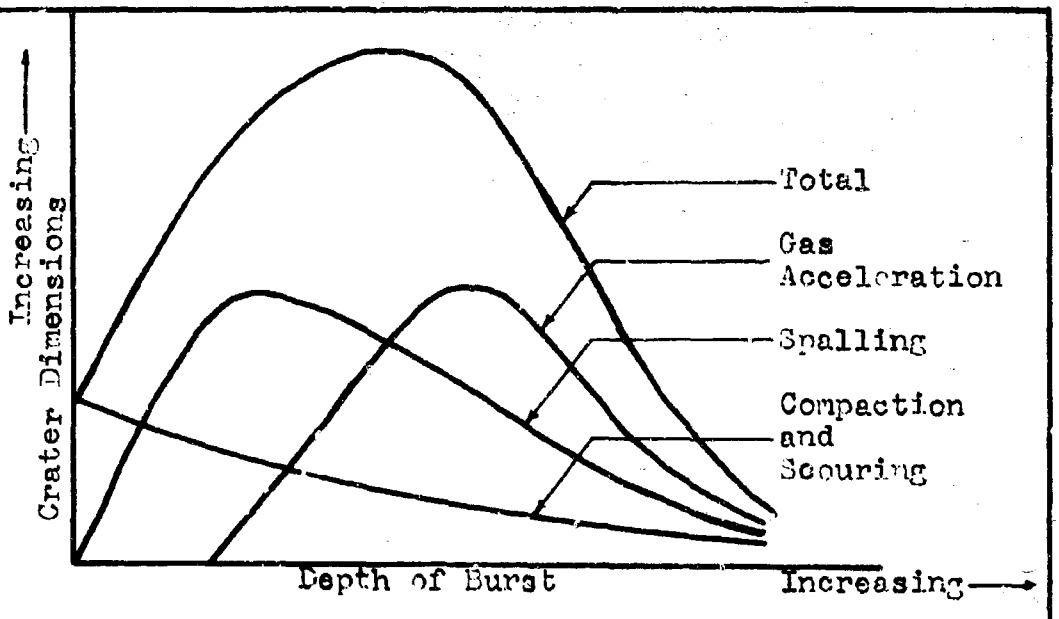

Figure 9

Relative Contributions of Processes to Crater Dimensions

Nordyke, summarizes the relative importance of the cratering processes as the DOB is increased (Ref 42:3457). Based upon the discussion contained in this section, it can be hypothesized that the ordinates of points on the total dimension curve in Fig. 9 vary inversely with gravity.

Summary

In this section, it was indicated that a change in gravity affects each cratering process. The effectiveness of the processes due to these changes and the effect on the crater depth and diameter are summarized below:

	Compaction	Scouring	Spalling	Gas Acceleration
Diameter	Varies inversely	Varies inversely	No change	No change
Depth	Varies inversely	Varies inversely	Varies inversely	Varies inversely

The processes of compaction and scouring are most significant at shallow depths of burst. At the optimum DOB, all cratering processes contribute to the crater formation. For deep depths of burst, gas acceleration is the most significant process. It is hypothesized that the combined effect of the processes results in crater dimensions varying inversely with gravity.

III. Experimental Procedure

The purpose of this experiment was to determine the effect of gravity on the formation of explosion craters. The experiment involved the detonation of a small explosive in a cohesionless medium under various gravity conditions. This section provides a brief explanation of the manner in which the experiment was conducted. The main steps in this experiment were (1) securing the materials and equipment, (2) calibrating the equipment, (3) conducting ground tests, and (4) conducting flight tests. For a more detailed explanation of the equipment, calibrations, sources of error, and false leads, refer to Appendix A.

Materials and Equipment

The aircraft for varying gravity was available in the Aeronautical Systems Division at Wright-Patterson Air Force Base, Ohio. The cratering medium selected was Flint Shot Ottawa Sand because of its characteristics of uniformity and purity and its cohesionless nature. Appendix B discusses in detail the properties of the cratering medium. The detonations were set off in sand on the floor of a plywood container which was 4 feet by 4 feet on a side and 5 feet high. The small explosive used was a 6.0-grain squib which disintegrates by a deflagration process. Photography was used to record the crater depths and diameters during the experiment.

Design and Calibration

The beginning phases of the experiment were concerned with the calibration of the equipment. The purpose of the calibration was (1) to insure that the planned method of obtaining data was yielding valid information, (2) to determine the degree of accuracy to which measurements could be made, and (3) to improve the efficiency of the data gathering techniques without sacrificing accuracy. The factors considered in calibration were (1) the area and depth of sand necessary to minimize boundary effects, (2) the best method of placement of the squib in the sand, and (3) the best method of extracting crater parameters from the films.

Ground Tests

Ground tests were performed to determine crater dimensions under 1.0 g conditions. These tests consisted of measuring craters formed under varying depths of burst. The depths of burst were varied in one-half inch intervals from surface bursts to a two inch DOB and in one inch intervals from a two inch DOB to depths where no crater was formed. Twenty bursts were recorded at each DOB to provide sufficient data for a statistical analysis. The steps in conducting a typical crater forming cycle were (1) preparing the medium, (2) setting the charge, and (3) detonating the charge and recording the crater dimensions.

Flight Tests

The flight tests were conducted in the same manner as the ground tests with the exception of the changes in the gravity field. The values of gravity chosen for the experiment were 0.17, 0.38, and 2.5 g.

These gravity levels could be maintained for a period of 15 seconds. The depths of burst were varied in the same manner as they were during the 1.0 g tests. Ten shots were taken for each condition of gravity and DOB. The value of gravity for each maneuver was recorded on an oscillograph for reference. In addition, five craters were formed at one and four inch depths of burst in flight under 1.0 g conditions. This was done to determine any possible effect on the crater dimensions due to aircraft vibrations.

IV. Discussion of Observed Gravity Effects

The data from the cratering experiment is evaluated in this section to determine the effect of gravity on crater formation. The experimental results are compared with the previously suggested effects of gravity on cratering. Conclusions are drawn concerning the influence of gravity on crater formation for small deflagrating processes in a dry cohesionless silica sand.

Diameters As a Function of Depth of Burst

Crater diameters can be displayed graphically as a function of the DOB of the charge. The data on which the graphs are based is tabulated in Appendix C. In addition, profiles of typical craters formed at each DOB and value of gravity are drawn in Appendix D. Each curve of diameter versus DOB is valid for a given value of gravity. Figures 10, 11, 12, and 13 are curves obtained from experimental data for diameters for 0.17, 0.38, 1.0, and 2.5 g, respectively. Figure 14 is a consolidation of these curves. Main points for discussion concerning gravity effects are (1) inherent scatter and possible errors, (2) significant differences in the diameters for a given DOB, (3) changes in optimum DOB, and (4) maximum DOB for which a crater is formed.

In Section II, it was hypothesized that crater diameters vary inversely with gravity. Figure 14 indicates that this hypothesis may be valid but before the conclusion can be accepted the inherent scatter and errors in the experimental data must be checked. An

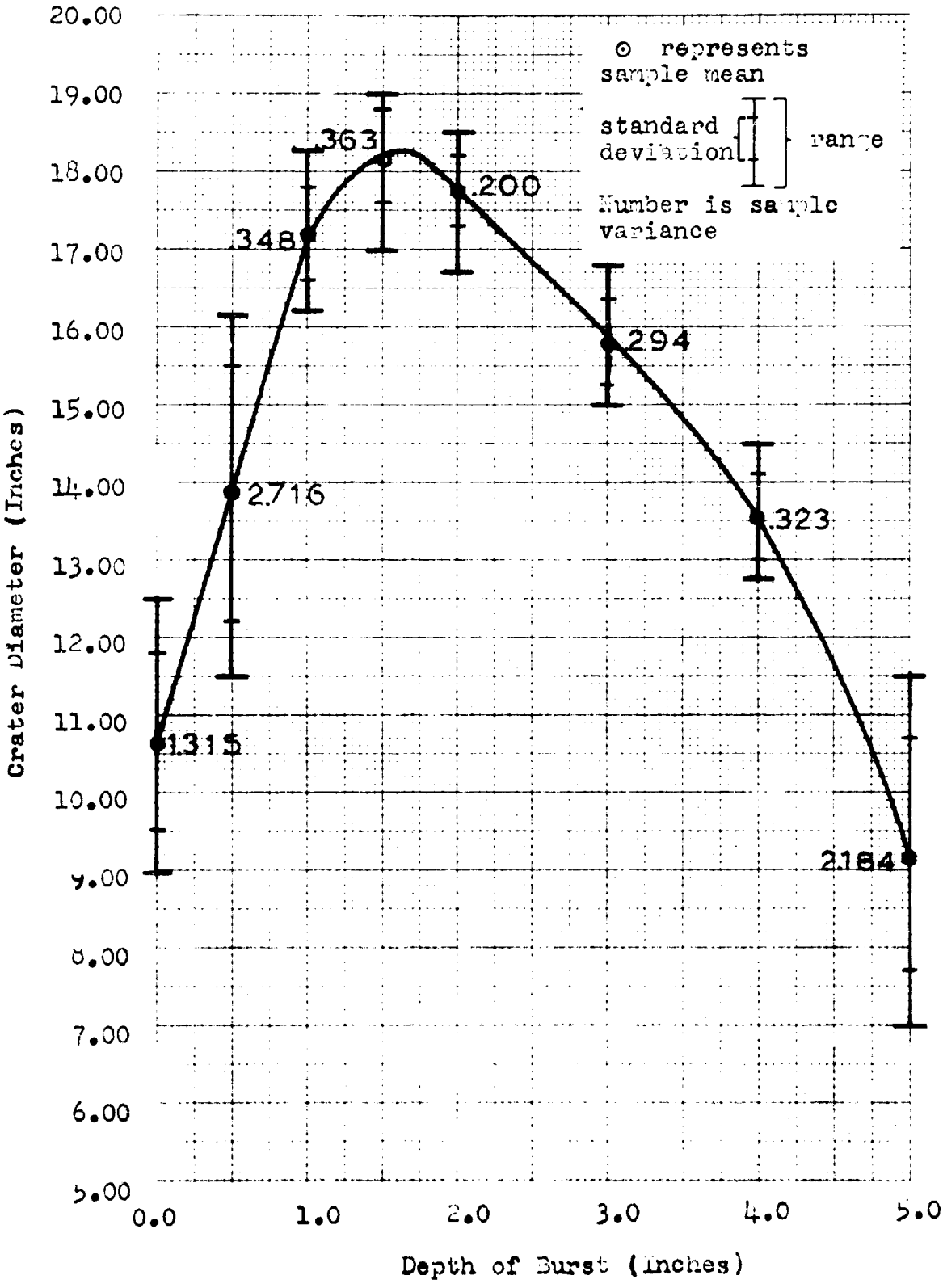

Figure 10

Diameter as a Function of Depth of Burst for .17 g

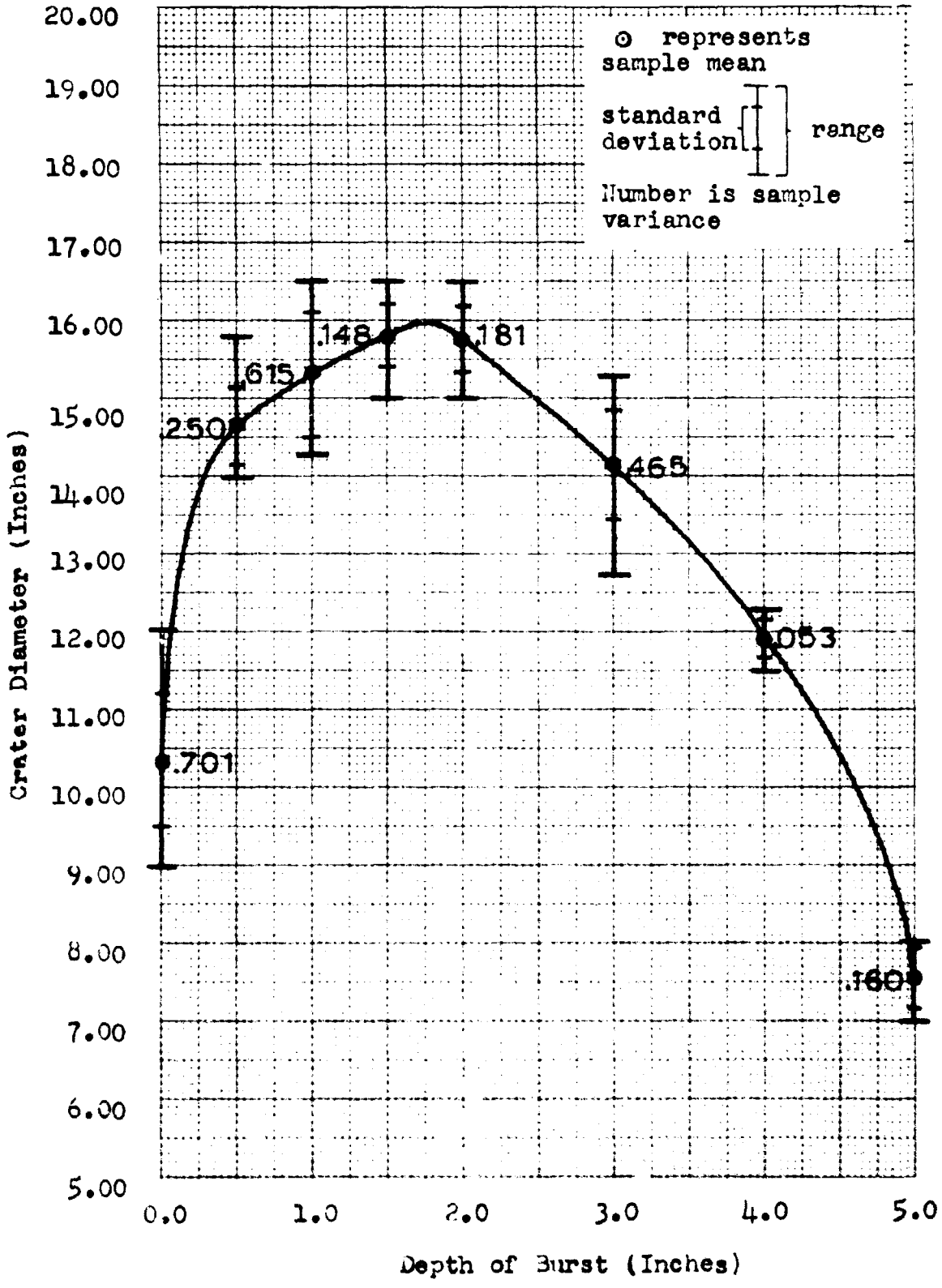

Figure 11

Diameter as a Function of Depth of Burst for .38 g

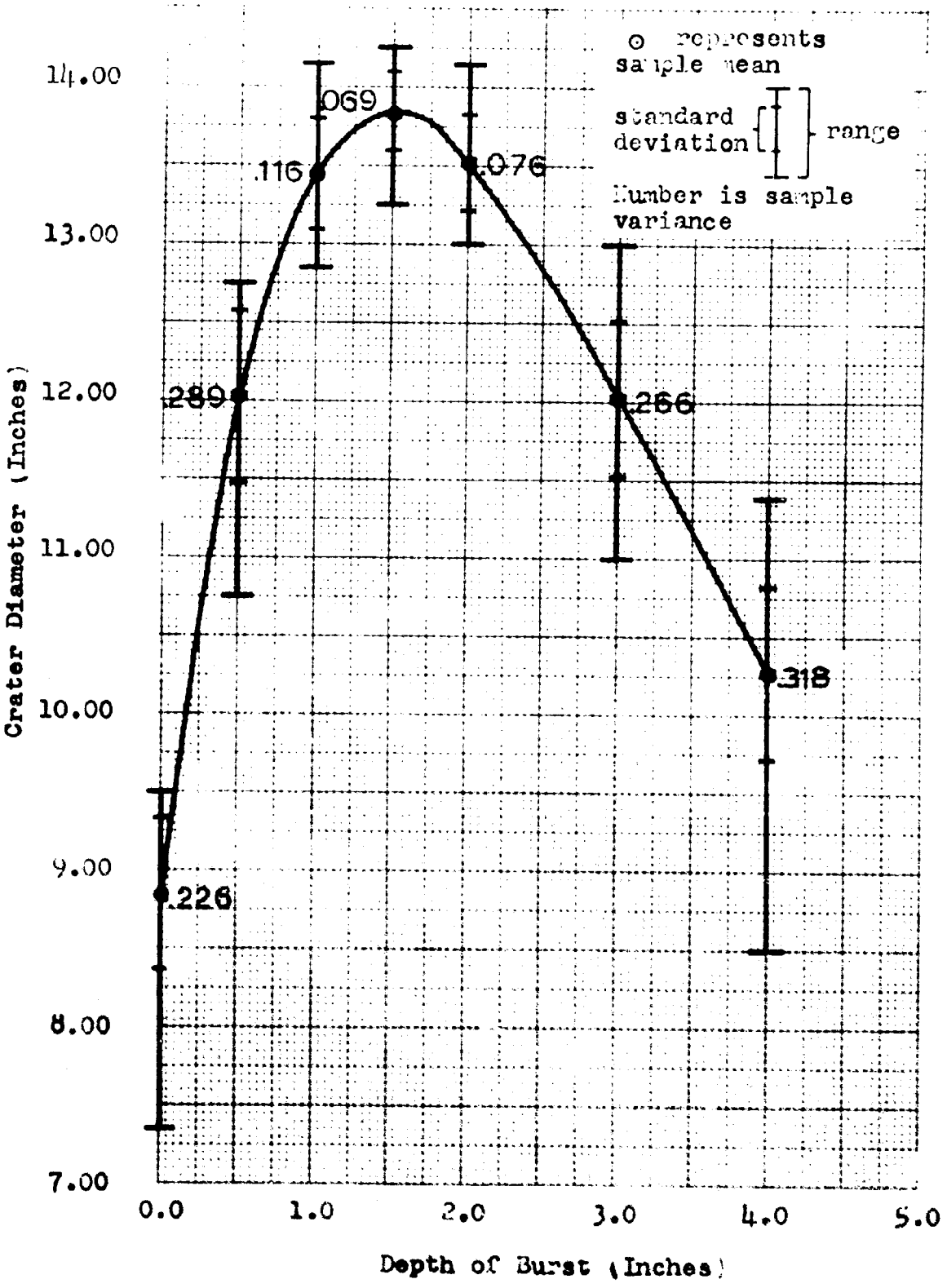

Figure 12

Diameter as a Function of Depth of Burst for 1.0 g

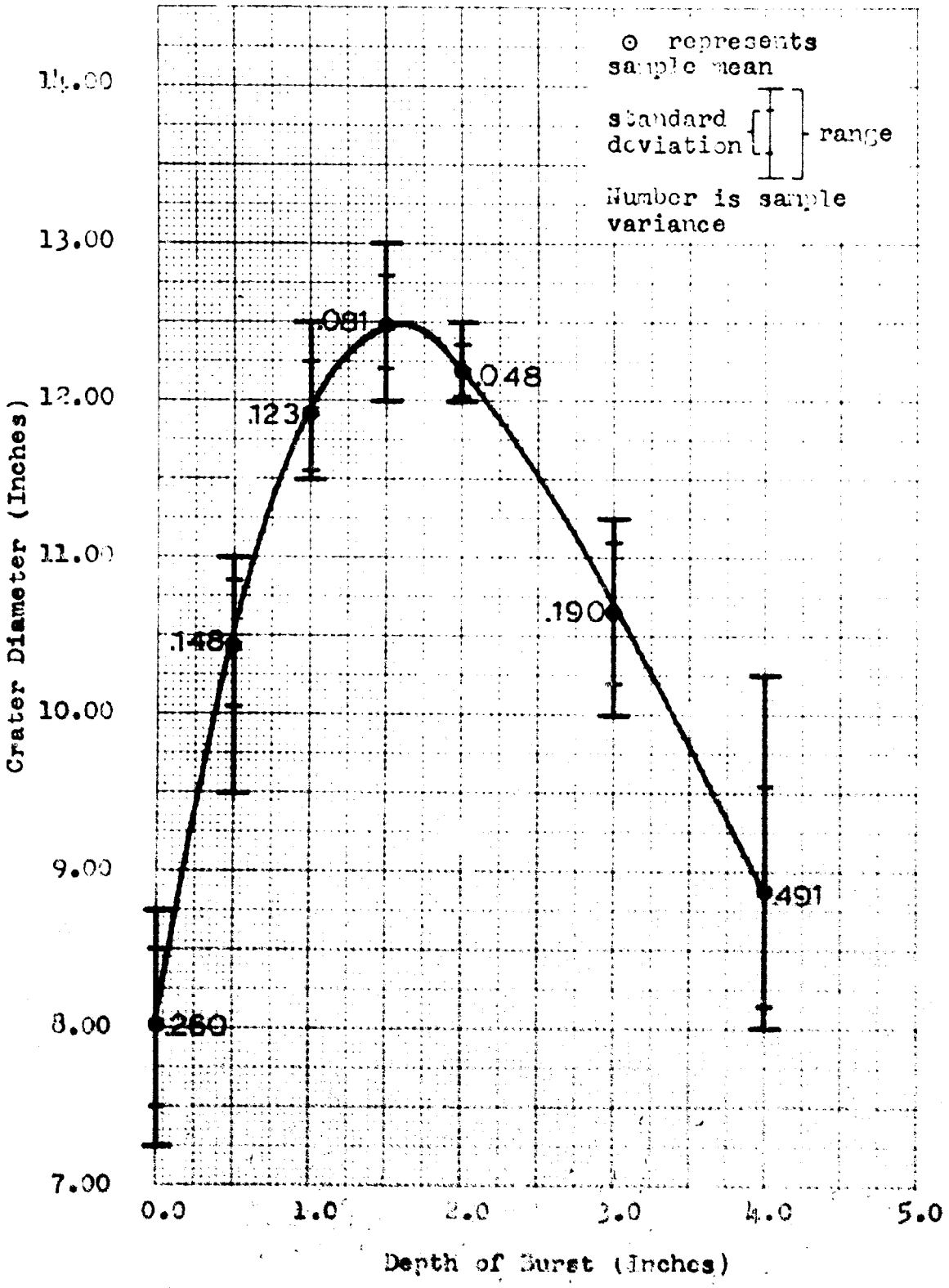

Figure 13

Diameter as a Function of Depth of Burst for 2.5 C

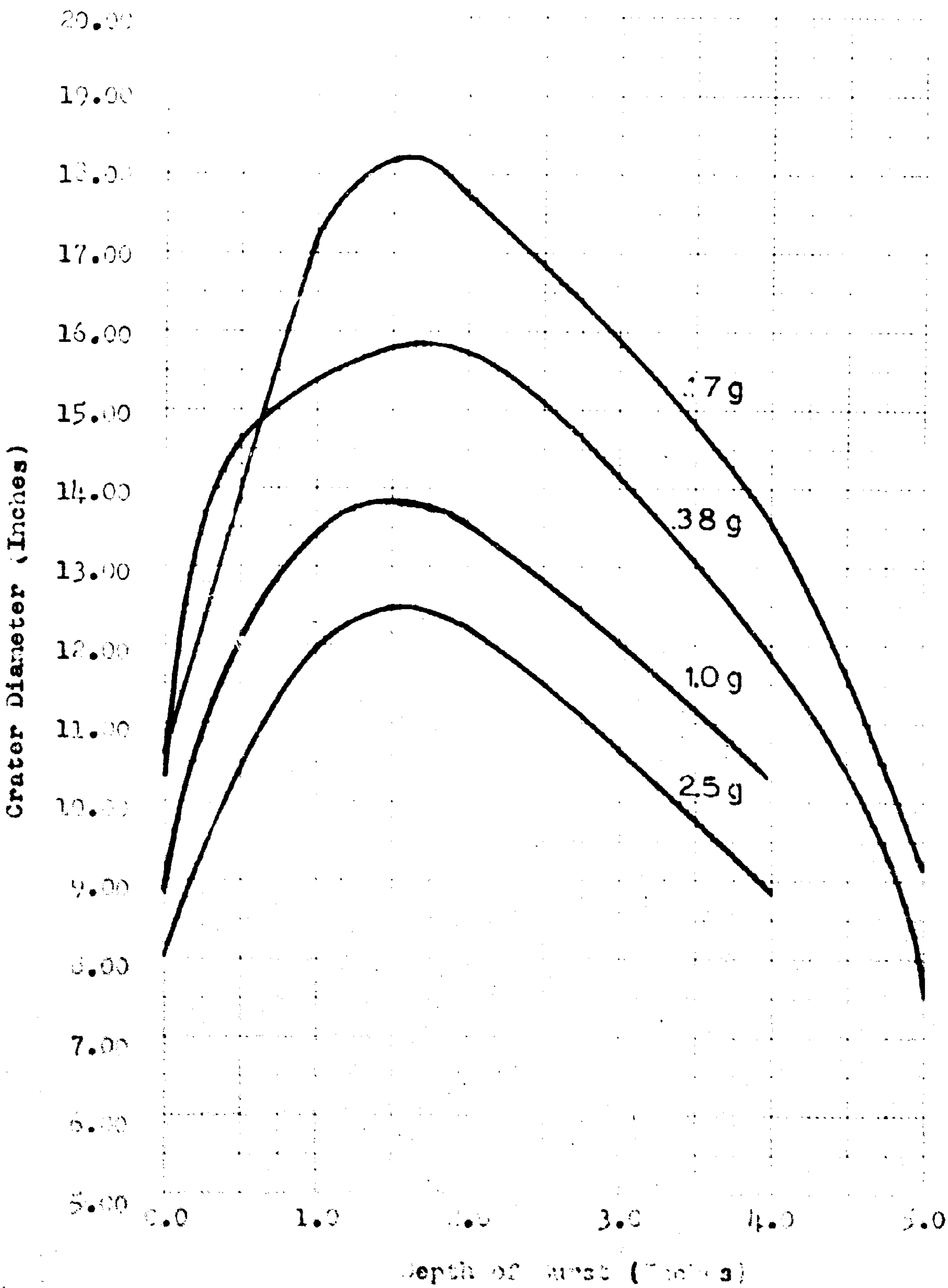
Crater Diameter (Inches)
17.00
16.00
15.00
14.00
13.00
11.00
9.00
7.00
5.00
1.0
3.0
4.0
5.0
7 g
.38 g
1.0 g
2.5 g

inspection of the variances and ranges of the samples listed in Table VI of Appendix C shows the samples for 0.0, 0.5, and 5.0 inch DOB at 0.17 g have the largest variances. The scatter can be attributed to aircraft vibration and difficulty in measuring crater depths and diameters for some craters of irregular shapes.

Although vibration should affect shallow depths of burst at all values of gravity, the effects are more pronounced at the low values of gravity. At low values of gravity, the lateral pressure of the sand and the weight of the squib are both decreased. This allows vibrations to move the squib from its desired position. During the experiment, it was noted that the squib, when set at shallow depths of burst, had a tendency to move upward. This was due to tension in the lead-in wires and firing wires. An effort was made to eliminate this tension by adjustment of the wires, but this was not always effective. Squib movement from desired settings has some influence on crater diameters as indicated in Table VII of Appendix C, where diameters are compared when the DOB is slightly varied from a given position. Diameters of craters that are formed when squibs move upward are smaller than diameters of craters formed when squib movement does not occur.

The scatter in the data for 5.0 inch depths of burst at 0.17 g is caused by measurement difficulties at this condition. The final crater shape was poorly defined and irregular because of the deep DOB. Craters were barely visible at 5.0 inch DOB at 0.38 g and no craters were formed at all for this DOB at 1.0 and 2.5 g.

In summary, the charge did not remain at the desired DOB at shallow depths of burst and lower values of gravity. If the charge had

remained at the desired DOB, the ordinate values of the curves would have been somewhat higher than those shown in Figs. 10 through 16. Crater shapes for deep depths of burst were difficult to measure which increased the scatter in the data.

An understanding of the nature of the scatter and errors in the experiment permits a more reliable estimate to be made concerning significant gravity effects on crater diameters. A statistical analysis of the experimental data was made which compared diameters at given depths of burst but which were formed at two different gravity values. The test used is called the two-sample t-test and the hypothesis tested was that the mean diameters of the compared samples were equal. The alternative condition was that the sample mean for diameters formed under a given gravity field was greater than the sample mean for diameters formed under a higher gravity field. If the hypothesis that the means were equal could be rejected, gravity had an effect on crater formation. Appendix E gives a detailed explanation of the t-test and contains the tabulated results of this test. This tabulated data reveals that the changes in diameters are statistically significant for all comparisons except two.

One of the comparisons where the hypothesis could not be rejected was at 0.0 inch DOB for 0.17 and 0.38 g. At this DOB, the squib was completely unconfined by the cratering medium. The lack of confining pressure on the squib can result in a large portion of the charge being scattered without burning. This property of the squib is explained in the performance characteristics section of the specifications shown in Fig. 41, Appendix A. The high speed films taken of the

cratering process verified that portions of the explosive mixture were scattered from the point of detonation for surface bursts. Such scattering resulted in a reduction in the effective yield of the explosive. The effective yield of an explosive is defined here to be that portion of the total energy yield which contributes to crater formation. Because the reduction in the effective yield is an uncontrolled variable at this DOB, the variance of the data is increased. This large variance tends to mask the gravity effects on the cratering process for 0.17 and 0.38 g. When larger increments of gravity are taken in the t-test, the gravity effects on crater dimensions become apparent. If an instantaneous detonation could have been achieved in the experiment, the scatter of the explosive mixture would not have occurred. One can reasonably speculate that the effective yield would not have been reduced and the gravity effects might have been statistically significant between 0.17 and 0.38 g for surface bursts.

The other comparison for which the hypothesis cannot be rejected is between 0.17 and 0.38 g at 0.5 inch DOB. For this DOB, lack of adequate confinement on the squib is again an important factor. In this instance, the confinement on the squib is due to the lateral pressure exerted on the squib by the medium. According to a duPont technical representative, the minimum condition for consistency of the detonation process is to have the squib completely covered with sand in a 1.0 g field (Ref 14). This condition is achieved at 0.5 inch DOB for 1.0 or 2.5 g. However, for reduced gravity, the lateral pressure at a given depth is reduced. This reduction would be especially critical for 0.17 g and shallow depths of burst. The gravity

dependent confining pressure affects the explosive effective yield and may be responsible for the crossing in the 0.17 and 0.38 g curves as shown in Fig. 14. If an instantaneous detonation could have been achieved, the crossover in the curves might not have been present.

For all other comparisons in the t-test, statistically significant changes were noted for crater diameters as a function of gravity. The experimentally observed changes in the diameters vary inversely with changes in gravity.

Optimum and Maximum Depth of Burst for Diameters

A point of interest on Fig. 14 is the value for the optimum depth of burst. The optimum depth of burst is the DOB where the maximum crater diameter is produced from the detonation. A change in gravity, while changing crater diameters, does not appear to influence the DOB for optimum diameters. It was hypothesized in the discussion of gravity effects that for constant depths of burst crater diameters are influenced only by changes in the compaction and scouring processes. If this hypothesis is true, the change is shown in Fig. 15, a modification of Fig. 9. A change in the ordinate values of the compaction and scouring curve is reflected in a similar change in the ordinate values of the total curve. A change of this nature does not appear to shift the location of the optimum DOB.

It can be observed from Fig. 14 that the maximum DOB at which a crater with a measurable diameter is formed varies inversely with gravity. This observation may be explained by the fact that the maximum depth at which shear failure can develop along a plane varies inversely with gravity. This influences the maximum DOB at which a

crater diameter is formed.

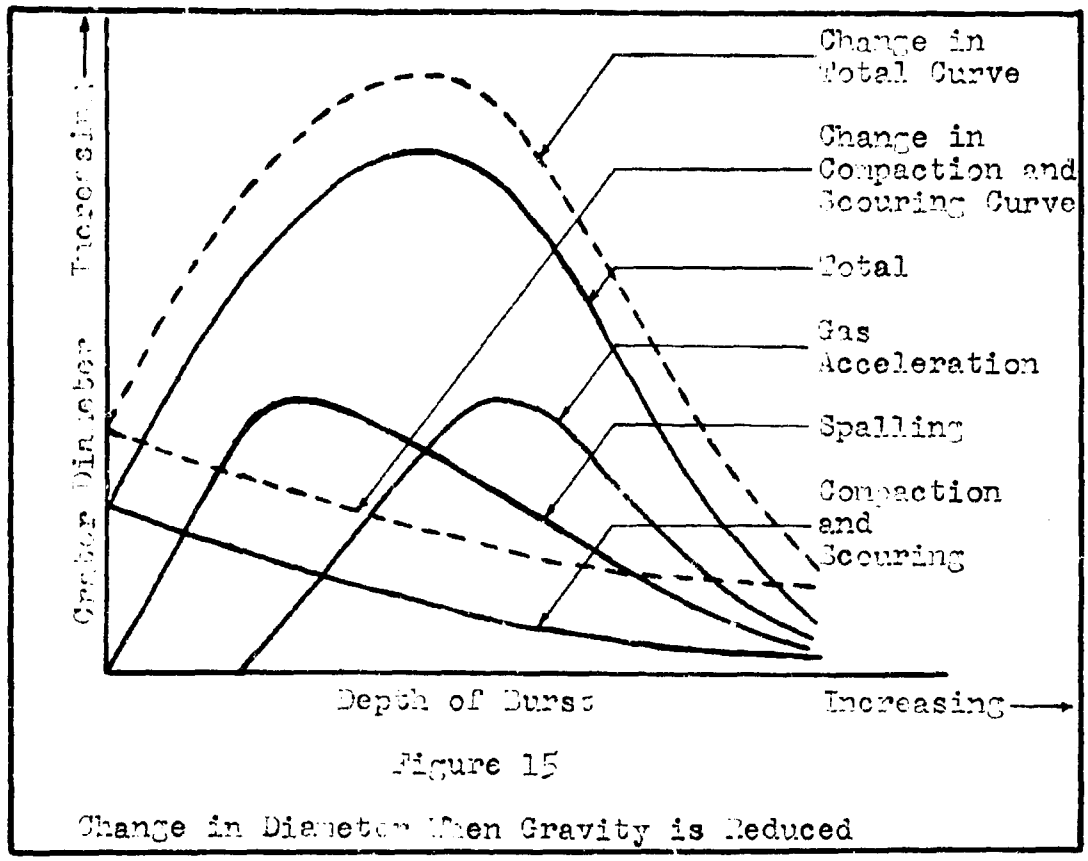

Figure 15

Change in Diameter When Gravity is Reduced

Depths as a Function of Depth of Burst

The depth of a crater can also be analyzed as a function of the DOB when gravity is varied. Figures 16, 17, 18, and 19 are curves of depth versus DOB for 0.17, 0.38, 1.0, and 2.5 g, respectively. Figure 20 is a consolidation of these curves.

Some of the scatter in the data for crater depths is due to aircraft vibration. Additionally, it is noted that the curve in Fig. 17 for 0.38 g has two maximum points. Of the four curves, this is the only one which has this characteristic. A detailed investigation was made to determine the reason for this anomaly. A check of the gravity values attained during the flight and a remeasurement of the craters

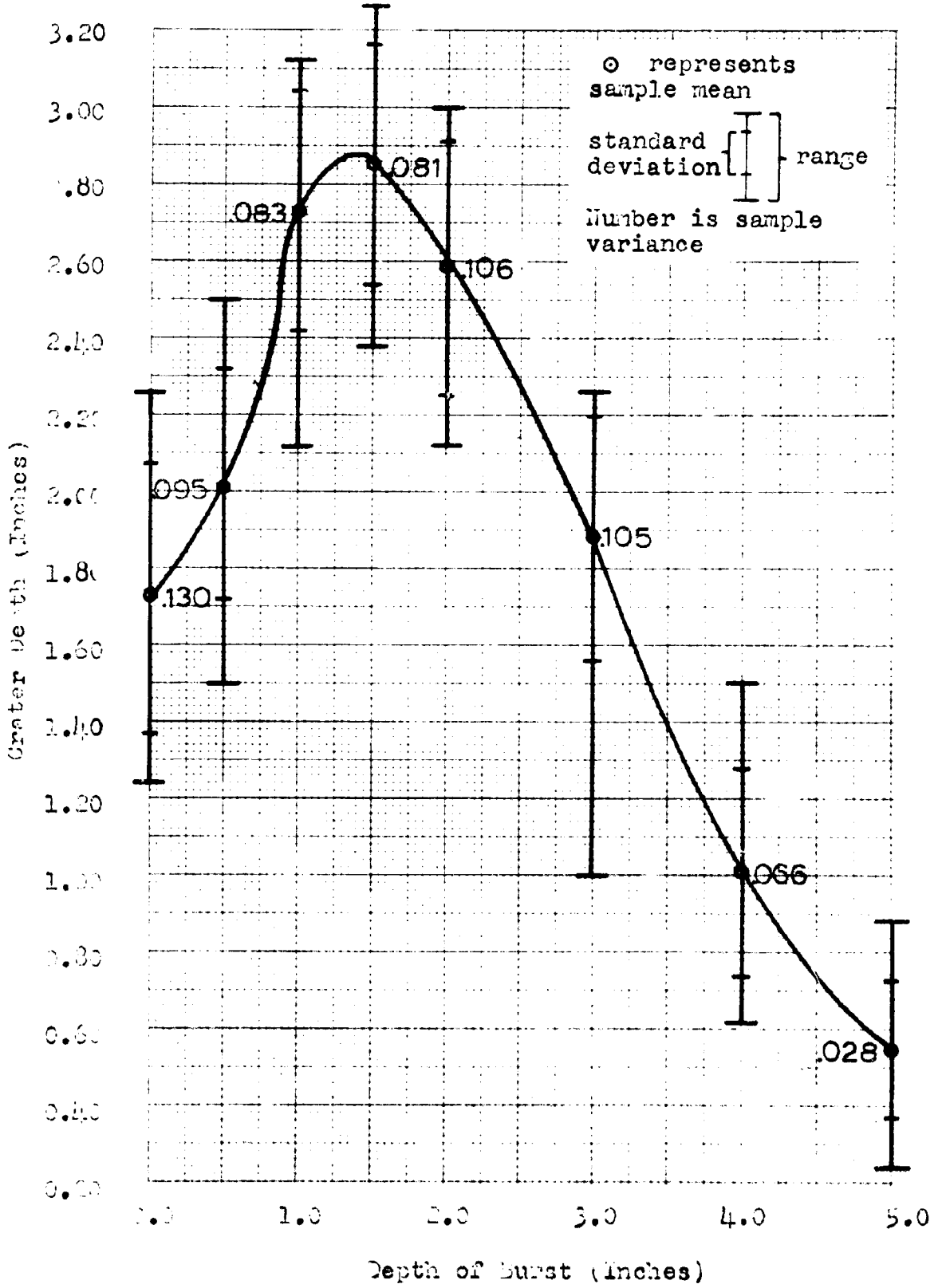

Figure 16

Depth as a Function of Depth of Burst for .17 g

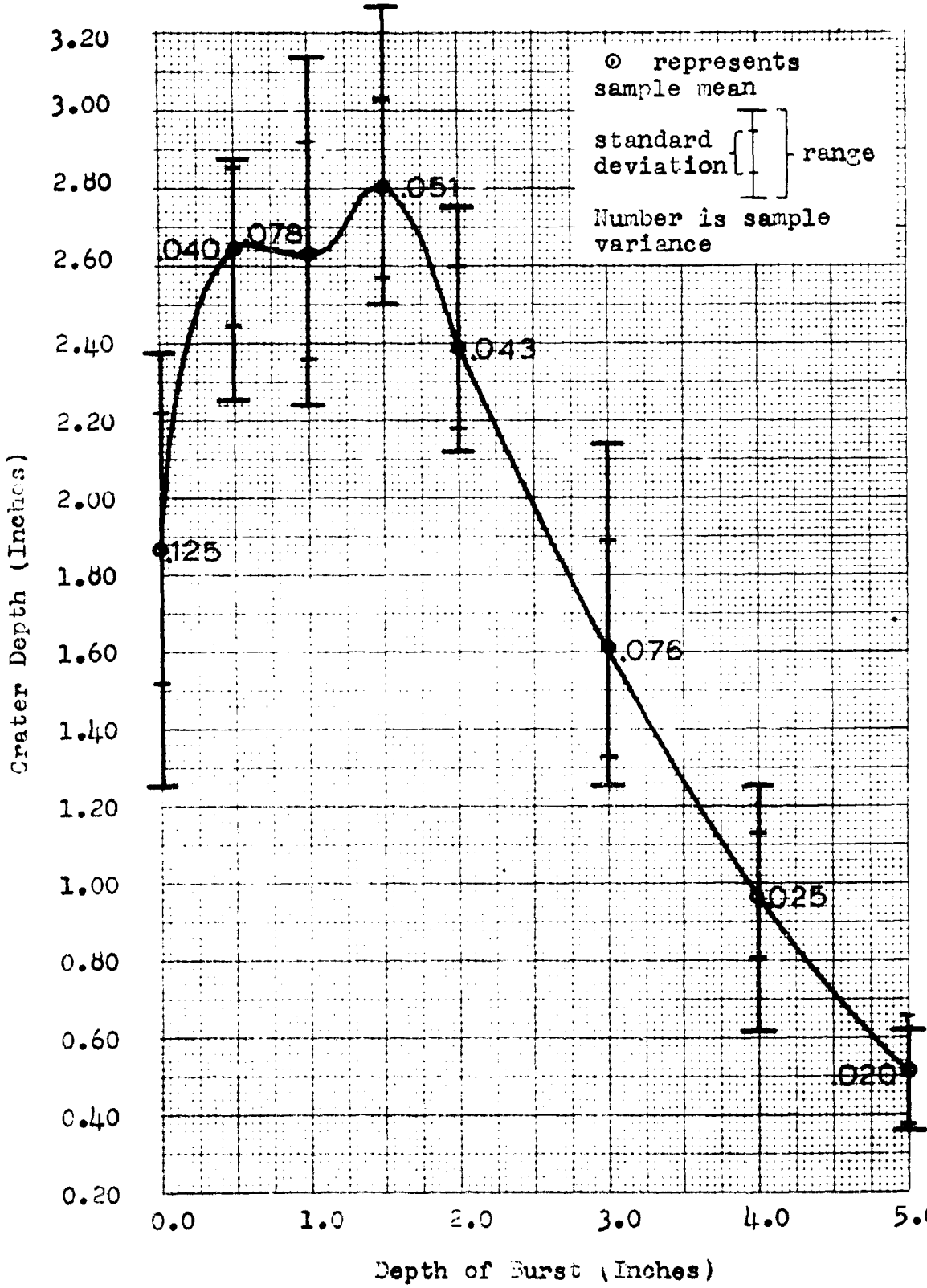

Figure 17

Depth as a Function of Depth of Burst for .38 g

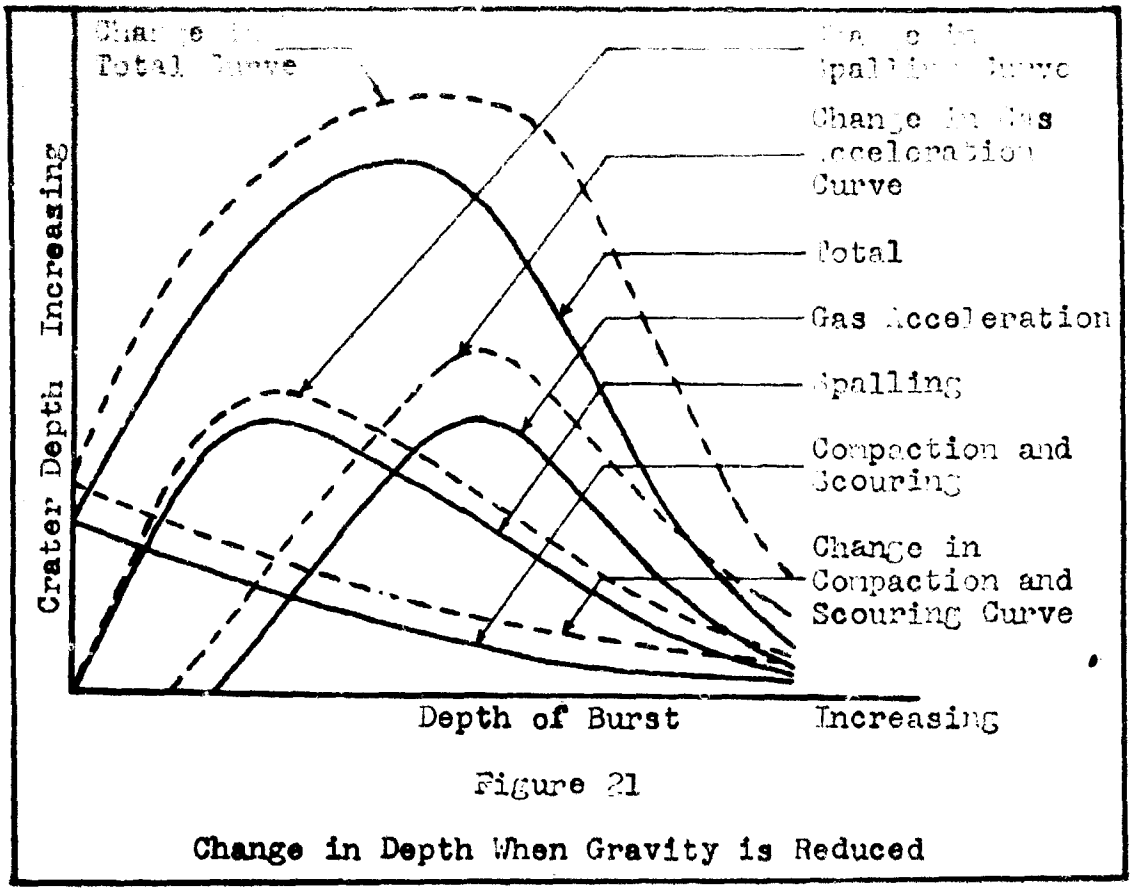

Figure 21

Change in Depth When Gravity is Reduced

inversely with gravity, the maximum DOB also varies inversely with gravity.

Relationship Between Dimensions and Gravity

At this point, it has been established that crater dimensions vary inversely with gravity. The next step is to try to determine a mathematical relationship for the dimensions as a function of gravity.

The dimensions should have some finite value even as the gravity field approaches zero. The dimensions of craters formed at very low values of g are determined by the manner in which the sand dissipates the energy of the detonation through inertial resistance.

Examining the limiting condition when the gravity field becomes very large, one expects the crater dimensions to approach zero as a

limit. This is based upon the inability of the energy of the explosion to overcome the large shear resistance which is present. In addition, the range of any particle which is given an initial velocity becomes negligible as is illustrated by Eq. (6). Considering the above limiting cases which must be satisfied, an exponential function for the dimension in terms of gravity appears to be a suitable relationship to assume.

Plots of diameters and depths as a function of gravity for a given DOB are shown in Figs. 22 through 35. It can be seen that the sample points do indeed exhibit a trend toward a decreasing exponential function as the gravity field is increased. In order to obtain parameters so that gravity effects could be analyzed, an exponential function was assumed of the form

$$D = Ae^{-gB} \tag{10}$$

where D = dimension of the crater

A = arbitrary constant

B = measure of sensitivity of dimension to gravity changes

g = acceleration due to gravity

The parameters A and B were adjusted to achieve the best fit to the experimental data in the least-squares sense. The effectiveness of this curve fitting technique was limited by the availability of only four data points for each curve. Values of A and B obtained in the curve fitting calculations and the least-squares deviations are listed in Table I. In addition, Figs. 22 through 35 show plots of Eq. (10) for the different depths of burst using values of A and B as calculated

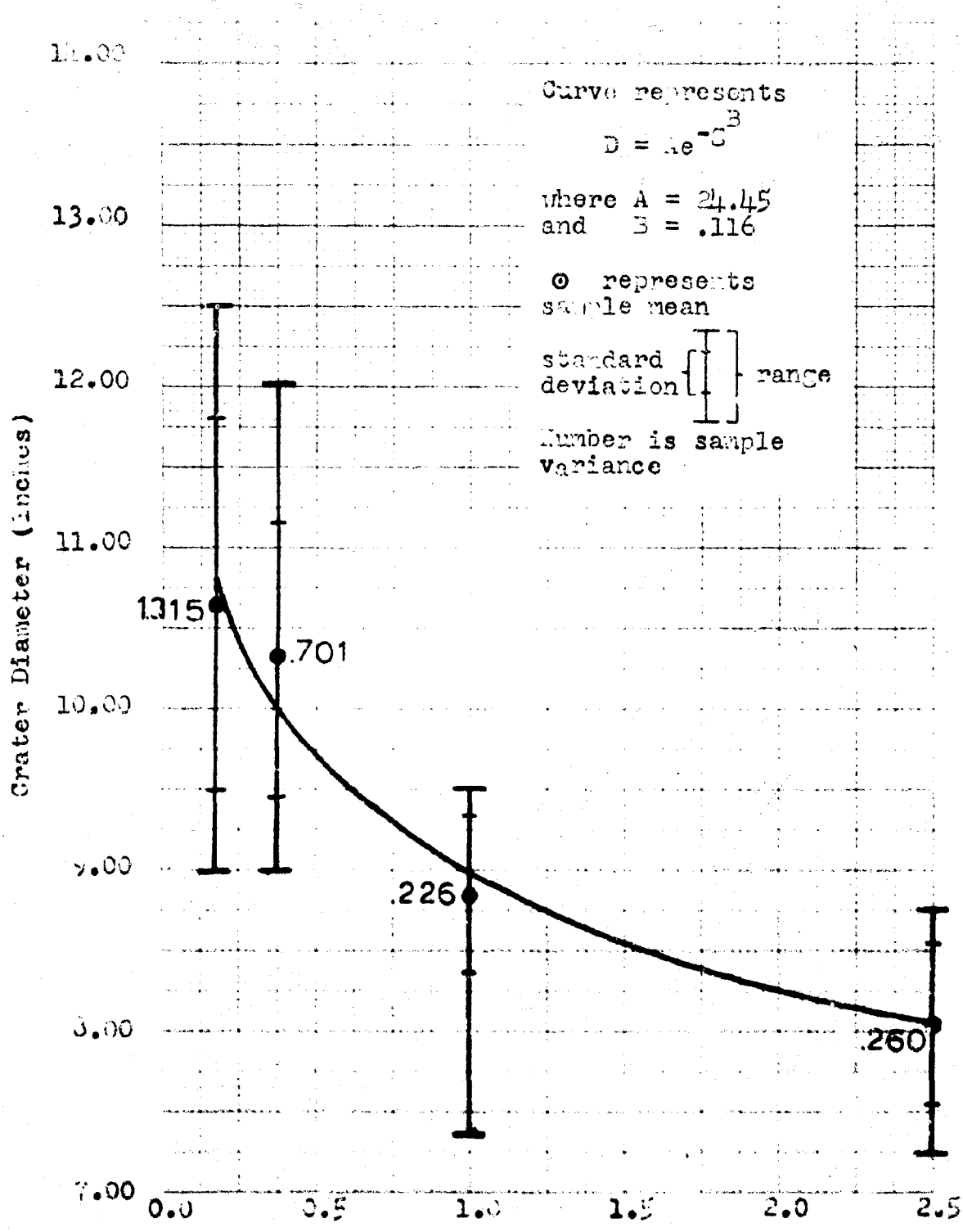

Figure 22

Diameter as a Function of Gravity at 0.0 Inch DOB

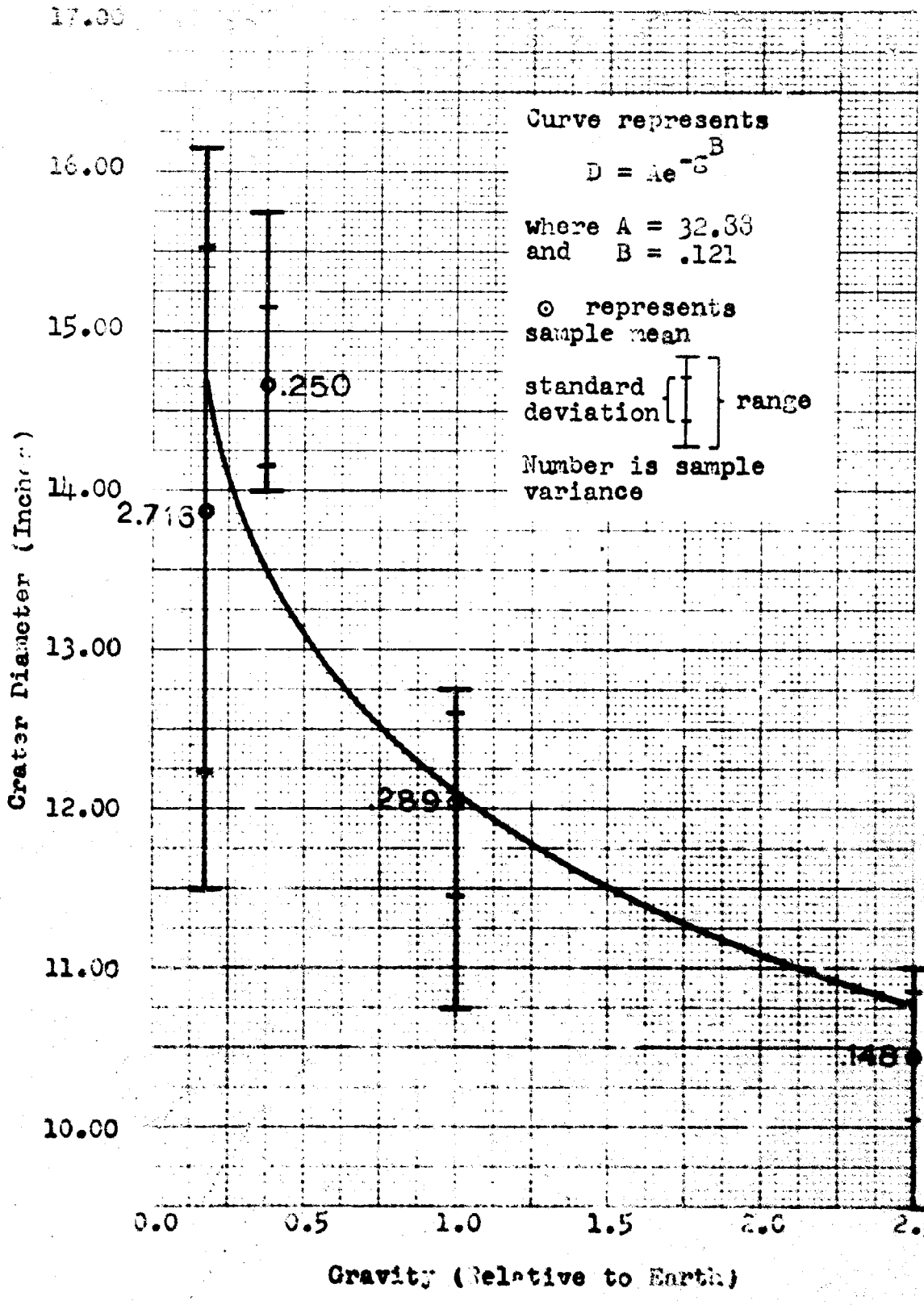

Figure 23

Diameter as a Function of Gravity at 0.5 Inch DOB

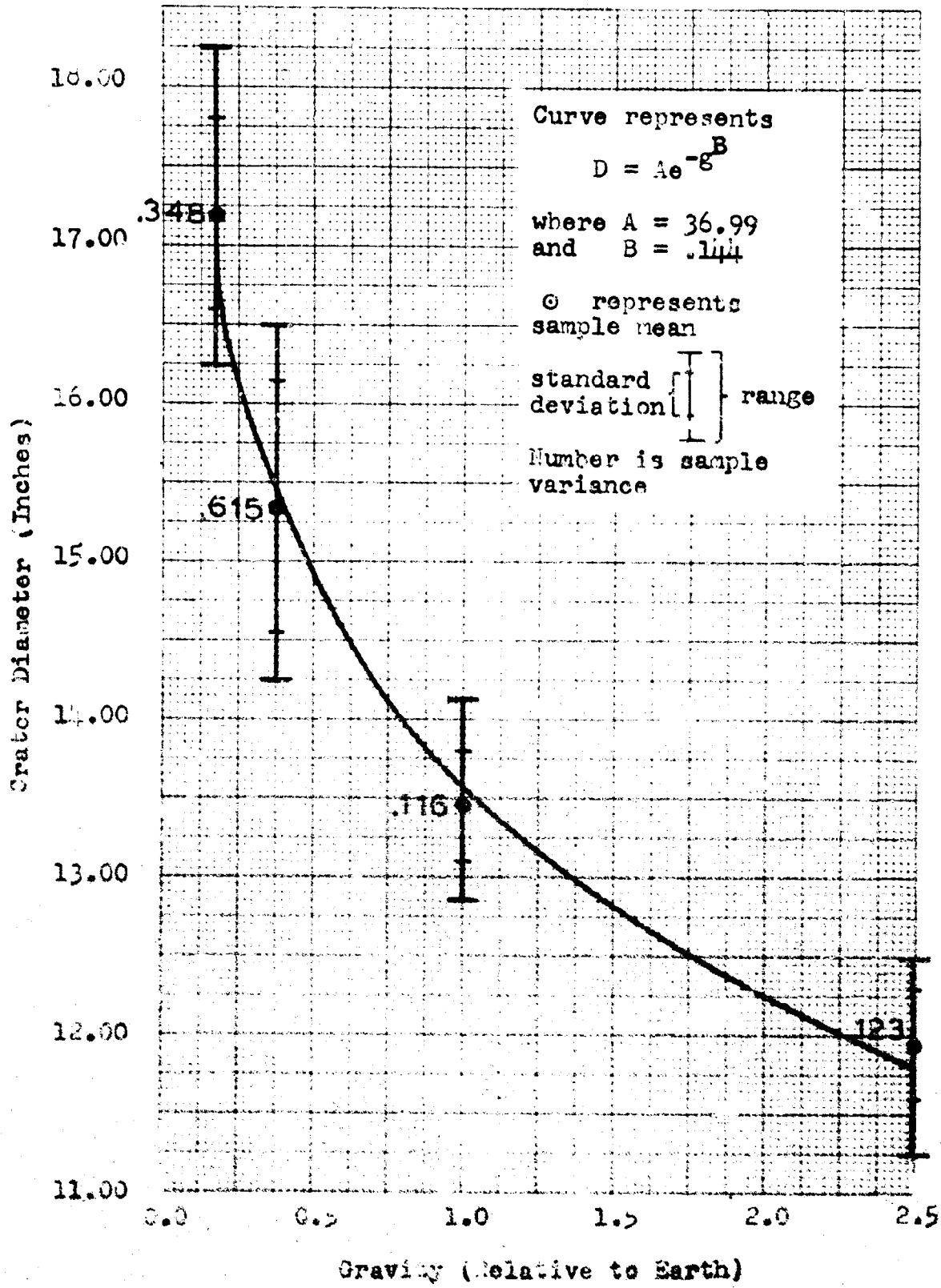

Figure 24

Diameter as a Function of Gravity at 1.0 Inch DOB

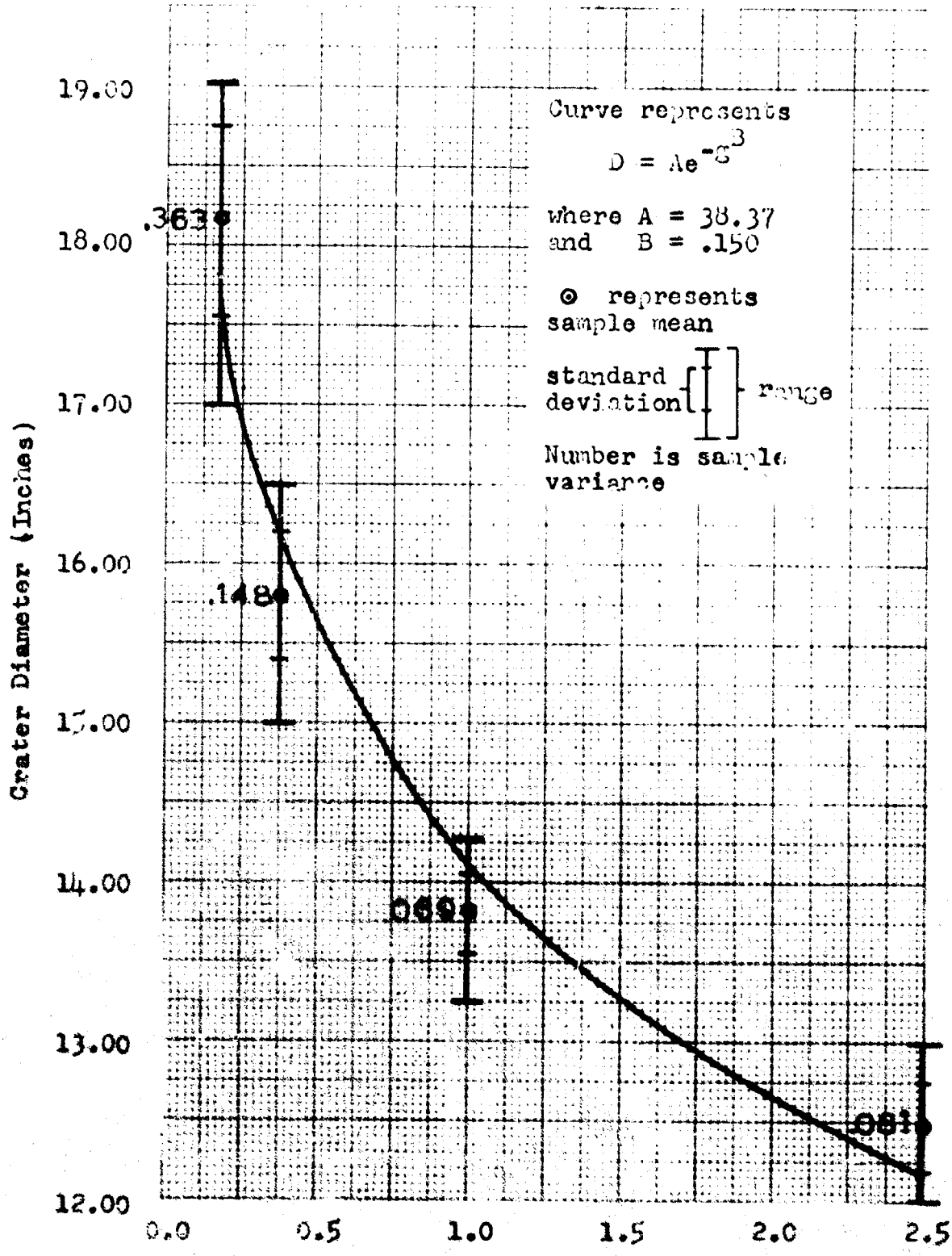

Figure 25

Diameter as a Function of Gravity at 1.5 Inch DOB

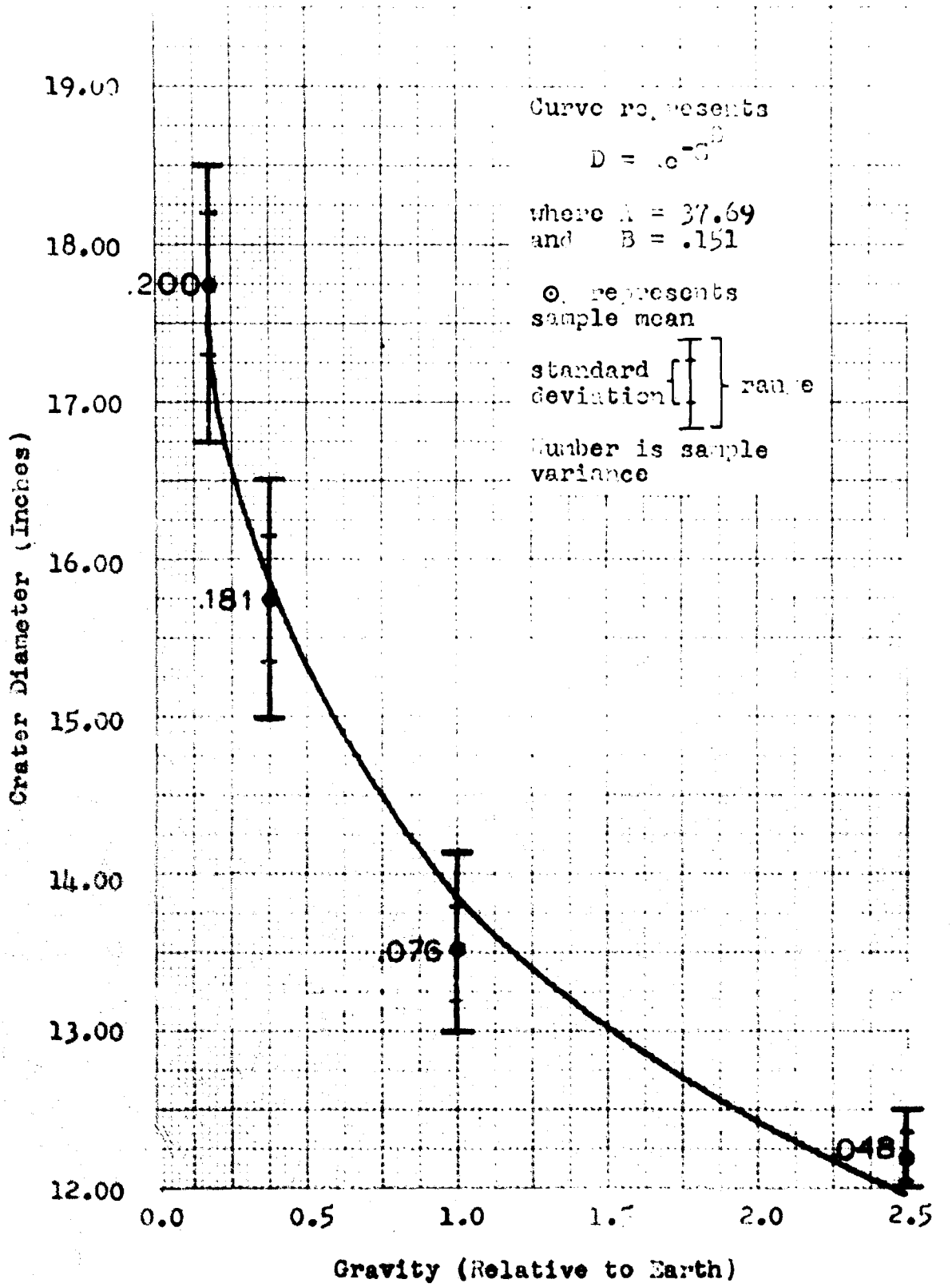

Figure 26

Diameter as a Function of Gravity at 2.0 Inch DOB

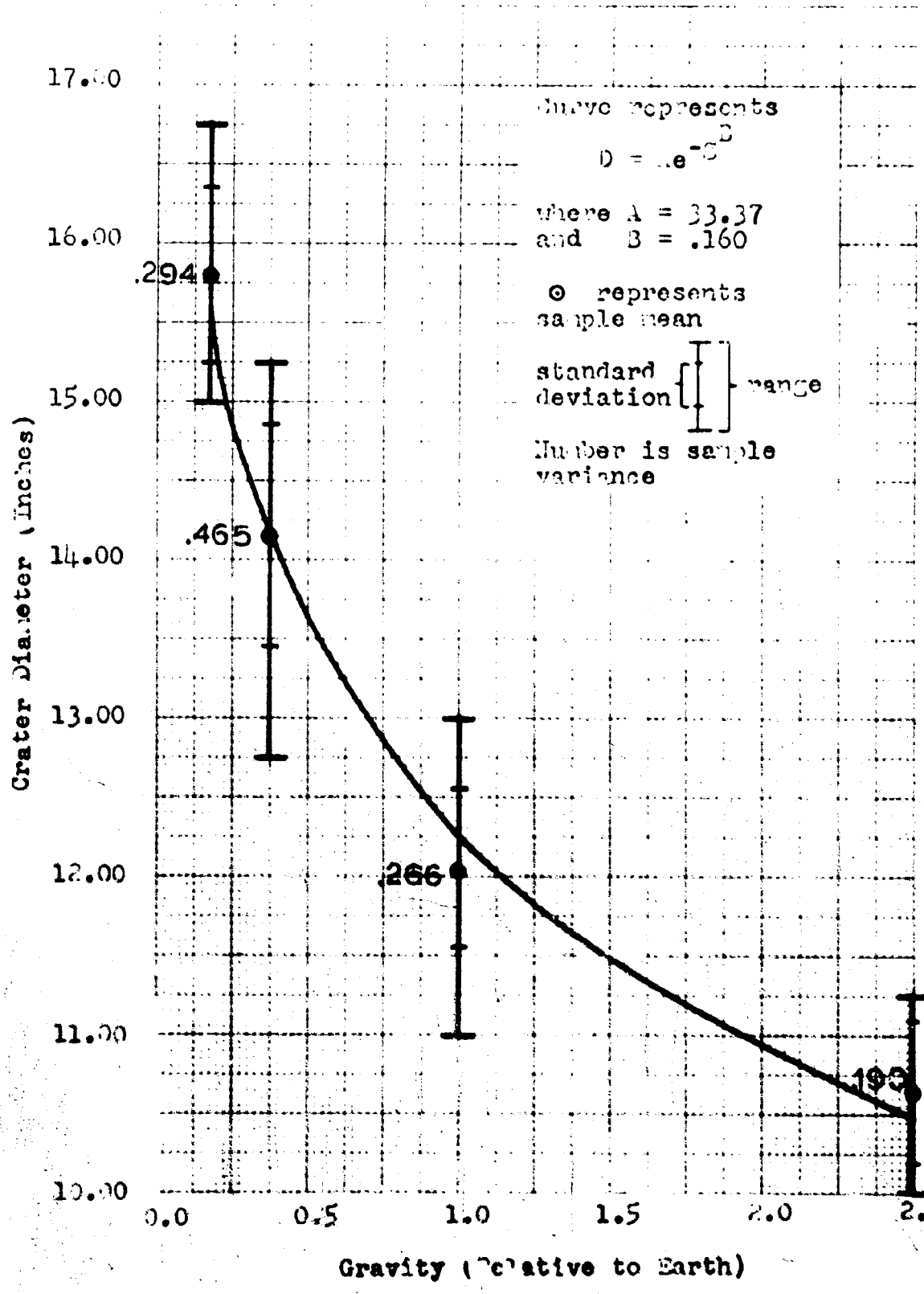

Figure 27

Diameter as a Function of Gravity at 3.0 Inch DOB

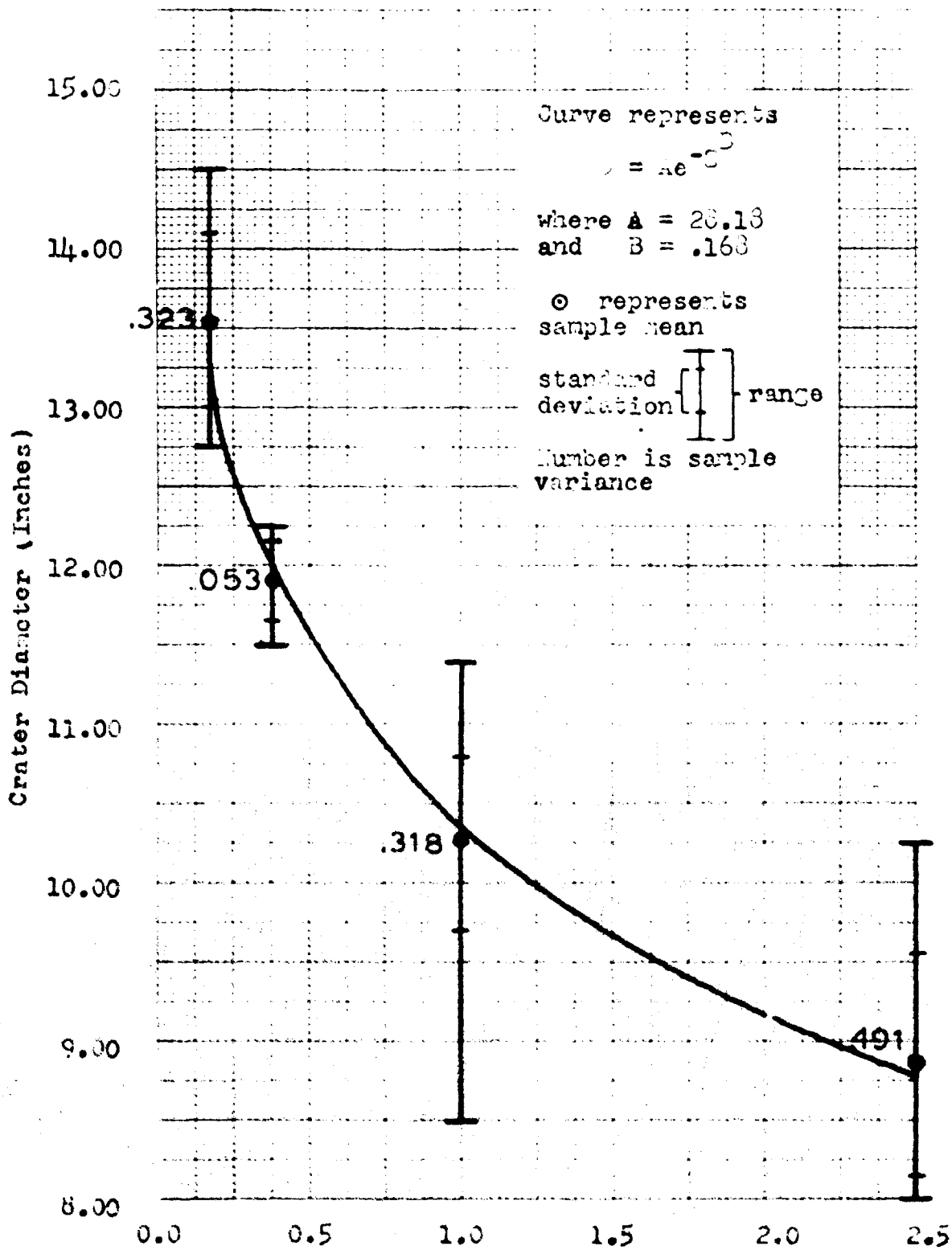

Figure

Diameter as a Function of Gravity at 4.0 Inch DOB

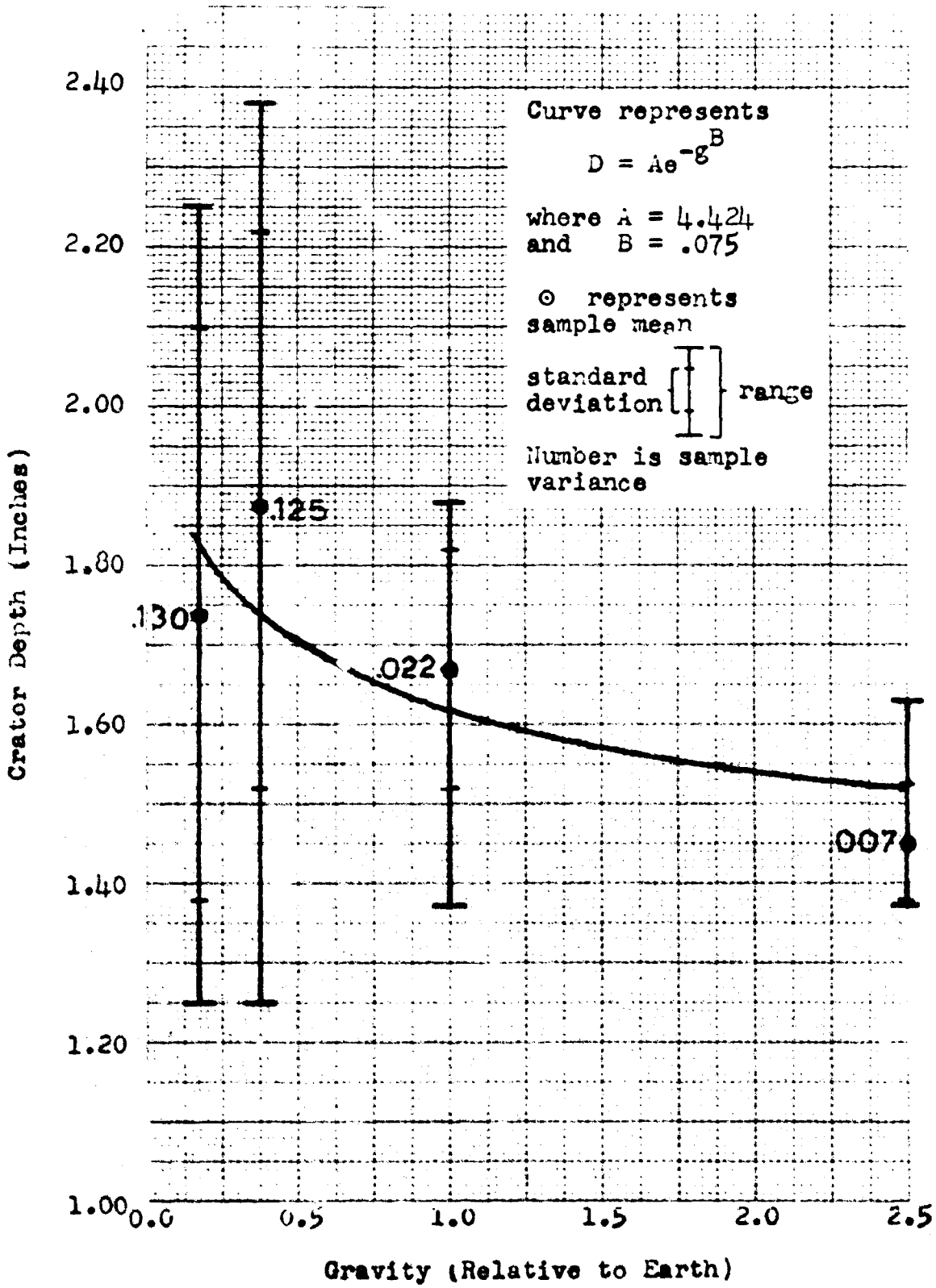

Figure 29

Depth as a Function of Gravity at 0.0 Inch DOB

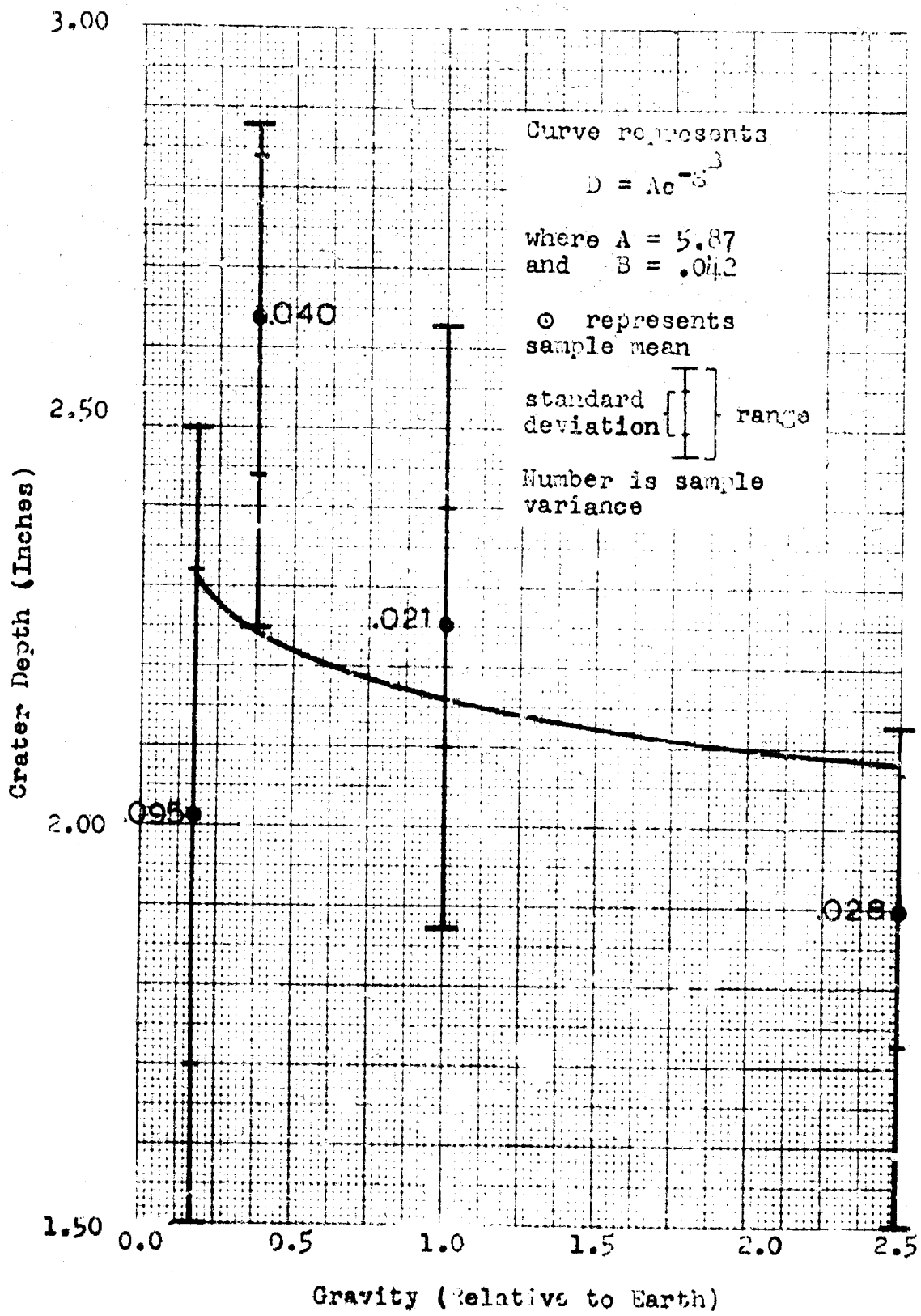

Figure 30

Depth as a Function of Gravity at 0.5 Inch DOB

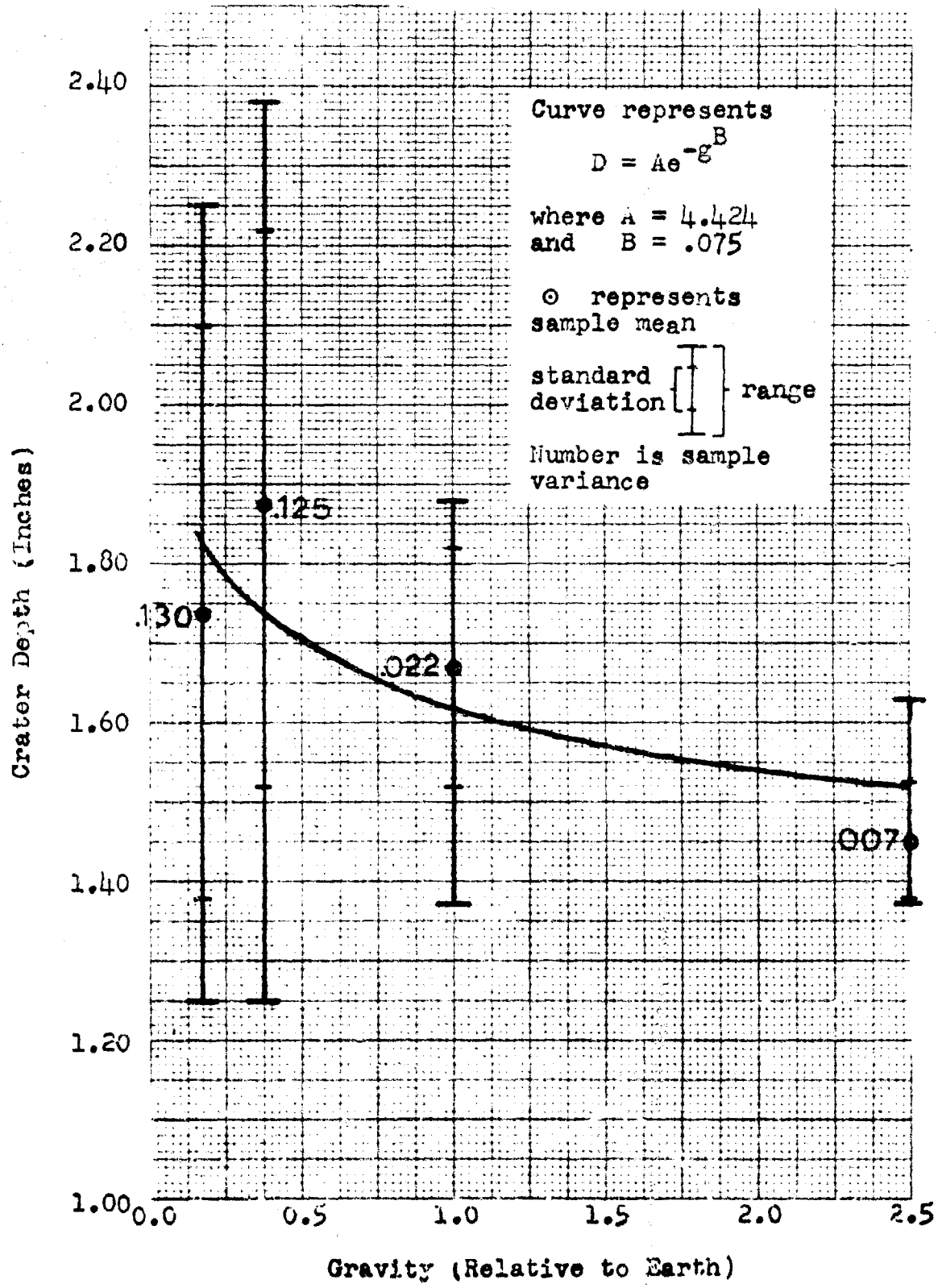

Figure 29

Depth as a Function of Gravity at 0.0 Inch DOB

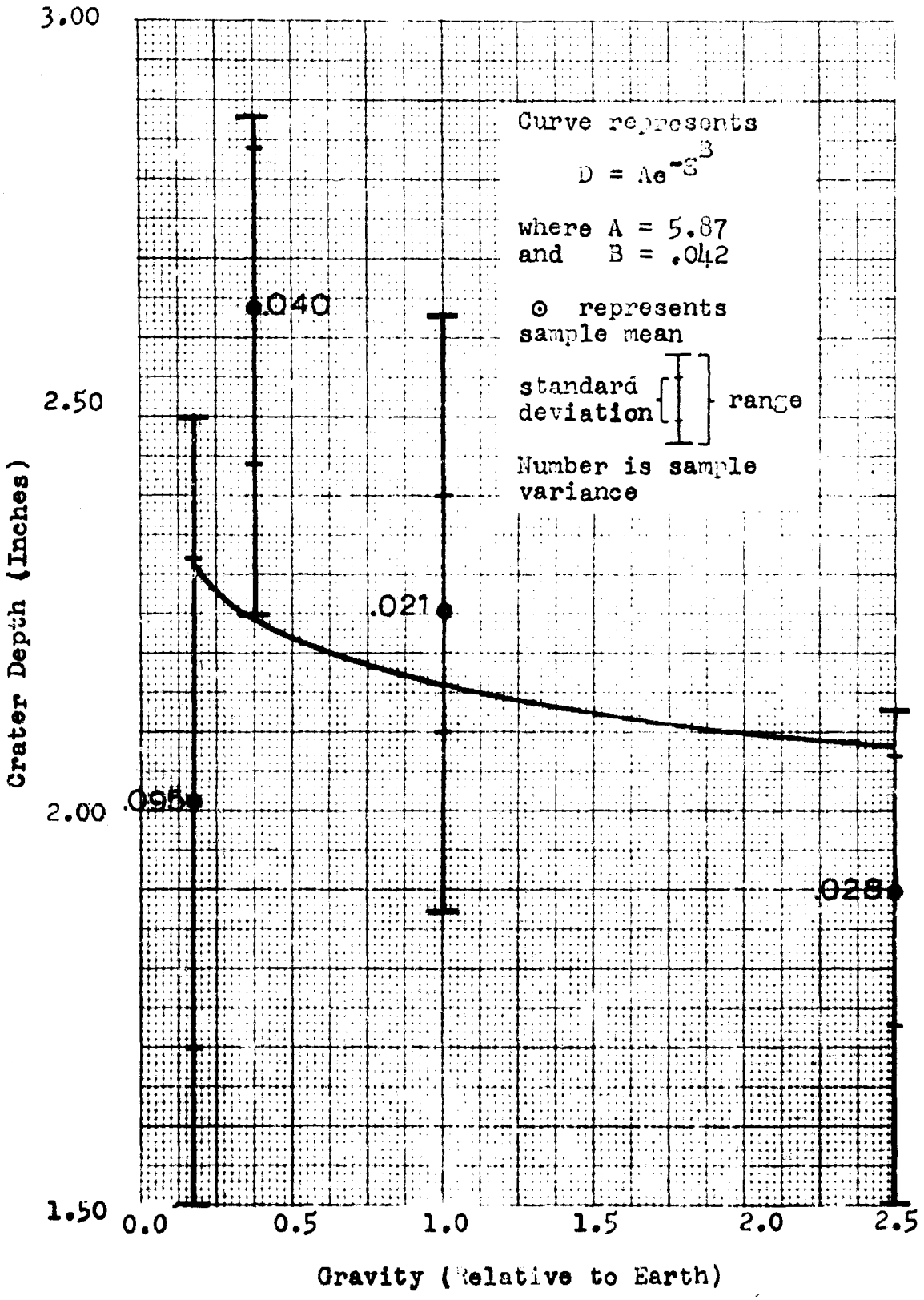

Figure 30

Depth as a Function of Gravity at 0.5 Inch DOB

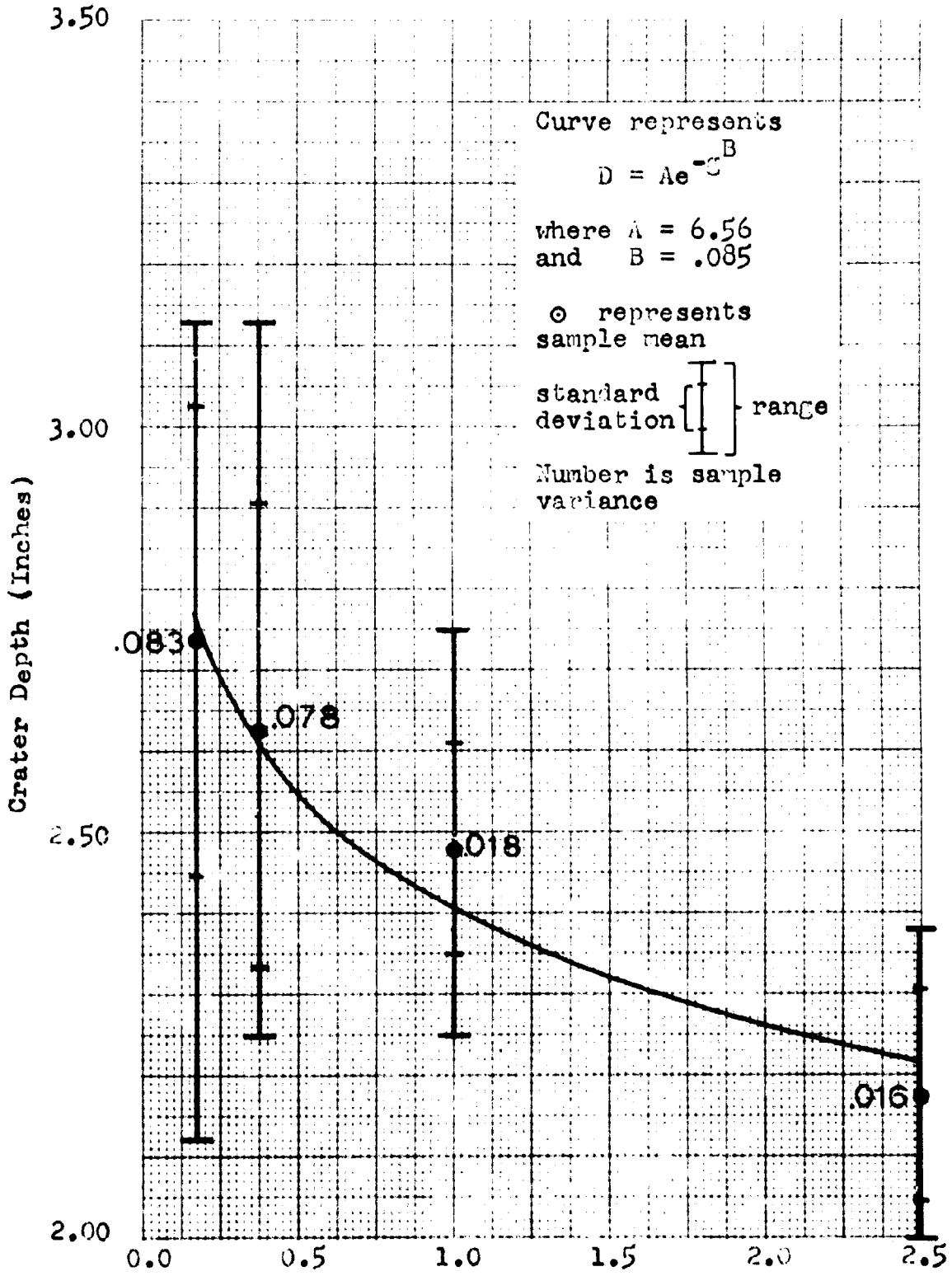

Figure 31

Depth as a Function of Gravity at 1.0 Inch DOB

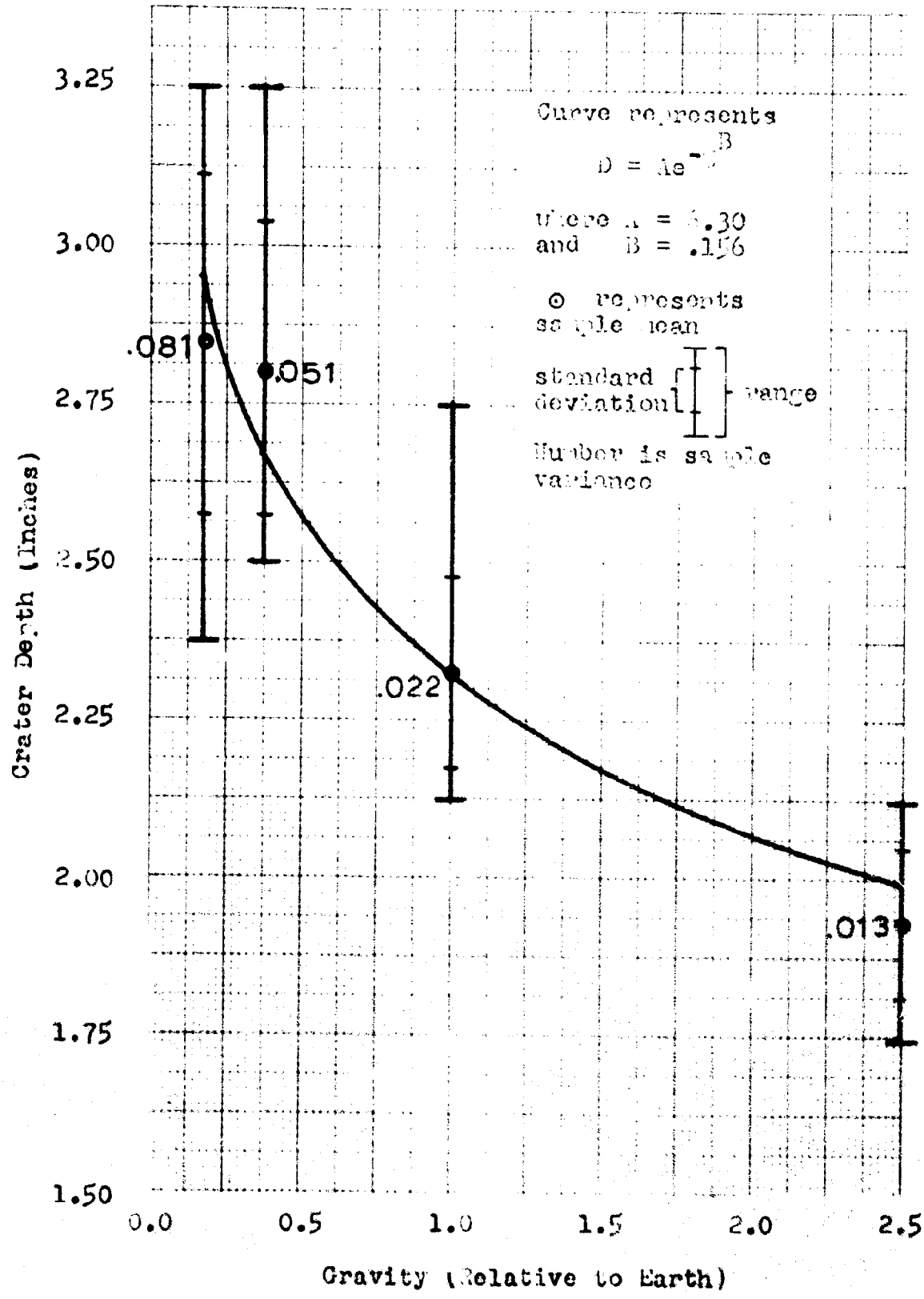

Figure 32

Depth as a Function of Gravity at 1.5 Inch DOB

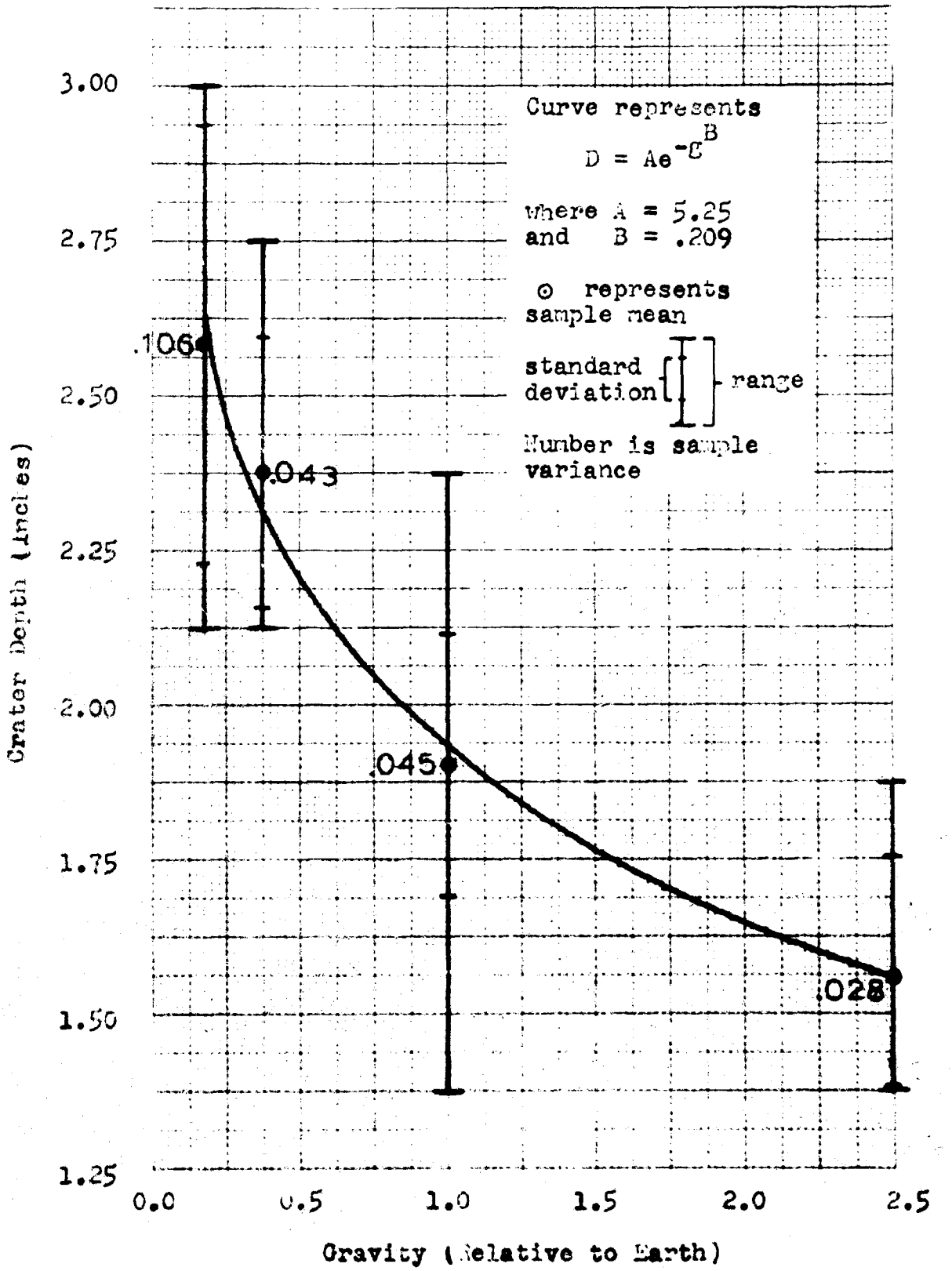

Figure 33

Depth as a Function of Gravity at 2.0 Inch DOB

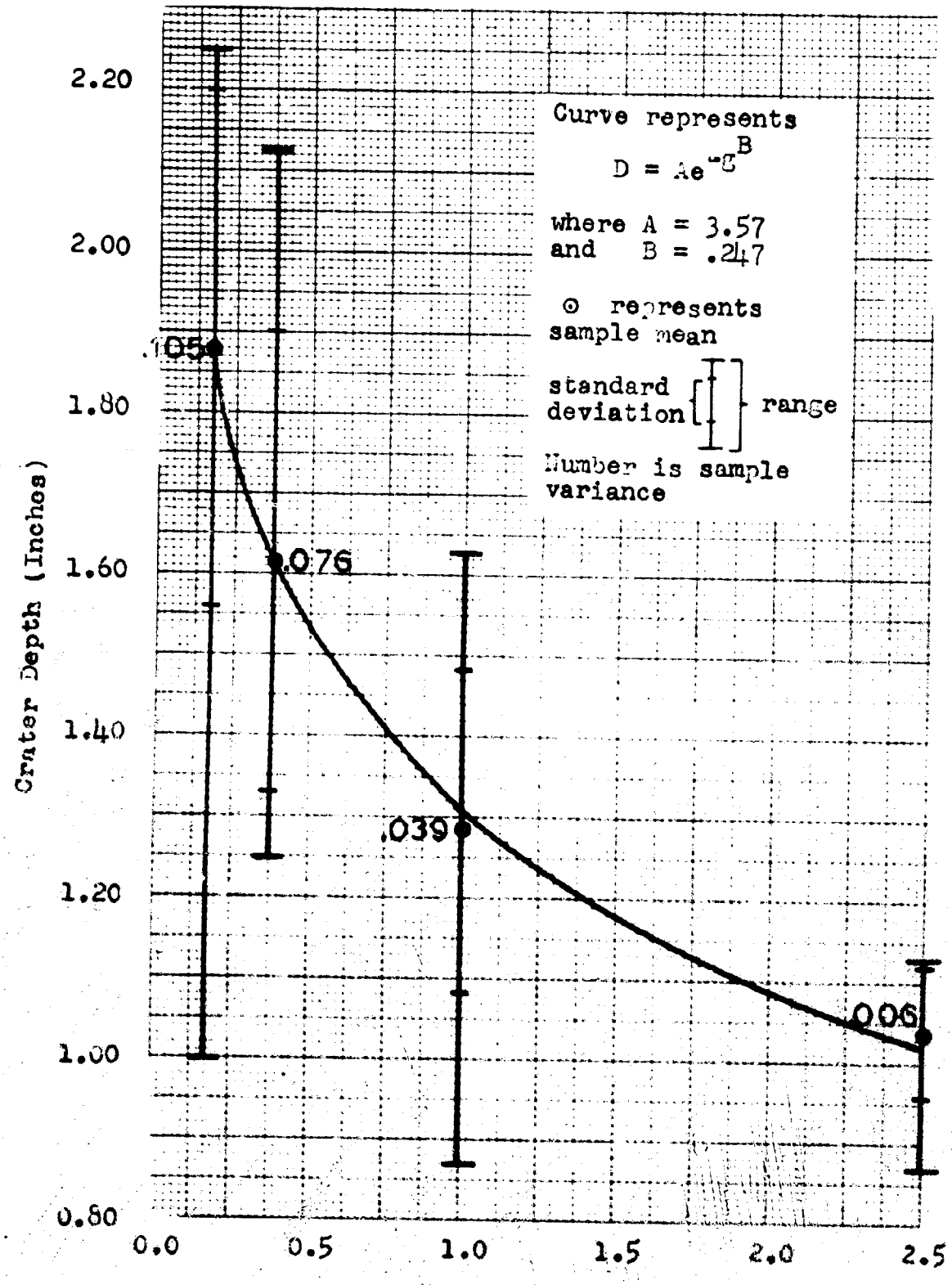

Figure 34

Depth as a Function of Gravity at 3.0 Inch DOB

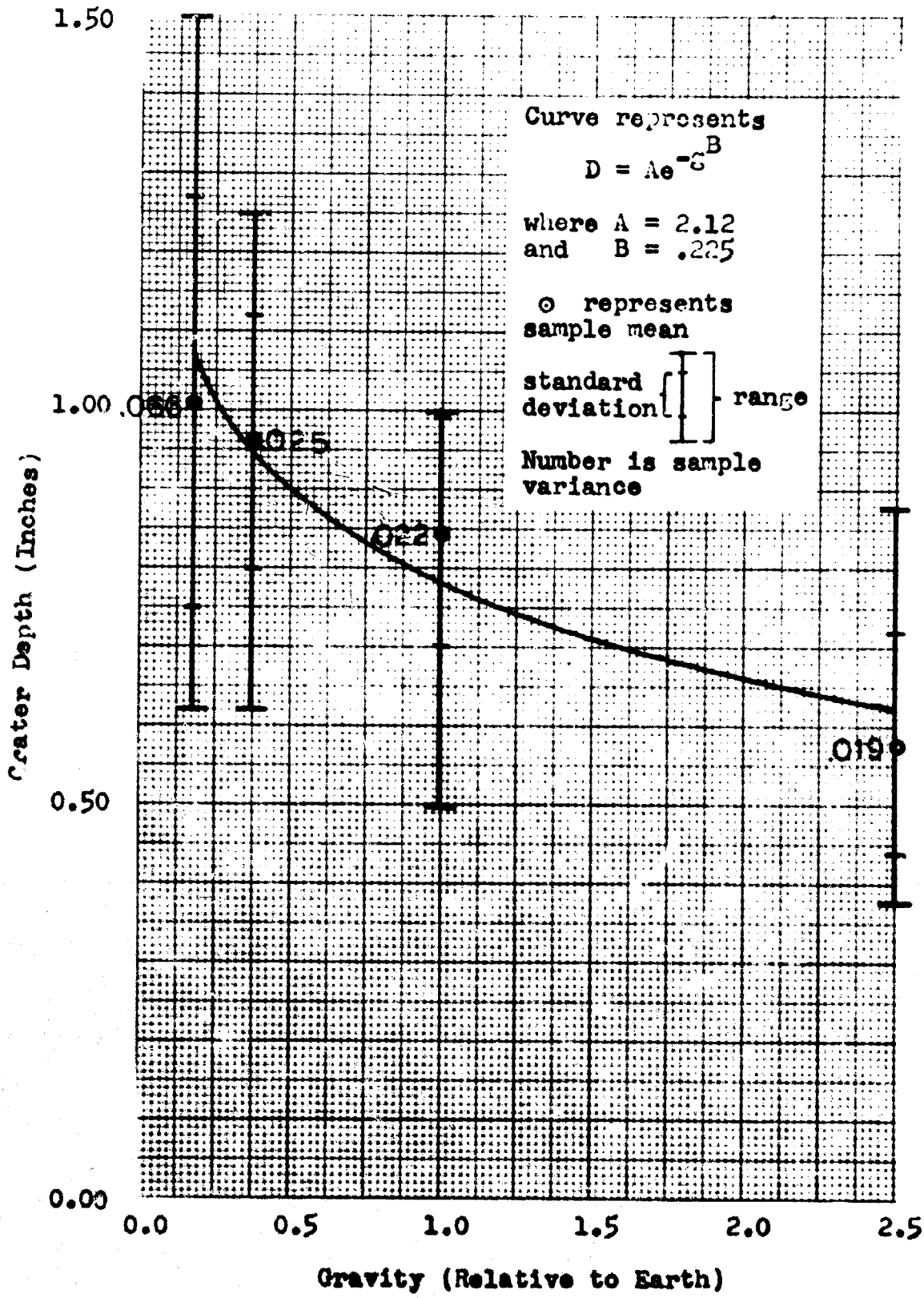

Figure 35

Depth as a Function of Gravity at 4.0 Inch DOB

TABLE I

VALUES OF A AND B AS A FUNCTION OF
DEPTH OF BURST AND CRATER DIMENSIONS

DOB in inches	B	A	Least-Squares Deviation *
		Diameter	
0.0	0.116	24.4529	0.1581
0.5	0.121	32.8782	2.0721
1.0	0.144	36.9874	0.0844
1.5	0.150	38.3664	0.4196
2.0	0.151	37.6850	0.2413
3.0	0.160	33.3658	0.0924
4.0	0.168	28.1812	0.0582
		Depth	
0.0	0.075	4.4240	0.0339
0.5	0.042	5.8720	0.2882
1.0	0.085	6.5554	0.0087
1.5	0.156	6.3021	0.0309
2.0	0.209	5.2473	0.0074
3.0	0.247	3.5691	0.0014
4.0	0.225	2.1196	0.0075

* The deviation is the value of the sum of the squares of the differences between the set of data points for the dimensions at a given DOB and the assumed exponential curve, $D = Ae^{-gB}$.

The magnitude of the deviation from a perfect fit is the determining factor in the least-squares technique. Table I and the graphs show that all the deviations are less than 1.0 except at 0.5 inches DOB for crater diameters. The dependence of effective yields on gravity causes this large deviation. In addition values of B change with depth of burst. These trends are illustrated in Figs. 36 and 37, which are consolidations of the plots of Eq. (10). In these figures, the value of B is reflected in the slopes of the curves.

The range of B is small for diameters when compared to the range of B for crater depths. This is expected because only compaction and scouring cause incremental changes in the diameter when gravity is varied. The B values slowly increase as the DOB increases from 0.0 to 4.0 inches. The increase means that the relative importance of compaction and scouring due to changes in gravity increases with increasing DOB.

The larger range of B for depths than for diameters may be explained by the hypothesis that all cratering processes cause changes in the depth of a crater when gravity is varied. The relatively low values of B at 0.0, 0.5, and 1.0 inch DOB are caused by the low angle of ejection and high initial velocities of the ejected particles which throw them clear of the crater regardless of the value of gravity. At depths of burst less than 1.0 inches, the change in depth is determined mostly by compaction. The particularly low value of B at 0.5 inch DOB reflects the influence of gravity on the effective yield of the explosive. The increase in the fallback with increasing DOB is evidenced by larger values of B at 1.5, 2.0, and 3.0 inch DOB. The

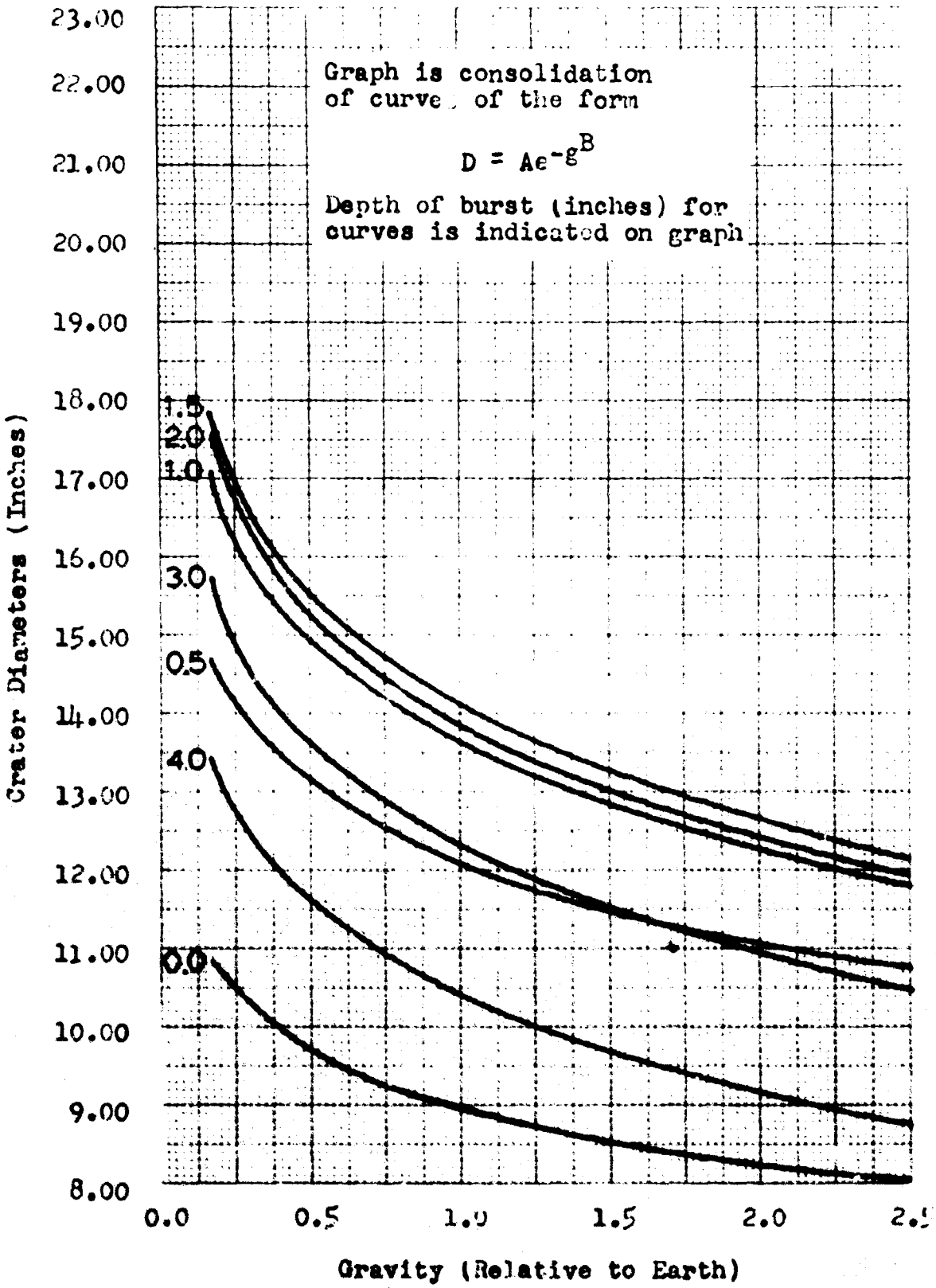

Figure 36

Crater Diameters as a Function of Gravity with Depth of Burst as a Parameter

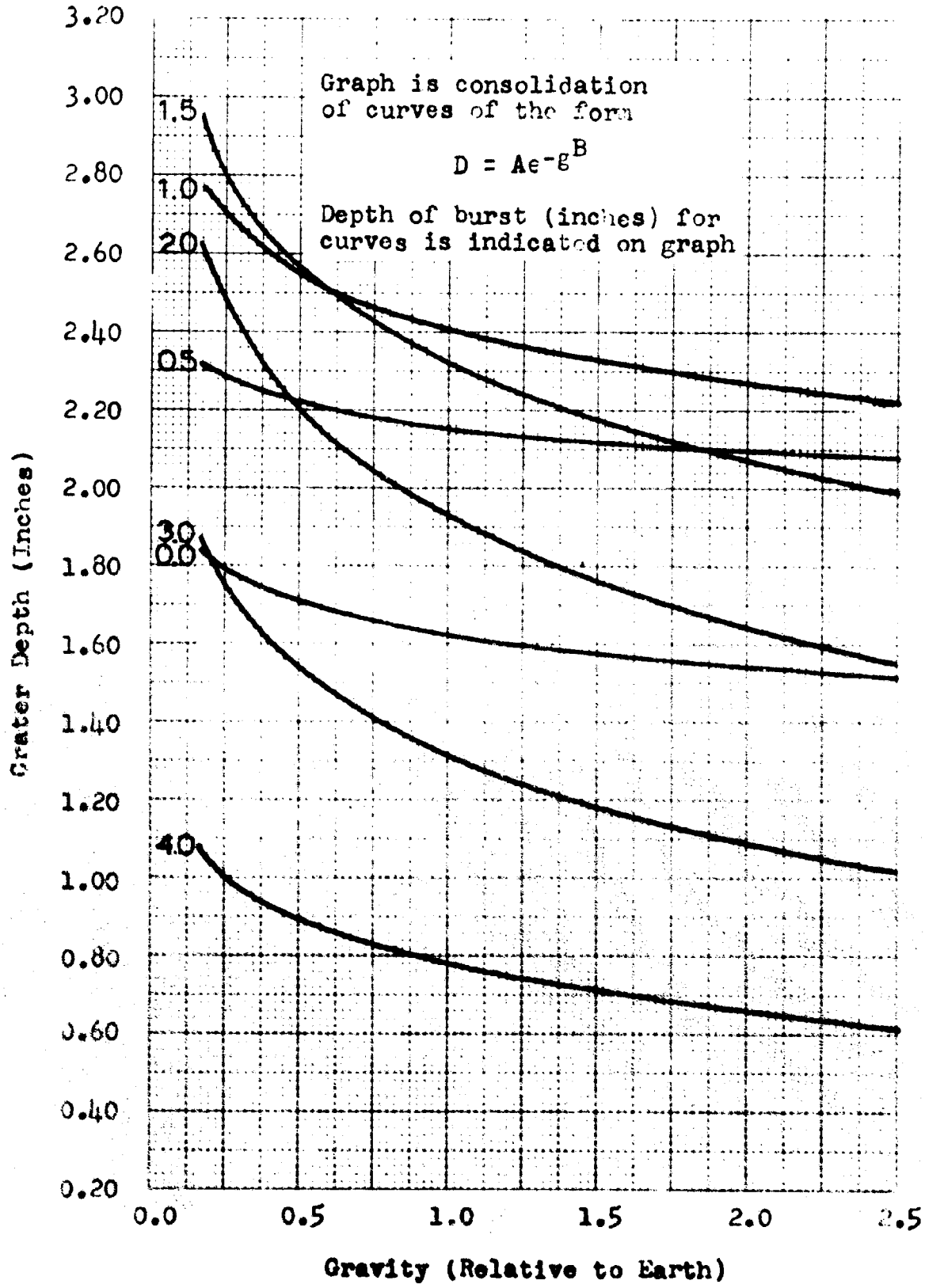

Figure 37

Crater Depths as a Function of Gravity
with Depth of Burst as a Parameter

large increase in B with greater depths of burst tends to support the hypothesis that the gas acceleration process is more influenced by gravity changes than the other processes when depths are considered. This hypothesis was put forth as an explanation for the shift in the optimum DOB for depths. The B values reach a maximum and decrease in the vicinity of 3.0 inch DOB. This decrease occurs because the angle of ejection of particles at depths of burst greater than 3.0 inches become so nearly vertical that the effect of gravity on particle ranges is reduced.

It should be emphasized here that the exponential expression which was chosen to represent crater dimensions as a function of gravity may not be the correct expression since a complete theoretical analysis was not developed which proves the validity of this relationship. However, this exponential expression approximates the data well enough to determine that the sensitivity of crater dimensions to changes in gravity is a function of the DOB.

V. Conclusions and Recommendations

Conclusions

The main points to be made from this experiment are:

1. Crater parameters which vary inversely with gravity are:

   a. crater depths and diameters

   b. optimum depth of burst for crater depths

   c. maximum depth of burst for which a visible crater is formed.

2. The optimum depth of burst for crater diameters is not a function of gravity.

3. The sensitivity of changes in crater dimensions to changes in gravity is a function of the depth of burst.

Recommendations

The following topics in the field of cratering in varied gravity are recommended for further study:

1. Use of an explosive with a higher detonating velocity to compare results from a deflagrating explosive.

2. High speed analysis of the cratering process to include calculations of throwout patterns.

3. Cratering in different mediums.

4. Measurement of crater volumes.

5. Quantitative theoretical study of cratering in varied gravity fields based on the discussion developed in this paper.

Bibliography

1. AFSWC TDR-63-47. Experimental Study of the Effect of Material Properties on Coupling of Explosion Energy. Kirtland AFB, New Mexico: Air Force Special Weapons Center, May 1963.

2. Anderson, E. E., et al. Project Buckboard. Final Report, SC-4675 (RR). Albuquerque, New Mexico: Sandia Corporation, August 1962.

3. ASTFP FTP 63-47. Flight Test Plan C-131B and KC-135 Zero "g" Studies. Wright-Patterson AFB, Ohio: Aeronautical Systems Division, December 1963.

4. Baldwin, R. B. Measure of the Moon. Chicago: The University of Chicago Press, 1963.

5. Bass, R. C., Hawk, H. L. and A. J. Chabai. Hugoniot Data for Some Geologic Materials. SC-4903 (RR). Albuquerque, New Mexico: Sandia Corporation, June 1963.

6. Bishop, R. J., et al. Project Stagecoach, 20-ton HE Cratering Experiments in Desert Alluvium, Final Report. SC-4596 (RR). Albuquerque, New Mexico: Sandia Corporation, May 1962.

7. Bjork, R. L. and H. L. Brode. Cratering From a Megaton Surface Burst. RM-2600. Washington: U. S. Air Force, June 1960.

8. Brownlee, K. A. Statistical Theory and Methodology in Science and Engineering. New York: John Wiley and Sons, Inc., 1960.

9. Chadwick, P., Cox, A. D. and H. G. Hopkins. Mechanics of Deep Underground Explosions. R.A.R.D.E. Report (b) 8/62. Fort Halstead, Kent, Great Britain: Royal Armament Research and Development Establishment, October 1962.

10. Circeo, L. J. Engineering Properties and Applications of Nuclear Excavations. Livermore, California: University of California Lawrence Radiation Laboratory, February 1964.

11. Cook, M. A. The Science of High Explosives. New York: Reinhold Publishing Corporation, 1958.

12. Cole, R. H. Underwater Explosions. Princeton, New Jersey: Princeton University Press, 1948.

13. Courant, R. and K. O. Friedrichs. Supersonic Flow and Shock Waves. New York: Interscience Publishers, Inc., 1948.

Bibliography (Contd)

14. Cramer, E. H. Technical Representative, E. I. duPont, Inc. Pompton Lakes, New Jersey. Personal Communication, June 1965.

15. Cushing, V., Losaw, W. and D. Reily. Characteristic Emissions From an Underground Explosion. DASA-1484. Rockville, Maryland: Engineering-Physics Company, February 1964.

16. Department of the Army. Operation Jangle. Underground Explosion Theory. Washington: Armed Forces Special Weapons Project, April 1962.

17. Department of Ordnance, United States Military Academy. Elements of Armament Engineering. West Point, New York: U.S.M.A., 1958.

18. Doll, E. B. and V. Salmon. Scaled HE Tests-Operation Jangle. Final Report. Project 1(9)-1. Melno, California: Stanford Research Institute, December 1952.

19. DuBosar, A. Professor of Civil Engineering. University of Dayton, Dayton, Ohio. Personal Communication, March, 1965.

20. Freund, J. E. Mathematical Statistics. Englewood Cliffs, New Jersey: Prentice-Hall, Inc., 1963.

21. Green, J. The Geology of the Lunar Base. SID 61-358, Revised. Downey, California: North American Aviation, May 1962.

22. Gudzent, D. "The Propagation of Shock Waves Induces by Underground Explosions", in Dynamic Behavior of Materials and Structures. Durham, North Carolina: U.S. Army Research Office, September 1962.

23. Halajian, J. D. "Gravity Effects on Soil Behavior", in The Lunar Surface Layer, Edited by J. W. Salisbury and P. E. Glaser. New York: Academic Press, 1964, pp. 67-91.

24. Hendron, A. J. and J. N. Strange. Method for Predicting the Shape of Explosion-Produced Craters. Misc Paper No. 1-667. Vicksburg, Mississippi: USA Engineer Waterways Experiment Station, October 1964.

25. Hess, W. N. and M. D. Nordyke. "Throwout Calculations for Explosive Craters". Journal of Geophysical Research, 66: 3405-3412 (October 1961).

Bibliography (Contd)

26. Johnson, G. P. and R. J. Talbot. A Theoretical Study of the Shock Wave Origin of Shatter Cones. Master's Thesis. Wright-Patterson AFB, Ohio: Air Force Institute of Technology, 1964.

27. Johnson, S. W. Criteria for the Design of Structures for a Permanent Lunar Base. Doctor's Thesis. Urbana, Illinois: University of Illinois, 1964.

28. Kennedy, N. D. "Explosions and Explosives in Air", in Effects of Impact and Explosion. Vol I. Summary Technical Report of Division 2, NDRC. Washington: Office of Scientific Research and Development, 1946, pp. 64-109.

29. Kinney, G. F. Explosive Shocks in Air. New York: MacMillian Company, 1962.

30. Kisslinger, C. The Generation of the Primary Seismic Signal by a Contained Explosive. 4410-48-X. Ann Arbor, Michigan: University of Michigan, 1963.

31. Lambe, W. T. Soil Testing for Engineers. New York: John Wiley and Sons, Inc., 1964.

32. Lampson, C. W. "Explosions in Earth", in Effects of Impact and Explosion. Vol I. Summary Technical Report of Division 2, NDRC. Washington: Office of Scientific Research and Development, 1946, pp. 110-132.

33. Langhaar, H. L. Dimensional Analysis and Theory of Models. New York: John Wiley and Sons, Inc., 1951.

34. Langseth, M., Perkins, B. and W. Townsend. Mechanics of Crater Formation in Sand and Clay Produced by Underground Explosions. BRL Memo Report 1381. Aberdeen Proving Grounds, Maryland: Ballistic Research Laboratories, December 1961.

35. Lawrence, F. V. The Response of Soils to Dynamic Loadings. Research Report R63-8. Boston: MIT Department of Civil Engineering, March 1963.

36. Lockheed Missiles and Space Company. Study of Deployment Procedures for Lunar Exploration Systems for Apollo (LESA). Final Report, Volume II. Sunnyvale, California: Lockheed Missiles and Space Company, February 1965.

Bibliography (Contd)

37. Lyakov, G. M. and G. I. Polrovsky. Underground Explosion Waves. FTD-TT 63-724 (Translation). Wright-Patterson AFB, Ohio: Foreign Technology Division, February 1964.

38. Maenchen, G. and J. Nuckolls. "Calculations of Underground Explosions". Proceedings of the Geophysical Laboratory-Lawrence Radiation Laboratory Cratering Symposium. Livermore, California: University of California Lawrence Radiation Laboratory, March 1961.

39. Markov, A. V. The Moon. Chicago: University of Chicago Press, 1962.

40. Martin, D. L. and W. J. Hinze. Energy Partition of Underground Explosions. AFSWP-789. Fort Belvoir, Virginia: U. S. Army Research and Development Laboratories, March 1958.

41. Murphy, B. F. and L. F. Vortman. "High Explosive Craters in Desert Alluvium, Tuff, and Basalt". Journal of Geophysical Research, 66: 3389-3404 (October 1961).

42. Nordyke, M. D. "Nuclear Craters and Preliminary Theory of the Mechanics of Explosive Crater Formation". Journal of Geophysical Research, 66: 3439-3459 (October 1961).

43. Ottawa Silica Company. The Silica Sands of Ottawa. Ottawa, Illinois: Ottawa Silica Company, 1960.

44. Plowshare Series: Part II. Excavation. Proceedings of the Second Plowshare Symposium. UCRL-5676. Livermore, California: University of California Lawrence Radiation Laboratory, May 1959.

45. Rinehart, J. S. "The Role of Stress Waves in the Comminution of Brittle, Rocklike Materials", in International Symposium on Stress Wave Propagation in Materials, Edited by Norman Davids. London: Interscience Publishers, Ltd., 1960, pp. 247-269.

46. Sachs, D. C. and L. M. Swift. Small Explosion Tests, Project Mole. Vol I, Final Report AFSWP-291. Melno, California: Stanford Research Institute, December 1955.

47. Sauer, F. M. Nuclear Geoplosics. Part One-Theory of Directly-Induced Ground Motion. DASA-1285 (I). Menlo Park, California: Stanford Research Institute, May 1964.

Bibliography (Contd)

48. - - - - - - -. Nuclear Geoplosics. Part Two-Mechanical Properties of Earth Materials. DASA-1285 (II). Menlo Park, California: Stanford Research Institute, May 1964.

49. - - - - - - -. Nuclear Geoplosics. Part Four-Empirical Analysis of Ground Motion and Cratering. DASA (IV). Menlo Park, California: Stanford Research Institute, May 1964.

50. Spangler, M. G. Soil Engineering. Scranton, Pennsylvania: International Textbook Company, 1963.

51. Stromer, P. R. Shock Wave Propagation in Solids: An Annotated Bibliography. Special Bibliography SB 63-31. Sunnyvale, California: Lockheed Missiles and Space Company, March 1963.

52. Taylor, D. W. and R. V. Whitman. The Behavior of Soils Under Dynamic Loadings. AFSWP-117. Boston: Massachusetts Institute of Technology, July 1953.

53. Terzaghi, K. and R. B. Peck. Soil Mechanics in Engineering Practice. New York: John Wiley and Sons, Inc., 1948.

54. Thompson, A. A. A Comparison of the Dynamic and the Static Stress-Strain Curve of Sand Under Confined and Unconfined Conditions. Memorandum Report Number 1262. Aberdeen Proving Ground, Maryland: Ballistic Research Laboratories, April 1960.

55. - - - - - - -. The Comparison of Strain and Kinetic Energy in a Plastic Wave Moving Through Sand. BRL Memo Report No. 1263. Aberdeen Proving Ground, Maryland: Ballistic Research Laboratories, April 1960.

56. TM 5-541. Control of Soils in Military Construction. Washington: Department of the Air Force and Army, September 1954.

57. U. S. Army Corps of Engineers. Craters Formed by Small Explosions in Dry Sand. Miscellaneous Paper No. 2-524. Vicksburg, Mississippi: U. S. Army Engineer Waterway Experiment Station, September, 1962.

58. Vaile, R. B., Jr. "Pacific Craters and Scaling Laws". Journal of Geophysical Research, 66: 3413-3438 (October 1961).

59. Violet, C. E. "A Generalized Empirical Analysis of Cratering". Journal of Geophysical Research, 66: 3461-3470 (October 1961).

Bibliography (Contd)

60. Whitney, D. R. Elements of Mathematical Statistics. New York: Holt, Rinehart and Winston, 1961.

61. Woods, R. D. Preliminary Design of Dynamic-Static Direct Shear Apparatus for Soils and Annotated Bibliographies of Soil Dynamics and Cratering. RTD-TDR-63-3050. Kirtland AFB, New Mexico: Air Force Weapons Laboratory, 1963.

62. Yakovlev, Y. S. The Hydrodynamics of an Explosion. Washington: U. S. Department of Commerce, Office of Technical Services Translation, September 1963.

Appendix A

Details of Experimental Procedure

Equipment and Materials

The equipment and materials required for the experiment were a special aircraft for varying gravity conditions, a cohesionless sand, a container in which the cratering process could take place, a small explosive source, and devices to measure the crater parameters.

The Zero-Gravity Aircraft. The special aircraft, a twin-engined, propeller-driven, Air Force C-131B, was available in the Aeronautical Systems Division at Wright-Patterson Air Force Base, Ohio. Gravity was varied under controlled conditions during the flights. Figure 38 shows the nose of the aircraft and a flight profile which indicates the details of the maneuver performed to vary gravity inside the aircraft. By flying an electronically programmed maneuver similar to that for the zero gravity condition shown in Fig. 38, any value of g up to 1.0 g could be attained for periods up to 15 seconds. Values greater than 1.0 g and up to 2.5 g were achieved by performing tight turns instead of the parabolic maneuver. Details about the aircraft and its flight plan can be found in Reference 3.

The Cratering Medium. Because of its homogeneous qualities compared to other soils, a dry, cohesionless, silica sand was selected as the medium in which to form the craters. Flint Shot Ottawa Sand was the brand picked because of its availability and outstanding characteristics of uniformity and purity. Figure 39 illustrates these

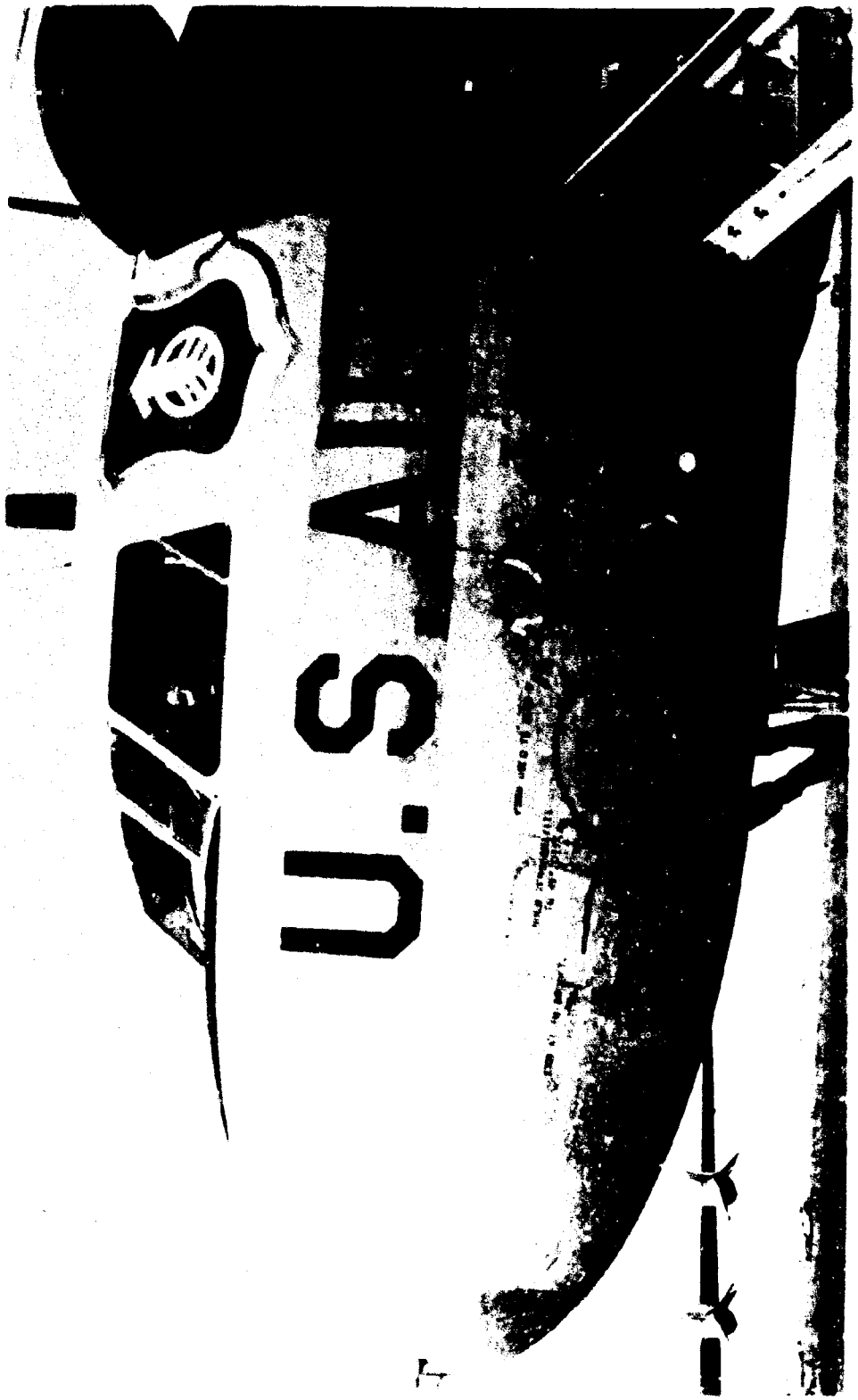

Figure 38

The Zero Gravity Aircraft

Figure 39

Close-Up of Cratering Medium

Scale Division is 1/32 Inches

characteristics by means of a close-up photograph of the sand particles. Based upon a number of soil mechanics tests, it was determined that the sand maintained consistent values of density and moisture content throughout the experiment. A discussion of these tests and their results are described in Appendix B.

The Sand Container. A container was necessary in order to confine the cratering process during the experiment. This was especially important on the aircraft as sand could not be permitted to come in contact with the mechanical and electrical equipment in the aircraft. The box was designed to be large enough so that it would not influence the cratering process and small enough to move it on and off the plane. Considering these criteria, the box was constructed from 3/4-inch plywood with a 4 feet by 4 feet base. The height of the box was 5 feet. One wall of the box was constructed as a door to allow access inside the box. In addition, a plexiglass section was mounted on top to allow observation of the cratering process. Figure 40 is a photograph of the container.

The Small Explosive Source. The dimensions of the sand container were primarily determined by the interior dimensions of the aircraft. This placed an upper limit on the magnitude of the explosive that could be used for the cratering process. An explosion of too great a magnitude would cause particles to rebound from the walls of the container and influence the final crater form by falling back into the crater when they would normally be thrown clear. The possibility of a reflected shock wave from the walls of the container interacting with the normal cratering process also had to be avoided. In addition,

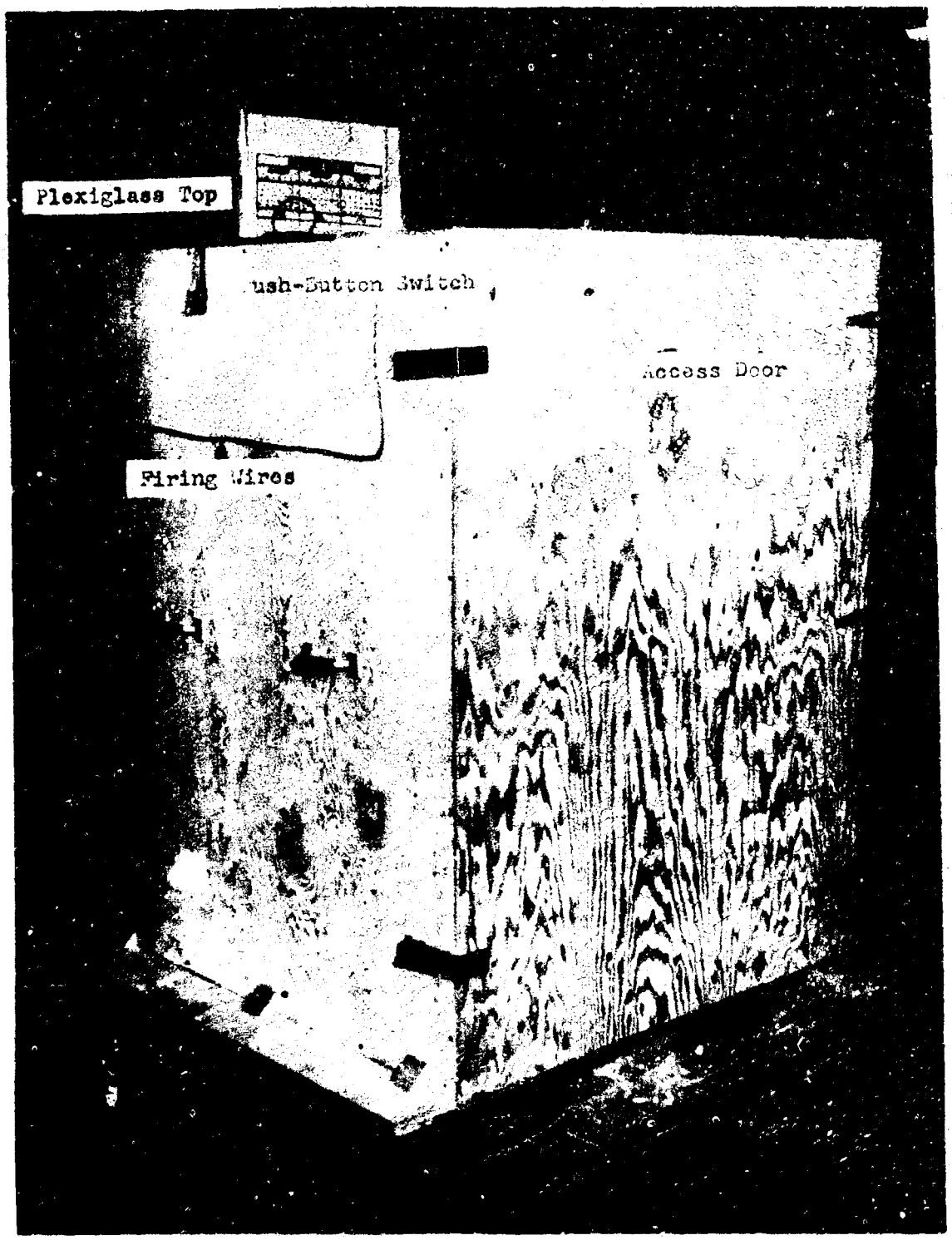

Figure 4C

Sand Container

flight safety demanded a detonation of small magnitude. A 6.0 grain explosive squib was found to be suitable as the explosive device under the described restrictions. The squibs that were used are electrically detonated explosives normally used to actuate release mechanisms such as wing tip tank releases on Air Force aircraft. Figures 41 and 42 show the details of the squib used in the experiment. The load tolerance of the squib is 6.0 ± 0.4 grains of explosive. The duPont 50/25/25 mixture in the squibs does not detonate instantaneously as is the case with an explosive like TNT. Instead, the mixture burns rapidly to produce high pressure levels. This type of mixture is known as a deflagrating compound and is in a different class from TNT. TNT expends its energy with a strong shock wave whereas the duPont 50/25/25 mixture expends its energy through a relatively slow build-up of pressure over a longer period of time than TNT. This results in a weaker shock wave.

Photographic Measurements. Photographic means were used to measure the crater parameters during the experiment. The crater parameters chosen for observation were crater depth and diameter. These dimensions are indicated on Fig. 1. Photography was chosen because aircraft vibrations disturbed craters before manual measurements could be made. This also allowed the maximum number of detonations to be performed during the limited flight time available for the experimental phase. A 16-mm motion picture camera of the BlA type was used with a 13-mm lens and a frame rate of 64 frames per second. The camera was electrically powered with a 28-volt direct current motor. Figure 43 shows the camera as it was mounted on the sand container in a position

DUPONT S-68 SQUIB (X-81)

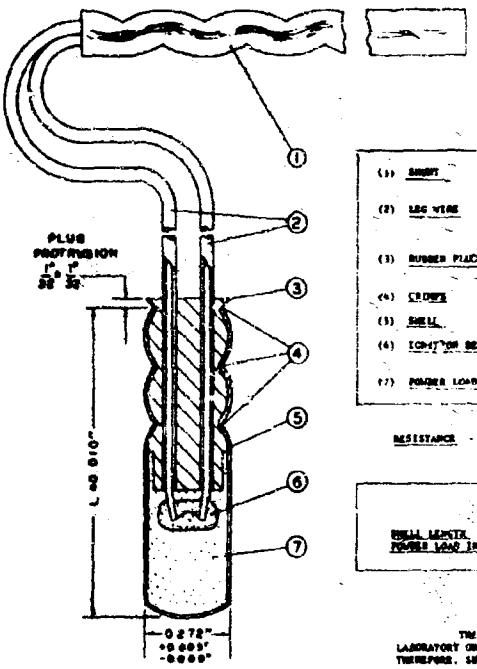

NOTICE

THIS DRAWING AND ACCOMPANYING DATA ARE INTENDED TO BE INFORMATIVE ONLY AND MUST NOT BE MADE THE BASIS FOR ANY SPECIFICATION WHATEVER.

(1)	SHUNT	- CELLOPHANE-LINED ALUMINUM FOIL, APPROXIMATELY 3-1/2 IN. LONG, SOLDERED AROUND BARED ENDS OF LEG WIRES.
(2)	LEG WIRE	- PLASTIC-INSULATED, ONE BLUE AND ONE YELLOW, 22 GAGE TINNED COPPER. CONDUCTOR ENDS BARED FOR A DISTANCE OF 1-7/8 TO 2-1/2 IN. TOLERANCES: 6.0 IN. MINIMUM & FT. +3.0 IN. -0 IN., 6 FT. AND OVER +3.0 IN. -2.0 IN.
(3)	RUBBER PLUG	- MOLDED INTO LEG WIRES, APPROXIMATELY 0.9019 IN. DIAMETER 60/20 NICHEL CHROMIUM BRIDGE WIRE SOLDERED TO BRIDGE POSTS.
(4)	CRIMPS	- THREE CRIMPS COMPLETELY AROUND SHELL.
(5)	SHELL	- COPPER ALLOY O.D. 0.272 IN. COLORED YELLOW - SEE TABLE BELOW FOR SHELL LENGTH.
(6)	IGNITION BEAD	- APPROXIMATELY 0.2 GRAINS OF DU PONT [illegible] A LEAD IGNITION MIXTURE LECHERED TO BRIDGE WIRE WITH RUBBER.
(7)	POWDER LOAD	DU PONT [illegible] 50/25/25 IGNITION MIXTURE. SEE TABLE BELOW FOR LOAD WEIGHT

RESISTANCE - THE RESISTANCE OF THIS SQUIB IS 1.37 OHMS ± 0.30 OHM PLUS 0.032 OHM FOR EACH DOUBLE FOOT OF LEG WIRE

	NOMINAL LOAD IN GRAINS							
	2	3	4	6	8	10	12	15
SHELL LENGTH	23/32	27/32	15/16	1-3/32	1-3/16	1-5/16	1-7/16	1-3/8
POWDER LOAD IN GRAINS	2.2	3.0	4	6	8	10	12	15

PERFORMANCE CHARACTERISTICS

THE PROPERTIES GIVEN BELOW ARE BASED ON BACKGROUND INFORMATION OR WERE DETERMINED IN THE LABORATORY ON INITIAL LOTS OF THE SQUIB. THE DATA MAY VARY WITH MORE EXHAUSTIVE TESTS AND ARE, THEREFORE, SUBJECT TO CHANGE.

GENERAL - THIS SQUIB WAS DEVELOPED IN 1949 TO REPLACE THE S-59 SQUIB FOR LOW-PRESSURE APPLICATIONS IN EXPLOSIVE RELEASE MECHANISMS. IT IS ALSO AN EXCELLENT AND FAST IGNITER FOR BLACK POWDER OR SIMILAR MATERIAL WHEN THE SQUIB AND MATERIAL BEING IGNITED ARE WELL CONFINED. IN THE OPEN, A LARGE PORTION OF THE CHARGE MAY SLATTER WITHOUT IGNITING, BUT UNDER LIGHT CONFINEMENT THE CHARGE BURNS COMPLETELY AND VIOLENTLY.

MINIMUM FIRING CURRENT - 0.30 AMP., AVERAGE (MAY VARY ± 10%). DID NOT FIRE WITH 0.30 AMP. APPLIED 5 MINUTES.

FIRING TIME - FIVE SQUIBS WERE TIMED, ON ELECTRONIC COUNTER, FOR EACH CONDITION. SEE GRAPH BELOW FOR FIRING TIMES AT 80°F IN AIR.

FIRING CURRENT AMP. (DC)	TEMPERATURE °F	FIRING TIME, MSEC.
1.5	160°F.	6.2
1.5	-107°F.	8.3
5.0	160°F.	2.0
5.0	-107°F.	2.7

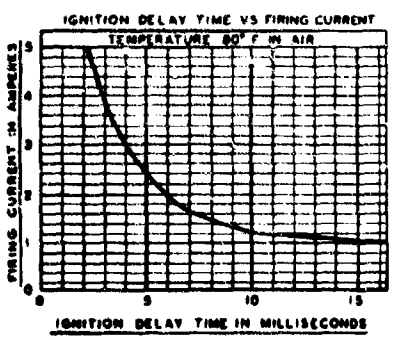

STATIC SUSCEPTIBILITY - MAXIMUM ENERGY BY CONDENSER DISCHARGE FOR IGNITION PROBABILITY OF ZERO. 0.090 JOULE.

WATER RESISTANCE - FUNCTIONED SATISFACTORILY AFTER 24 HOURS AT 70 PSI

HEAT RESISTANCE - FUNCTIONED SATISFACTORILY AFTER 6 HR. STORAGE AT 115°F.
4 HR. STORAGE AT 300°F.
1 YR. STORAGE AT 160°F.
2 YR. STORAGE AT 130°F.
WITHSTOOD THE DOUBLE JAN TEMPERATURE AND HUMIDITY CYCLE (MIL-STD 304) WITHOUT CHANGE.

LOW TEMPERATURE PERFORMANCE - NORMAL AT -65°F.

LOW PRESSURE PERFORMANCE - FUNCTIONED SATISFACTORILY AT A PRESSURE OF 1 MM. HG.

RESISTANCE TO AMMONIA - PERFORMANCE WAS UNAFFECTED BY 72 DAYS' EXPOSURE TO AMMONIA GAS AT 10 PSI GAGE, BUT SHELL WAS BADLY CORRODED.

Figure 41

Specifications and Schematic Drawing of Squib

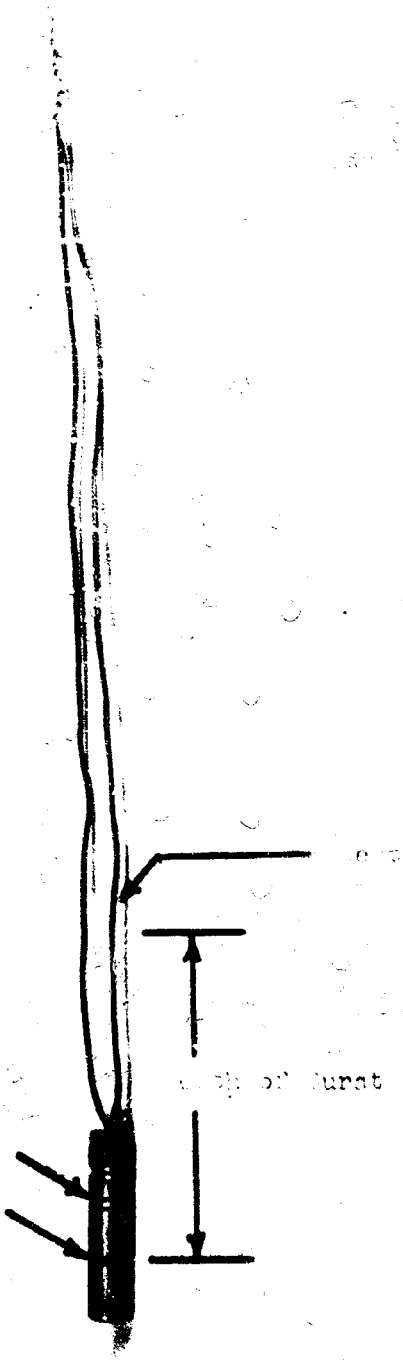

Figure 42

Close-Up of Squib

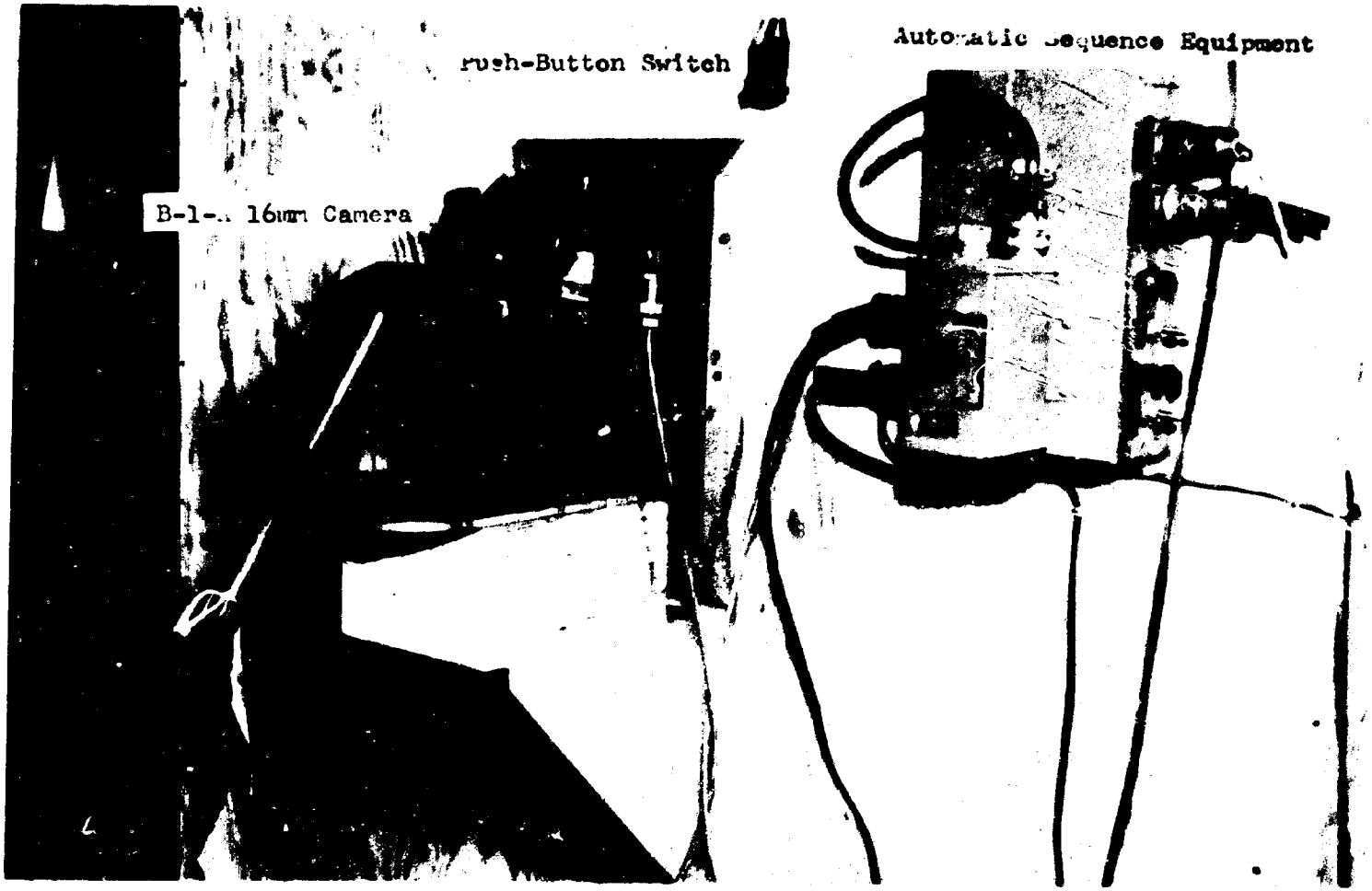

Figure 43

B-1-A Camera and Electronic Control Equipment

to record the cratering process. The electronic equipment that controlled the camera and cratering process is also shown in this figure. This circuitry enabled the experiment to be controlled by the activation of a single push-button switch. Pushing this button started the camera and flood light. After a 2 second delay, 28-volts were automatically sent to the prepared squib. After initiation of the squib, the camera and light continued to function for 3 seconds. The filming and lighting sequence then automatically terminated and a new cratering sequence could be started. A wiring diagram for the circuit is shown in Fig. 44. The lighting apparatus is shown in Fig. 45. These lights were energized by 110-volt alternating current.

In addition, high-speed photography was used to record the motion of the sand during the cratering process. A high speed sequence was taken of one crater for each condition of gravity and DOB. This was done to provide an additional means of analyzing the processes occurring during crater formations. The camera used was a 16-mm Fairchild Motion Analysis Camera, Model Number HS 101, powered by a 28-volt, direct current motor. A 13-mm lens was provided on the camera. The camera, which operated at a maximum rate of 2000 frames per second, is shown in Fig. 46.

Calibration Tests

The calibration phase of the experiment in this thesis included determinations of (1) the boundary effects due to the container and depth wire, (2) a satisfactory method of placement of the squib in the sand, and (3) satisfactory methods of extracting crater parameters from the films.

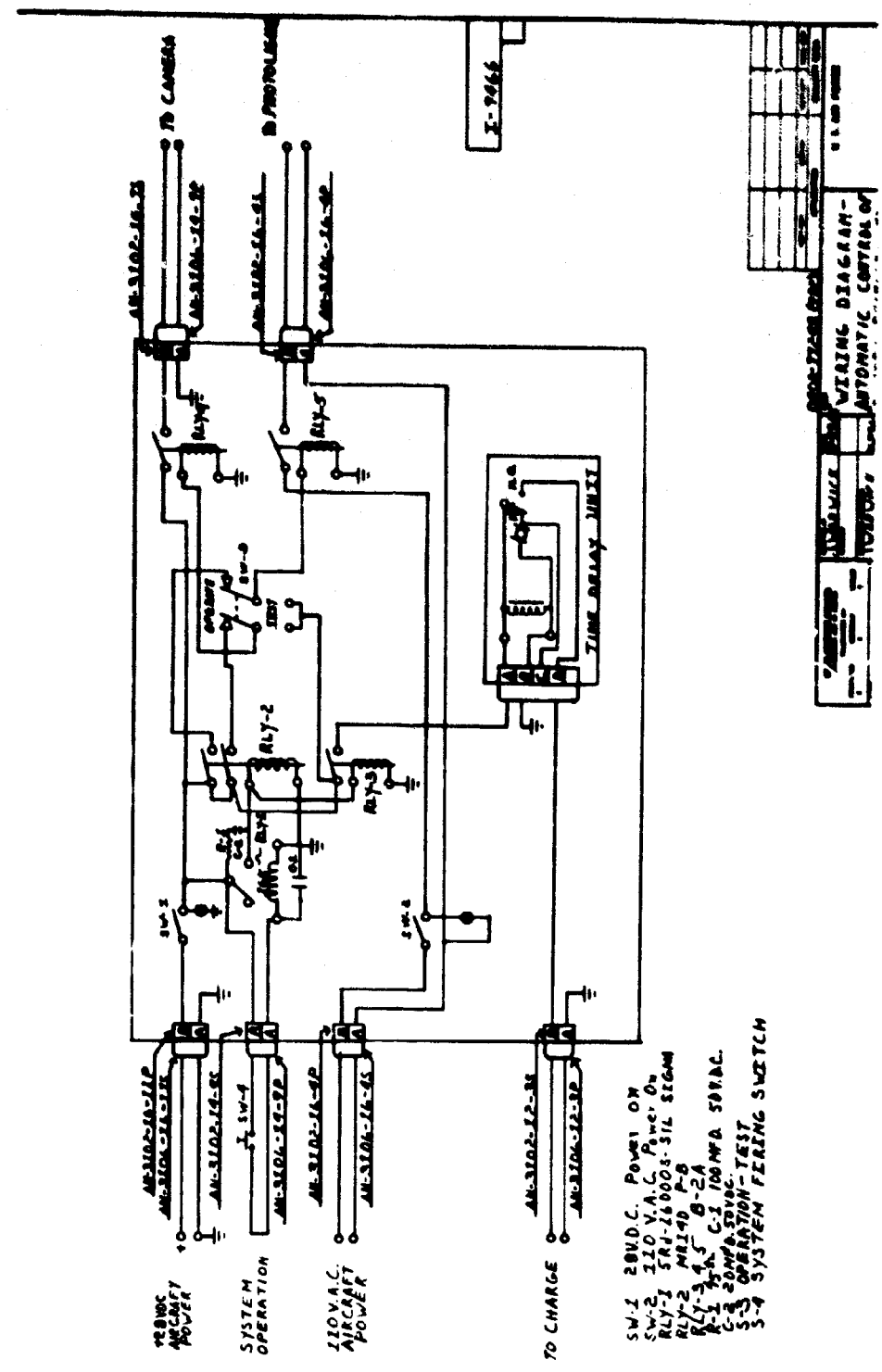

Figure 44

Wiring Diagram for Electronic Control Equipment

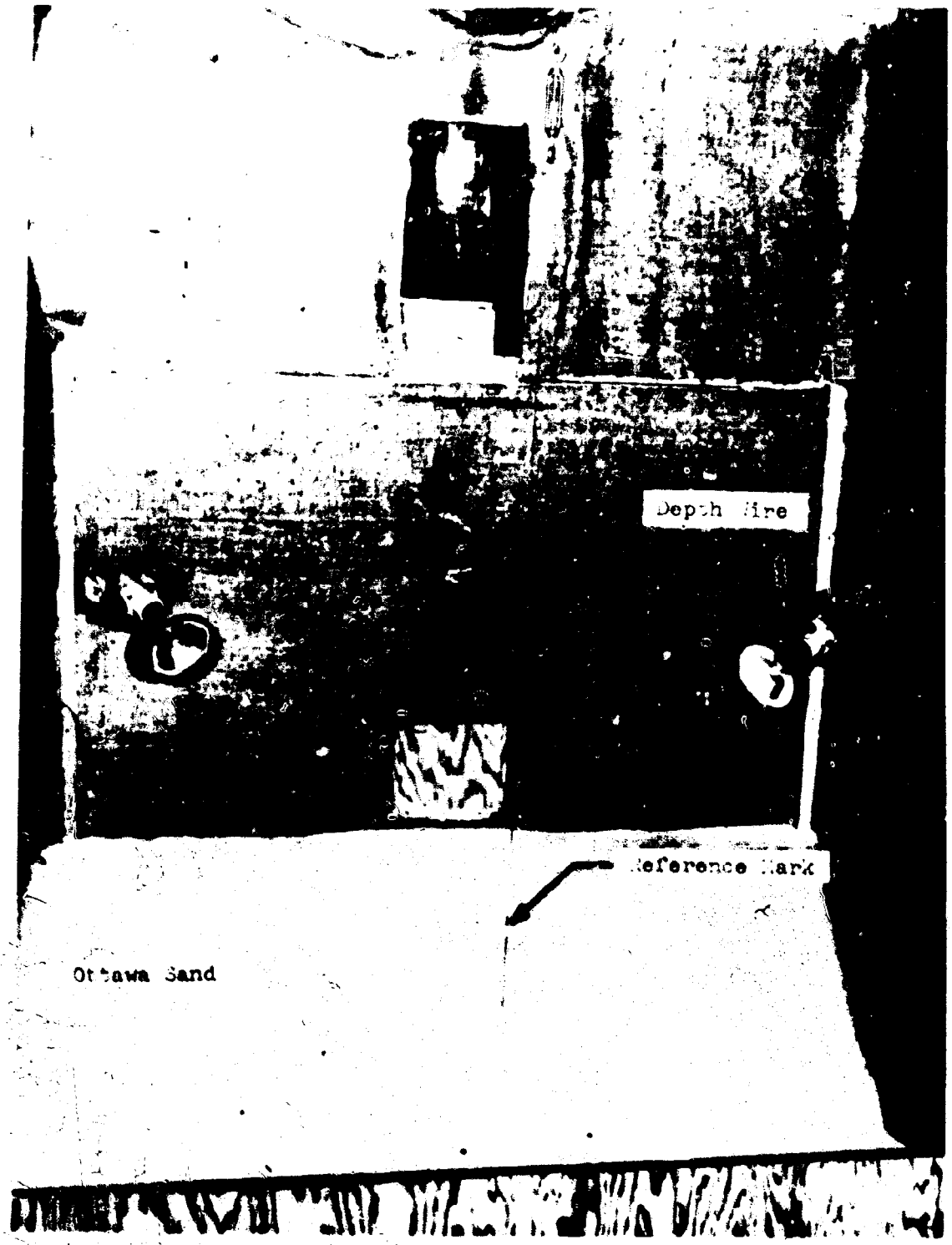

Figure 45

Lighting Apparatus for Photography

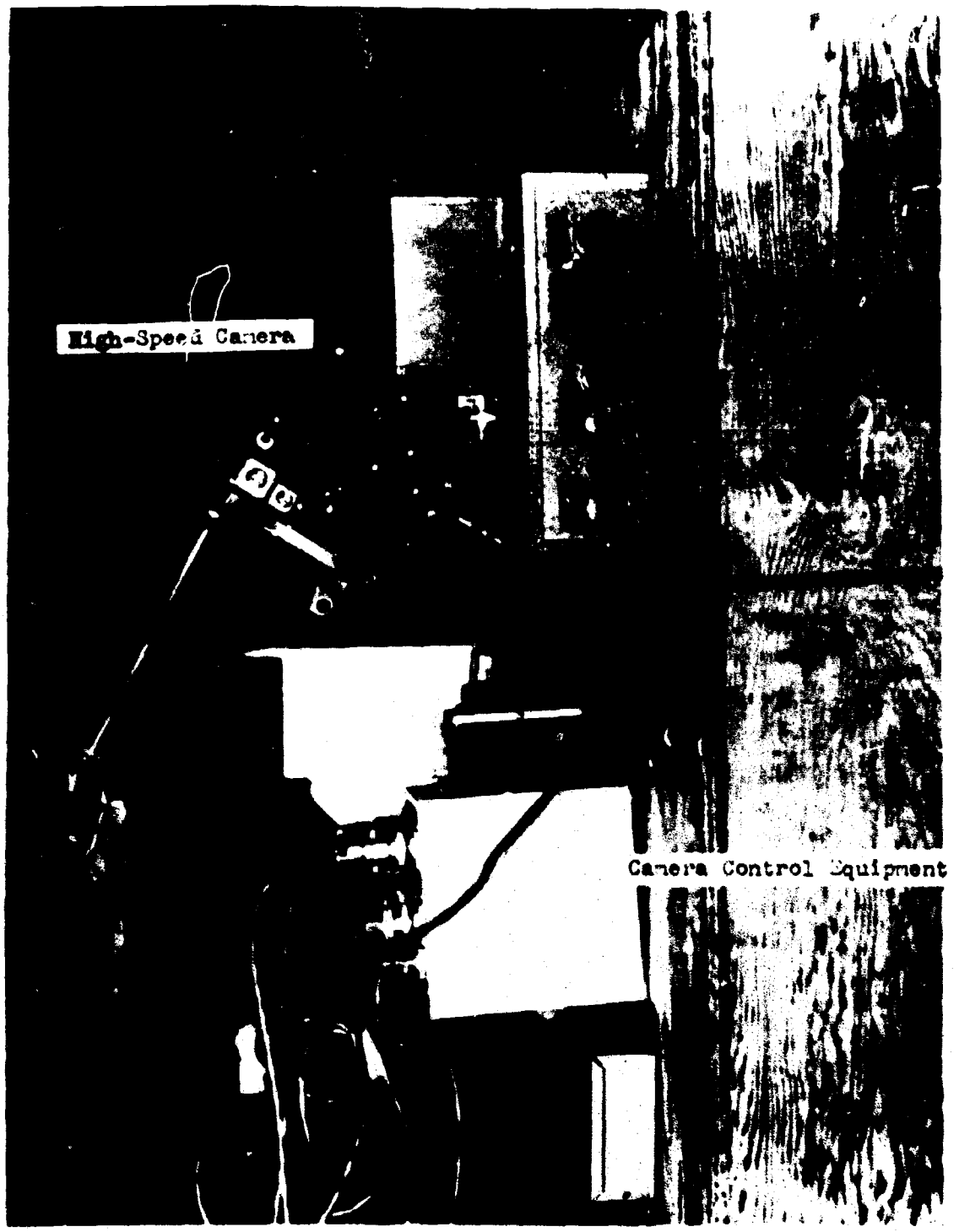

Figure 46

High-Speed Camera

Boundary Effects. In order to insure that the cratering process was not influenced by any reflections of the shock wave from the bottom of the container, the depth of sand used as the medium was carefully investigated. A comparison of crater parameters in different depths of sand indicated whether or not boundary effects were influencing crater dimensions. It was felt that enough sand between the explosion and the container would damp out any reflected shock waves that would adversely affect the crater. The different depths investigated were 5, 10, 12, 13, and 14 inches of sand. Different size craters were formed between 5, 10, 12, and 13 inches of sand for a constant source of energy and DOB. The differences were felt to be due to boundary effects from the container. A statistical analysis using the two-sample t-test indicated that there was not a significant difference in compared dimensions of craters formed in 13 and 14 inches of sand (see Appendix E). Therefore negligible boundary effects were present with 14 inches of sand in the container. Since there was more than 14 inches of sand between the point of detonation and the sides of the container, the assumption was made that there were no boundary effects from the side of the container.

The thin wire shown in Fig. 45 was used as an aid in extracting the crater dimensions from the motion picture film. This technique will be explained in the discussion of crater measurements contained in this section. The wire did not influence the crater dimensions as comparisons of depths and diameters of craters formed under the same conditions except with or without the wire showed no statistically significant difference.

Squib Placement. Several methods of placement of the squib to obtain the desired DOB were tested. The squib had to be (1) emplaced quickly to conserve time on the aircraft, (2) attached securely to withstand aircraft vibrations, and (3) positioned accurately at a given depth. It was determined that a placement of the squib with the wires pointing upward worked most effectively. The center of detonation was estimated from Fig. 41. Based upon this figure, the midpoint distance between the end of the squib and the first crimp was chosen as the center of the detonation. Distances were measured upward from this point and the desired depth settings were marked on the wires. After the sand was leveled to a depth of 14 inches, the squib was inserted into the sand at a point next to the depth wire with the lead-in wires pointing upward. In order to insure that the squib was vertical and that the lead-in wires were straight, the squib was inserted to a depth below the final desired depth and then pulled upward to the final position. The final position was noted by means of a mark painted on the lead-in wires. The above procedure proved to be the most accurate method of achieving the correct DOB. After the squib was attached to the firing wires, the container was closed and the firing sequence was initiated.

For depths of burst greater than two inches, it was necessary to slightly modify the above procedure due to the inability of inserting the squib to the desired depth without bending the lead-in wires. For these depths, a depression was made in the medium where the squib was to be emplaced. This technique is shown in Fig. 47. The depression allowed the squib to be placed at the desired depth without having to

Figure 47

Placement of Squib for Deep Depths of Burst

be forced through more than two inches of the medium. The depression was then filled in and the sand was leveled. Final positioning of the squib was accomplished by pulling the lead-in wires upward to insure the proper DOB and vertical attitude. Experimentation with this method indicated that the squib remained close to vertical and that the depth could be consistently set to within 1/8 inch of the desired depth. Some error in the data could have resulted from this method of squib placement, but the error was random rather than systematic.

Crater Dimension Measurements. The dimensions of the craters formed during this experiment were obtained from motion picture film. The validity and accuracy of the measurements taken from the film were checked by comparing the film measurements with manual measurements taken of the same crater.

The crater measurements were extracted from the film with the aid of a thin wire and a photographed scale. The wire was placed in the container as shown in Fig. 48 and a reference mark was painted on the wire. By observing on the film the intersection of this wire with the sand before and after the detonation, the depth of the crater was determined. The diameter was directly observed on the film as the rim-to-rim distance normal to the line of sight of the photograph. A photographed scale was required to convert the scaled depth and diameter as seen on the film to true depth and diameter. This was done with the scale that is shown in Fig. 49. This scale was formed by placing a vertical ruler along the depth wire with the 12-inch line adjacent to the top of the reference mark on the wire. The horizontal ruler was placed at the original ground level. Several feet of film were

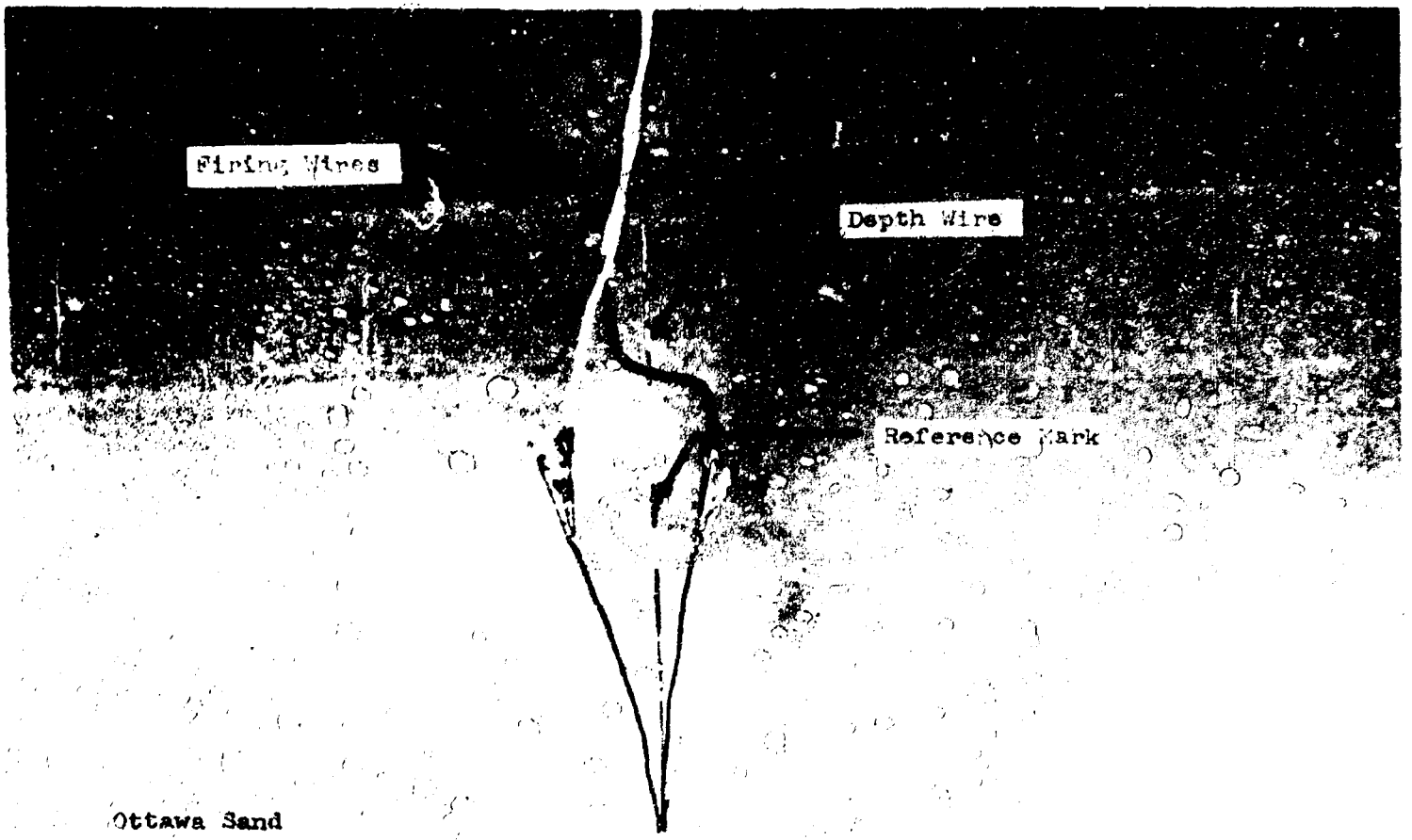

Figure 48

Pre-Detonation Condition

Figure 49

Scale Used for Crater Measurements

taken of this scale from the same location and with the same camera as used to photograph the craters.

The actual crater dimensions were obtained from the film by projecting the cratering sequence on a poster board screen. The pre-detonation conditions were recorded by marking the position of the wire reference mark and the original ground level on the screen. The intersection of the wire and the sand clearly located the original ground level. The film was advanced to the post-detonation position where the final crater was recorded. After relocating and superimposing the reference marks on the screen and film, the wire-sand intersection could again be marked. The wire-sand intersection is seen in Fig. 50. The distance between this mark and the original

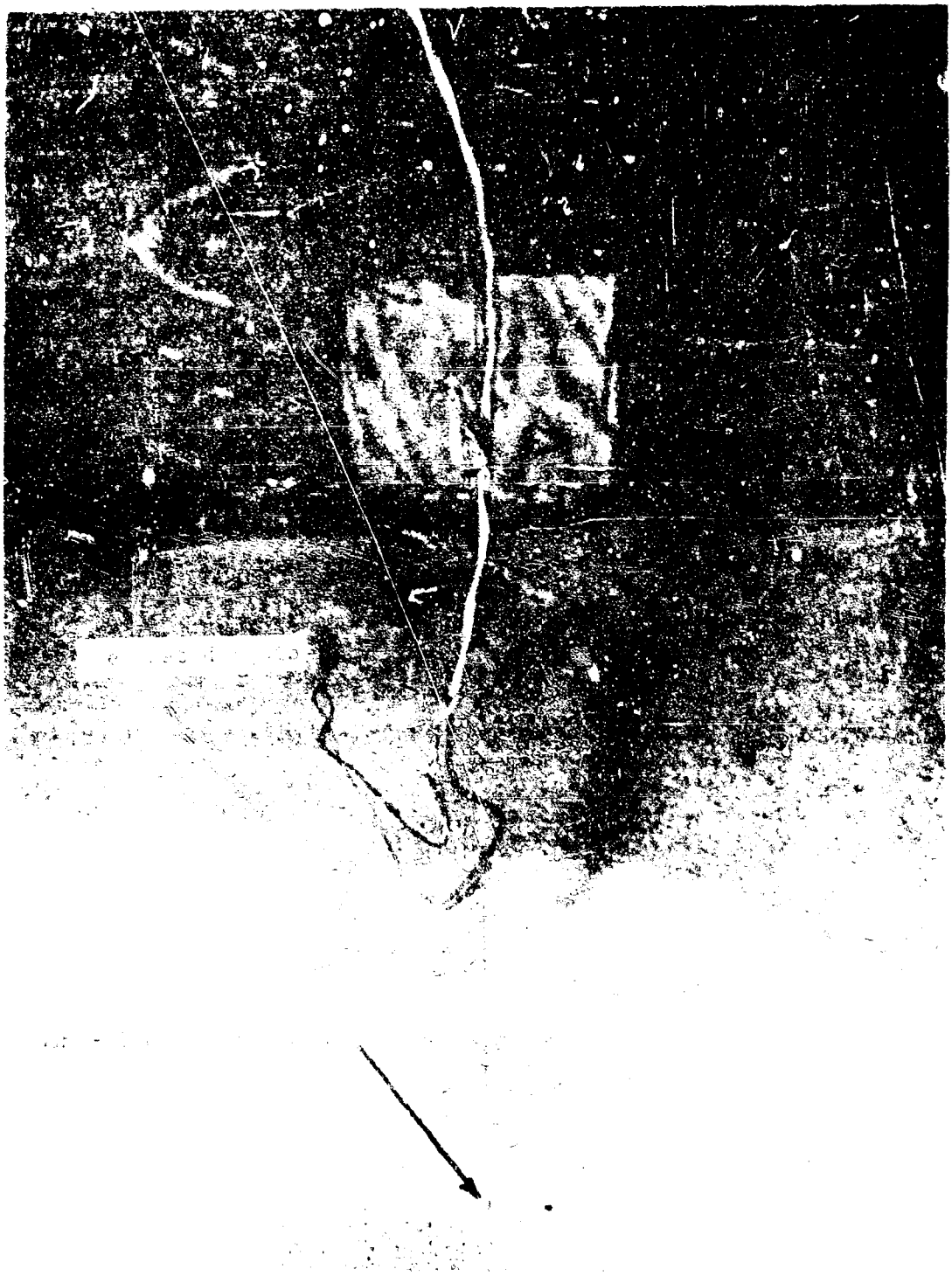

Figure 50

Final Crater and Wire-Sand Intersection

ground level was the scaled crater depth. The normal-to-the-line-of-sight rim separation distance across the center of the crater was marked as the scaled diameter. Figure 1 shows these dimensions. By projecting the photographed scale on the screen and aligning the reference marks again, the actual depths and diameters could be read directly. This procedure was further expedited by tracing the projected scale on acetate. The acetate was then placed over the screen and properly aligned to measure the actual crater dimensions. This system was valid as long as the screen-projector distance remained constant for the entire measuring procedure. This fixed distance was carefully maintained during the measurement of the craters.

The validity of this method of measurement was proven as the manual and film measurements agreed on the average to within ± 1/8 inch for the depths and ± 1/4 inch for the diameter. In addition, some of the craters were remeasured from the film at a later date as a check of the consistency of the measuring technique. The average change in the crater dimensions based upon the remeasured dimensions was ± 1/4 inch for the diameter and ± 1/8 inch for the depth. The limit of measurement of the photographed scale could be interpolated to the nearest 1/8 inch when projected on the screen.

Sources of Error

There were many possible sources of error in the experiment. The load tolerance of the squib was 6.0 ± 0.4 grains, which allowed an approximate 7% deviation in the explosive yield. The squib was constructed so that the detonation was not spherically symmetrical. This placed additional stress on the necessity for accurate placement

techniques. The small magnitude of the yield caused a small error in placement to be greatly magnified. In Appendix C are tabulated the dimensions of craters formed at a DOB of slightly less than 0.5 inches and slightly greater than 0.5 inches. The tabulated dimensions show that even a small error in placement can affect the crater dimensions.

An additional factor with the squib was the nature of its detonation. Since the squib burned rapidly instead of decomposing instantaneously, the lack of confinement of the charge at surface bursts permitted some scattering of unburned or burning compound.

Aircraft vibrations had some influence on the location of the squib between the time that it was placed and detonated. Vibrations may have also had some effect on crater formation. A t-test comparison of crater dimensions for 1.0 g conditions on and off the aircraft is shown in the tabulated data in Appendix E. The results of this test indicate that the diameters are only slightly influenced by vibrations but the depths show significant vibration changes. The error due to vibrations increase with increasing DOB.

The value of gravity in the aircraft was subject to variations of ± .01 g for any particular maneuver due to turbulence and limitations of pilot control. It was observed during the flights that occasional longitudinal acceleration of the aircraft was present during some of the maneuvers. This was due to improper throttle manipulations and, when noticed by the crew or technicians, was corrected. The presence of longitudinal acceleration primarily affected the depth of the crater rather than the diameter. At shallow depths of burst, more of the medium would slide back into the center of the crater after the

detonation process was completed. For deep depths of burst, longitudinal acceleration of the aircraft resulted in a shift of the fallback pattern. This resulted in a shift in the location of the crater center away from the depth wire. It was felt that longitudinal acceleration was the largest source of error in the flight tests. In addition, there were random errors in measurements due to the limits of resolution of the film.

False Leads

False leads encountered during the experiment are listed here briefly in hopes that they might possibly help future investigators save some time and effort in their research.

Other explosive sources than squibs were investigated. Exploding wires were considered but not used as the cost of constructing a device to explode wires was prohibitive when compared to squibs. Advantages of exploding wires are ease of control and safety. The explosion of a wire is not spherically symmetrical, however, and the energy partition is different from a chemical explosion.

Crater parameters other than depth and diameter were considered. An attempt to ascertain crater volumes proved fruitless from the films as the diameter of the crater was measured from the top of the crater rim rather than along the original ground level. The top of the crater rim was the only observable position from which to make a diameter determination from the film. The error in the measured volume when the rim-to-rim diameter was used instead of the proper ground level diameter ranged as high as 100%. Rim heights could not be measured because of the lack of reliable references on the films

and the small rim height. Rim heights seldom ranged over 1/2 inch.

An attempt to make depth determinations by painting the depth wire in known increments was made. By painting the wire in known increments, the depth of the crater could have been determined by simply counting the difference in the number of increments visible before and after detonation. The paint could not withstand the explosive force and the increments were either obscured or destroyed. The photographic scale was devised as an alternate means of measuring the crater depths.

Appendix B

Properties of the Cratering Medium

Ottawa sand is a high grade white silica sand which is mined exclusively from a silica sandstone of exceptional purity located in Ottawa, Illinois. Because of the high degree of uniformity and cleanliness, it has found extensive use as a standard for testing. In particular, the United States Government uses certain grades of Ottawa sand in calculating the energy content of chemical explosives (Ref 43:59).

Because the properties of the medium in which the crater is formed influence the size of the crater, it was imperative that these properties be known and that the variance in certain critical characteristics such as density and moisture content be limited throughout the experiment. In order to obtain this information, certain soil tests were performed. The results of these tests are discussed in the following paragraphs.

Grain Size Analysis

The process of separating a soil into particle-size groups by shaking it through a stack of wire screens with openings of known sizes is called sieve analysis. The definition of particle size is the size of a square opening on which the grain of soil is retained. The recommended procedure which is outlined in Section IV of Reference 31 was followed for the conduct of the test.

The result of the test is represented graphically in Fig. 51 by means of a grain size distribution curve. From the figure it is evident that the particles of the soil sample used as the cratering medium are uniform in size. A further indication of the general nature of the medium is given by the terms known as the coefficient of gradation and the uniformity coefficient. The coefficient of gradation is defined as

$$C_g = \frac{(D_{30})^2}{(D_{60})(D_{10})} \tag{11}$$

while the uniformity coefficient is defined as

$$C_u = \frac{D_{60}}{D_{10}} \tag{12}$$

where the D_i refers to the grain size which corresponds to the i% finer by weight point on a grain size distribution curve. In order to be classified as being uniformly graded, the value of the uniformity coefficient must be less than 4 while the value of the coefficient of gradation must be less than 1 or greater than 3 (Ref 56:281). For the Ottawa sand sample, the values of the two coefficients are $C_g = .92$ and $C_u = 1.47$. Based upon these coefficients, the medium is uniformly graded. For purposes of the investigation, a uniform soil sample was desired since this should decrease the variance in the density of the soil.

Density

Tests were conducted in order to determine if the density of the sample would exhibit only a limited variance. The first test consisted

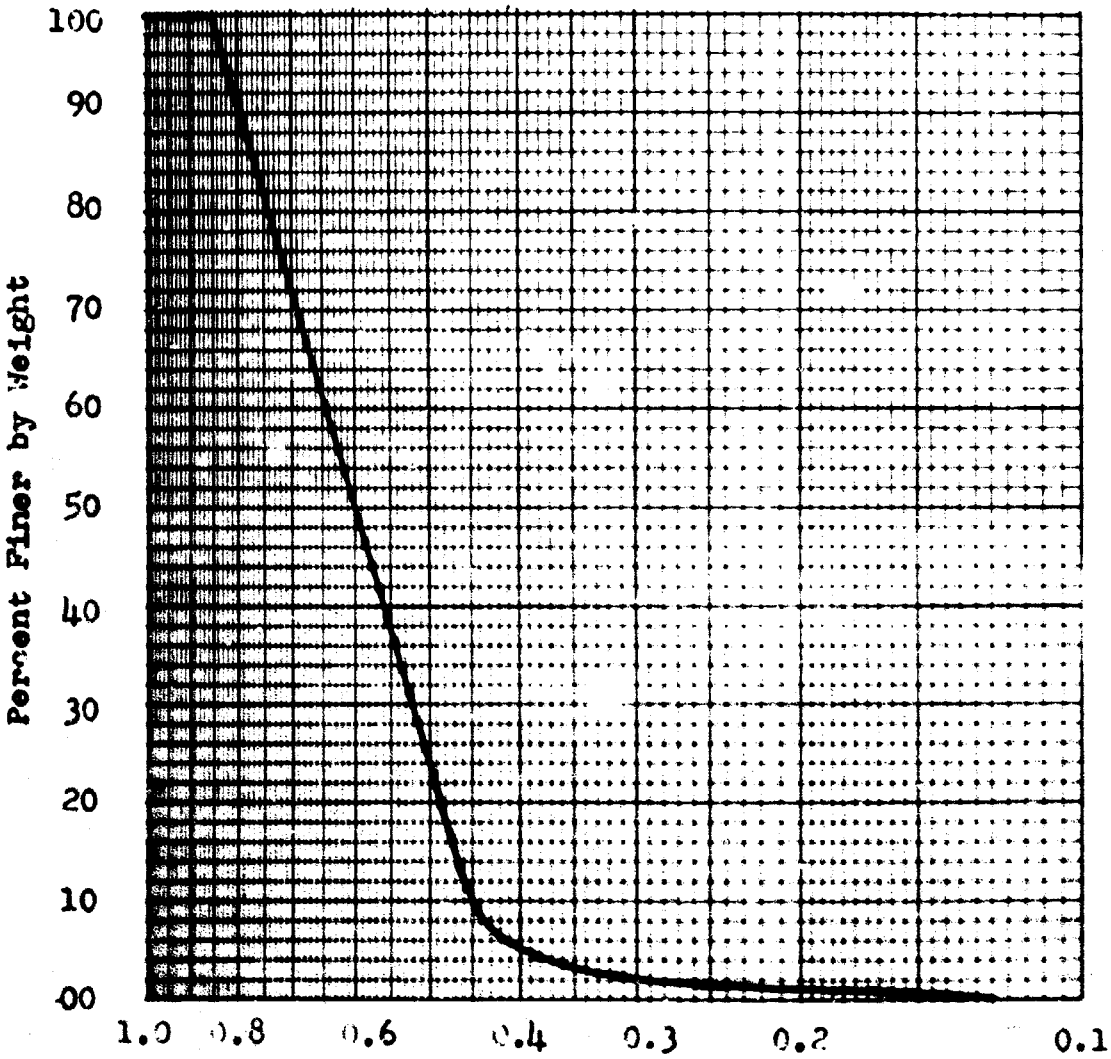

Figure 51

Grain Size Distribution Curve for Ottawa Sand

of placing the dry Ottawa sand in a standard compaction mold normally used for the Proctor compaction test. The sand was placed in as loose a manner as possible. Using the equation

$$\gamma_d = \frac{W}{V_m} \tag{13}$$

where W = weight of sand in mold in pounds

V_m = volume of the mold which was 1/30 of a cubic foot

γ_d = density of the sample in pounds per cubic foot (pcf)

a density of 96.8 pcf was attained.

The second test consisted of placing the dry Ottawa sand in the mold in a loose state and then subjecting the mold to a small amount of agitation and vibration such as it would be subjected to during the ground and flight tests. For this test, the density was calculated to be 107.5 pcf.

The final test consisted of performing a modified Proctor test on the dry sample in which the sand was placed in the mold in five layers with each layer being compacted by means of 25 blows with a ten pound hammer falling through a distance of 18 inches. A detailed explanation of such a test can be found in Chapter V of Reference 31. For this test the density was calculated to be 108 pcf.

Based upon the above tests, it was concluded that the variation in density due to the conditions of the experiment would be negligible.

Moisture Content

Since the assumption of negligible variation in density depended upon a negligible variation in the moisture content of the sand, tests

ditions.

In the first test, the moisture content of sand which had been stored in its original paper sack was determined according to the procedures outlined in Chapter III of Reference 31. The results of the tests on five different samples indicated zero moisture content.

A second moisture content determination was made on five samples of sand which were being used for the ground tests. In this case, the medium was stored in a heated building. Again zero moisture content was recorded.

A final test was made on five samples of sand which were stored in open containers in an unheated garage during three days of intermittent rain. During this time, the door of the garage remained open 24 hours a day in order to make the air in the garage as humid as possible. The moisture content for three of the samples was zero. For the other two samples, the moisture content was 0.1%. No water was ever added to the sand during the moisture content tests since the sand and the box in which it was contained were never exposed to any moisture except the water vapor in the air.

Based upon the above tests, it was concluded that there would be no variation in the moisture content of the sand during the course of the experiment.

Direct Shear Test

In a cohesionless soil, the angle of internal friction is the soil parameter which determines the shear resistance. In order to determine $\emptyset$, a strain-controlled direct shear test was conducted on a

dense sample of sand as outlined in Chapter X of Reference 31. In the direct shear test, a portion of the sand sample is caused to slide in relation to the rest of the sample. The tests were conducted by students at the University of Dayton, Dayton, Ohio. Plotting the data for all the tests and fitting a straight line to the data results in an angle of internal friction of 37°. This result is shown in Fig. 52 where each data point is the state of stress on the soil sample at the time of shear failure. Because a constant area of the sample is assumed, the scale is in terms of pounds of force. To compute the stress in psf, each value must be divided by 1/30 square foot.

Mention should be made of the fact that the line, which is really a plot of the Coulomb shear formula

$$s = c + p \tan \phi \qquad (14)$$

indicates that the sand apparently possesses some cohesion as indicated by the intercept on the axis. This is due to the presence of friction between the top of the shear box and the bottom of the shear box (Ref 19).

Summary

The sieve analysis indicated that the soil was uniformly graded. The densification tests showed that the variation in density under the conditions of the test would be negligible. Also, there was negligible moisture in the sand under the conditions of the test. The direct shear test indicated that the soil was cohesionless and had an angle of internal friction of 37°. Based upon these characteristics, the

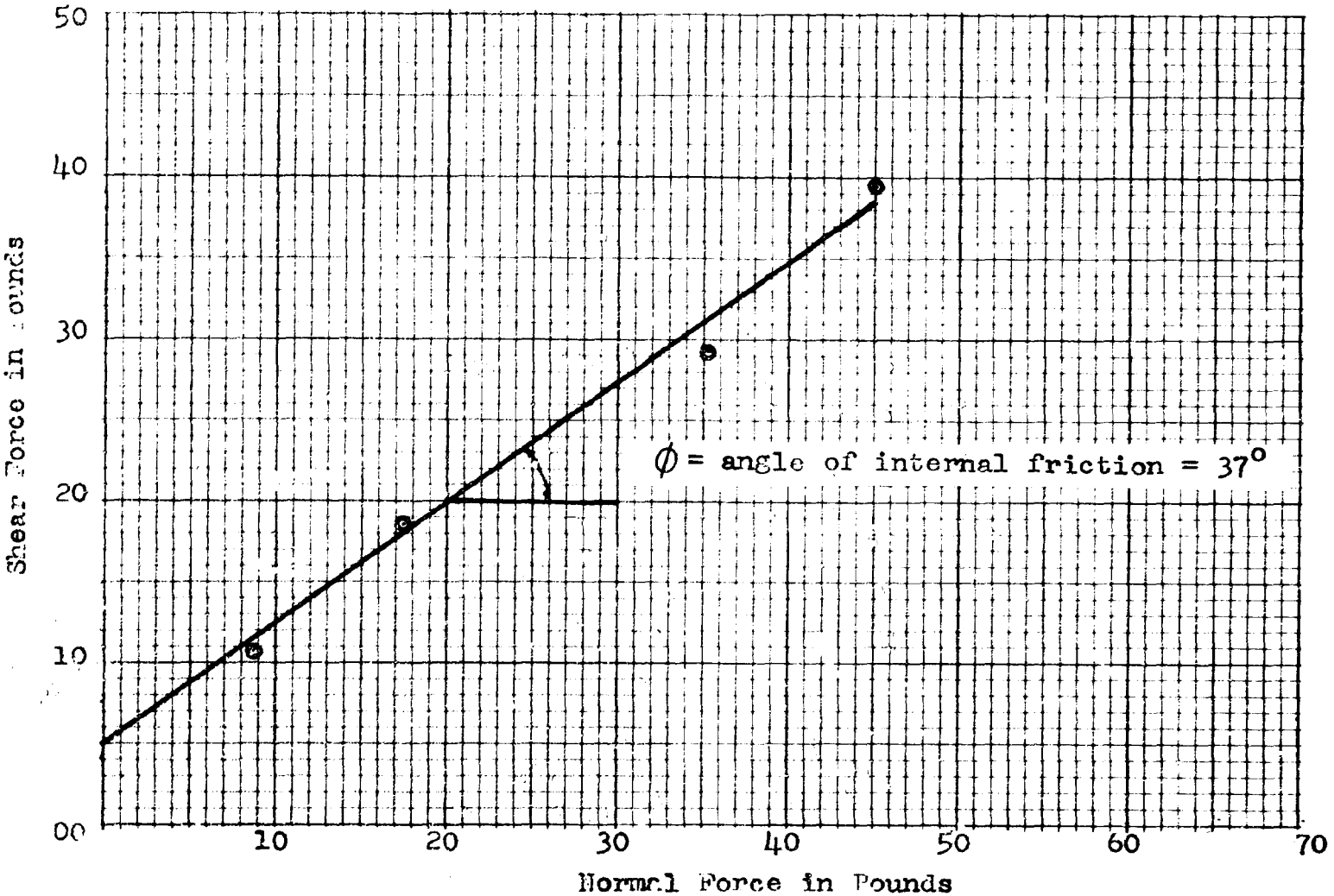

Figure 52

Graphical Calculation of Angle of Internal Friction

medium could be considered to be an ideal medium in which to investigate the effect of gravity on crater formation.

Appendix C

Tabulated Data

This appendix contains a listing of the dimensions of the craters formed during the calibration and test phases of the experiment. Also included are the means and variances of the craters formed under the various calibration and test conditions. All dimensions and depths of burst listed in the tables are expressed in inches.

TABLE II

DIMENSIONS OF CRATERS FORMED
UNDER .17 G CONDITIONS

0.0 Inch DOB			0.5 Inch DOB		
Index Number	Diameter	Depth	Index Number	Diameter	Depth
371	11.750	2.000	251	9.500	1.500
372	12.000	2.125	252	10.500	1.875
373	12.500	2.250	253	10.500	2.000
374	10.250	1.500	254	10.500	2.000
375	9.000	1.250	255	10.500	1.875
376	9.250	1.625	256	10.250	1.875
377	11.250	2.000	257	10.750	2.125
378	9.500	1.375	258	10.250	1.750
379	10.250	2.000	259	11.000	2.000
380	10.750	1.250	260	10.750	2.000
	1.0 Inch DOB			1.5 Inch DOB	
121	16.250	2.750	151	17.000	2.375
122	17.500	2.750	152	18.500	2.500
123	17.250	2.375	153	18.000	3.125
124	17.000	2.125	154	19.000	3.125
125	18.250	3.000	155	18.500	2.875
126	16.250	2.750	156	17.750	2.750
127	17.000	2.625	157	18.250	2.625
128	17.750	2.875	158	19.000	3.125
129	17.500	3.125	159	18.250	3.250
130	17.250	3.000	160	17.500	2.750

TABLE II (CONTINUED) DIMENSIONS OF CRATERS

	2.0 Inch DOB			3.0 Inch DOB	
Index Number	Diameter	Depth	Index Number	Diameter	Depth
141	17.500	2.375	161	15.000	1.875
142	18.000	2.125	162	15.250	2.000
143	16.750	2.000	163	15.250	1.000
144	17.500	2.375	164	16.000	1.875
145	17.750	2.750	165	16.000	1.875
146	18.000	3.000	166	16.750	2.250
147	18.000	2.785	167	16.250	1.875
148	18.500	2.750	168	16.250	2.125
149	17.500	2.750	169	15.750	1.875
150	18.000	2.875	170	15.750	2.125
	4.0 Inch DOB			5.0 Inch DOB	
181	12.750	1.250	201	7.000	.625
182	14.500	1.500	202	11.000	.875
183	14.000	1.250	203	8.500	.625
184	13.500	1.125	204	9.000	.500
185	14.000	1.125	205	7.500	.625
186	13.125	0.625	206	11.500	#
187	13.750	0.750	207	10.000	.500
188	12.750	0.750	208	#	.250
189	13.000	1.125	209	#	.375
190	14.000	1.000	210	9.000	.500

Crater not measureable

TABLE III

DIMENSIONS OF CRATERS FORMED
UNDER .38 G CONDITIONS

Index Number	0.0 Inch DOB Diameter	Depth	Index Number	0.5 Inch DOB Diameter	Depth
381	12.000	2.375	411	15.750	2.875
382	10.750	1.875	412	14.250	2.750
383	9.000	1.375	413	15.000	2.750
384	9.250	1.250	414	14.250	2.375
385	9.750	1.625	415	14.500	2.625
386	10.000	2.250	416	14.750	2.250
387	10.500	2.125	417	#	#
388	10.250	1.750	418	14.500	2.625
389	10.750	2.000	419	15.000	2.875
390	11.000	2.125	420	14.000	2.625
	1.0 Inch DOB			1.5 Inch DOB	
401	14.250	2.375	431	15.750	3.000
402	15.750	2.500	432	16.000	3.250
403	15.750	2.250	433	16.000	2.500
404	14.750	2.375	434	15.750	3.000
405	15.000	2.375	435	15.500	2.750
406	14.250	2.750	436	15.000	2.625
407	15.500	2.750	437	16.000	2.750
408	16.250	3.125	438	16.000	2.750
409	16.500	2.750	439	16.500	2.875
410	16.250	2.750	440	15.500	2.500

TABLE III (CONTINUED) DIMENSIONS OF CRATERS

2.0 Inch DOB			3.0 Inch DOB		
Index Number	Diameter	Depth	Index Number	Diameter	Depth
421	#	#	441	12.750	1.375
422	15.000	2.750	442	14.500	1.750
423	15.500	2.250	443	14.250	1.625
424	15.500	2.250	444	14.500	1.750
425	15.750	2.625	445	15.250	1.875
426	16.500	2.375	446	13.500	1.375
427	16.250	2.250	447	13.750	1.250
428	16.000	2.625	448	14.750	2.125
429	15.750	2.250	449	13.750	1.250
430	15.500	2.125	450	14.500	1.750
	4.0 Inch DOB			5.0 Inch DOB	
461	11.750	0.875	481	7.250	.625
462	11.500	1.000	482	#	.375
463	11.750	1.000	483	#	.375
464	12.250	0.625	484	#	.625
465	12.250	0.875	485	7.000	.375
466	11.750	1.000	486	7.500	.625
467	12.000	0.875	487	8.000	.625
468	12.000	1.000	488	8.000	.750
469	12.000	1.125	489	#	.375
470	11.750	1.250	490	#	.375

Crater not measureable

TABLE IV

DIMENSIONS OF CRATERS FORMED
UNDER 1.0 G CONDITIONS

0.0 Inch DOB			0.5 Inch DOB		
Index Number	Diameter	Depth	Index Number	Diameter	Depth
101	8.750	1.875	501	10.750	1.875
102	9.000	1.875	502	11.250	2.250
103	8.500	1.500	503	11.750	2.250
104	9.250	1.750	504	12.750	2.250
105	8.250	1.500	505	11.750	2.250
106	9.000	1.500	506	11.000	2.250
107	8.250	1.375	507	12.750	2.250
108	8.875	1.625	508	12.000	2.375
109	7.375	1.500	509	12.000	2.250
110	8.500	1.500	510	12.000	2.250
111	9.000	1.750	511	12.500	2.500
112	9.000	1.875	512	12.000	2.125
113	9.000	1.750	513	12.500	2.625
114	9.250	1.750	514	11.750	2.250
115	9.250	1.625	515	12.250	2.250
116	9.000	1.750	516	12.500	2.125
117	9.500	1.625	517	12.250	2.250
118	9.250	1.875	518	12.500	2.375
119	9.250	1.625	519	12.000	2.125
120	8.750	1.750	520	12.500	2.250

TABLE IV (CONTINUED) DIMENSIONS OF CRATERS

1.0 Inch DOB			1.5 Inch DOB		
Index Number	Diameter	Depth	Index Number	Diameter	Depth
1	13.750	2.500	521	13.250	2.500
2	13.375	2.625	522	13.500	2.250
3	12.875	2.500	523	13.500	2.750
4	14.125	2.500	524	13.750	2.375
5	13.125	2.500	525	14.000	2.500
6	13.125	2.500	526	13.750	2.125
7	13.250	2.375	527	13.500	2.250
8	13.375	2.500	528	13.750	2.250
9	13.125	2.375	529	13.750	2.250
10	13.125	2.375	530	13.500	2.500
11	13.125	2.250	531	14.000	2.375
12	13.500	2.500	532	14.000	2.375
13	13.250	2.250	533	14.000	2.250
14	14.000	2.750	534	14.000	2.375
15	13.500	2.375	535	13.750	2.250
16	14.000	2.500	536	14.250	2.250
17	13.750	2.500	537	14.250	2.250
18	13.625	2.375	538	14.000	2.125
19	13.500	2.750	539	14.000	2.250
20	13.750	2.625	540	14.000	2.500

Mech/GSF-65-35

TABLE IV (CONTINUED) DIMENSIONS OF CRATERS

2.0 Inch DOB			3.0 Inch DOB		
Index Number	Diameter	Depth	Index Number	Diameter	Depth
21	13.375	1.875	41	12.125	1.625
22	13.500	2.125	42	12.000	1.125
23	13.875	2.250	43	11.875	1.625
24	13.375	2.000	44	11.875	1.125
25	13.500	1.875	45	12.000	1.250
26	14.125	2.000	46	12.000	1.250
27	13.625	1.625	47	12.000	1.375
28	13.375	1.875	48	11.000	1.000
29	13.125	1.875	49	12.250	1.375
30	13.625	1.875	50	11.625	1.000
31	13.750	2.125	51	13.000	1.625
32	13.375	1.875	52	11.000	0.875
33	13.875	2.375	53	11.750	1.375
34	13.000	1.375	54	12.750	1.500
35	13.625	1.875	55	12.500	1.375
36	13.375	1.750	56	12.625	1.375
37	13.750	1.875	57	12.750	1.500
38	13.125	1.750	58	11.500	1.250
39	13.750	2.000	59	12.000	1.125
40	13.375	1.750	60	12.125	1.250

TABLE IV (CONTINUED) DIMENSIONS OF CRATERS

4.0
Inch DOB

Index Number	Diameter	Depth
61	10.250	1.000
62	10.250	0.750
63	10.875	0.750
64	9.875	0.500
65	11.000	1.000
66	11.375	1.000
67	10.625	0.750
68	8.500	0.875
69	10.250	0.875
70	10.500	0.750
71	10.000	1.000
72	10.500	0.750
73	10.500	1.000
74	10.250	0.750
75	10.000	1.000
76	10.500	0.750
77	10.000	0.625
78	10.500	0.750
79	9.750	1.000
80	10.000	1.000

TABLE V

DIMENSIONS OF CRATERS FORMED
UNDER 2.5 G CONDITIONS

0.0 Inch DOB			0.5 Inch DOB		
Index Number	Diameter	Depth	Index Number	Diameter	Depth
391	8.750	1.500	251	9.500	1.500
392	8.750	1.375	252	10.500	1.875
393	8.000	1.500	253	10.500	2.000
394	8.500	1.500	254	10.500	2.000
395	7.750	1.625	255	10.500	1.875
396	8.500	1.375	256	10.250	1.875
397	7.750	1.500	257	10.750	2.125
398	7.500	1.375	258	10.250	1.750
399	7.750	1.375	259	11.000	2.000
400	7.250	1.375	260	10.750	2.000
	1.0 Inch DOB			1.5 Inch DOB	
241	12.500	2.375	271	12.250	1.875
242	12.250	2.000	272	12.500	1.875
243	11.750	2.000	273	12.250	1.875
244	12.000	2.250	274	12.250	1.875
245	12.250	2.125	275	12.500	1.750
246	11.750	2.125	276	12.750	2.000
247	11.750	2.125	277	12.750	2.125
248	11.250	2.250	278	12.000	2.000
249	11.750	2.125	279	13.000	2.125
250	12.250	2.375	280	12.500	1.875

TABLE V (CONTINUED) DIMENSIONS OF CRATERS

2.0 Inch DOB			3.0 Inch DOB		
Index Number	Diameter	Depth	Index Number	Diameter	Depth
261	12.000	1.875	281	10.250	1.125
262	12.250	1.750	282	11.250	1.000
263	12.000	1.500	283	10.750	1.000
264	12.500	1.625	284	11.250	1.125
265	12.000	1.625	285	10.000	1.000
266	12.500	1.375	286	10.750	1.125
267	12.000	1.500	287	11.000	1.000
268	12.500	1.375	288	10.750	1.125
269	12.250	1.500	289	10.000	1.000
270	12.000	1.375	290	10.500	0.875

4.0 Inch DOB		
301	8.250	.750
302	8.000	.375
303	8.750	.500
304	8.500	.500
305	10.250	.875
306	8.500	.500
307	9.250	.625
308	10.000	.500
309	8.500	.500
310	8.750	.625

TABLE VI

MEANS AND VARIANCES OF CRATER DIMENSIONS

	0.17 g					0.38 g			
	Diameter		Depth			Diameter		Depth	
DOB	Mean	Variance	Mean	Variance	DOB	Mean	Variance	Mean	Variance
0.0	10.650	1.315	1.738	.130	0.0	10.325	.701	1.875	.125
0.5	13.875	2.716	2.013	.095	0.5	14.667	.250	2.639	.040
1.0	17.200	0.348	2.738	.083	1.0	15.350	.615	2.625	.078
1.5	18.175	0.363	2.850	.081	1.5	15.800	.148	2.800	.051
2.0	17.750	0.200	2.588	.106	2.0	15.750	.181	2.389	.043
3.0	15.800	0.294	1.888	.105	3.0	14.150	.463	1.613	.076
4.0	13.550	0.323	1.050	.066	4.0	11.900	.053	0.963	.025
5.0	9.188	2.184	0.542	.028	5.0	7.550	.160	0.513	.020
	1.0 g					2.5 g			
0.0	8.850	.226	1.669	.022	0.0	8.050	.260	1.450	.007
0.5	12.038	.289	2.256	.021	0.5	10.450	.148	1.900	.028
1.0	13.463	.116	2.481	.018	1.0	11.950	.123	2.175	.016
1.5	13.825	.069	2.338	.022	1.5	12.475	.081	1.938	.013
2.0	13.525	.076	1.906	.045	2.0	12.200	.048	1.560	.028
3.0	12.038	.266	1.288	.039	3.0	10.650	.190	1.038	.006
4.0	10.275	.318	0.844	.022	4.0	8.875	.191	0.575	.019

TABLE VII

DIMENSIONS OF CRATERS FORMED
DURING CALIBRATION TESTS AT 1 g

Craters Formed In Thirteen Inches of Sand

DOB	Number	Diameter	Mean	Variance	Depth	Mean	Variance
	13-1	10.625			0.750		
	13-2	9.500			0.750		
4.0	13-3	10.250	10.075	.160	1.000	.850	.009
	13-4	10.250			0.875		
	13-5	9.750			0.875		

Craters Formed Without Reference Wire

	WW-1-1	13.250			2.500		
	WW-1-2	13.375			2.500		
1.0	WW-1-3	13.625	13.400	.021	2.500	2.550	.010
	WW-1-4	13.500			2.500		
	WW-1-5	13.250			2.750		
	WW-4-1	10.000			1.000		
	WW-4-2	9.750			0.875		
4.0	WW-4-3	10.000	10.200	.635	0.875	.850	.009
	WW-4-4	9.500			0.750		
	WW-4-5	11.750			0.750		

TABLE VII (CONTINUED) DIMENSIONS OF CRATERS FOR CALIBRATION

Craters Formed For Vibration Tests

DOB	Number	Diameter	Mean	Variance	Depth	Mean	Variance
	V-1-1	13.750			2.125		
	V-1-2	14.000			2.125		
1.0	V-1-3	13.500	13.450	.160	2.125	2.225	.015
	V-1-4	13.000			2.375		
	V-1-5	13.000			2.375		
	V-4-1	11.000			.500		
	V-4-2	9.500			.625		
4.0	V-4-3	9.750	9.750	.450	.750	.500	.031
	V-4-4	9.500			.375		
	V-4-5	9.000			.250		

TABLE VII (CONTINUED) DIMENSIONS OF CRATERS FOR CALIBRATION

Craters Formed to Determine Effect of DOB Placement

DOB	Number	Diameter	Mean	Variance	Depth	Mean	Variance
	E-1	10.750			2.250		
	E-2	11.250			2.000		
0.5(-)	E-3	11.750	11.250	.100	2.125	2.050	.016
	E-4	11.250			1.875		
	E-5	11.250			2.000		
	E-6	12.000			2.250		
	E-7	12.500			2.250		
0.5(+)	E-8	12.250	12.400	.065	2.250	2.275	.003
	E-9	12.500			2.250		
	E-10	12.750			2.375		

Appendix D

This appendix contains photographs and profiles of typical craters formed at each depth of burst and in each gravity field. The shape of the profile was obtained from direct observation of the craters, examination of the cratering films, and the measured depth and diameter. The crater rim-to-rim diameter and crater depth are accurately represented while the remaining dimensions such as rim width and height are estimated. However, the photographs and profiles do give an indication of the trend in the crater size and shape as gravity and depth of burst are varied.

In certain of the crater profiles, a hummocky rim is noted. During the experiment, some of the fallback would occasionally trap the expanding gases before they vented into the air. This resulted in a secondary scouring action as the gases escaped from the additional entrapment. This secondary scouring, which appeared to be independent of gravity, is believed to be the reason for the hummocky rims.

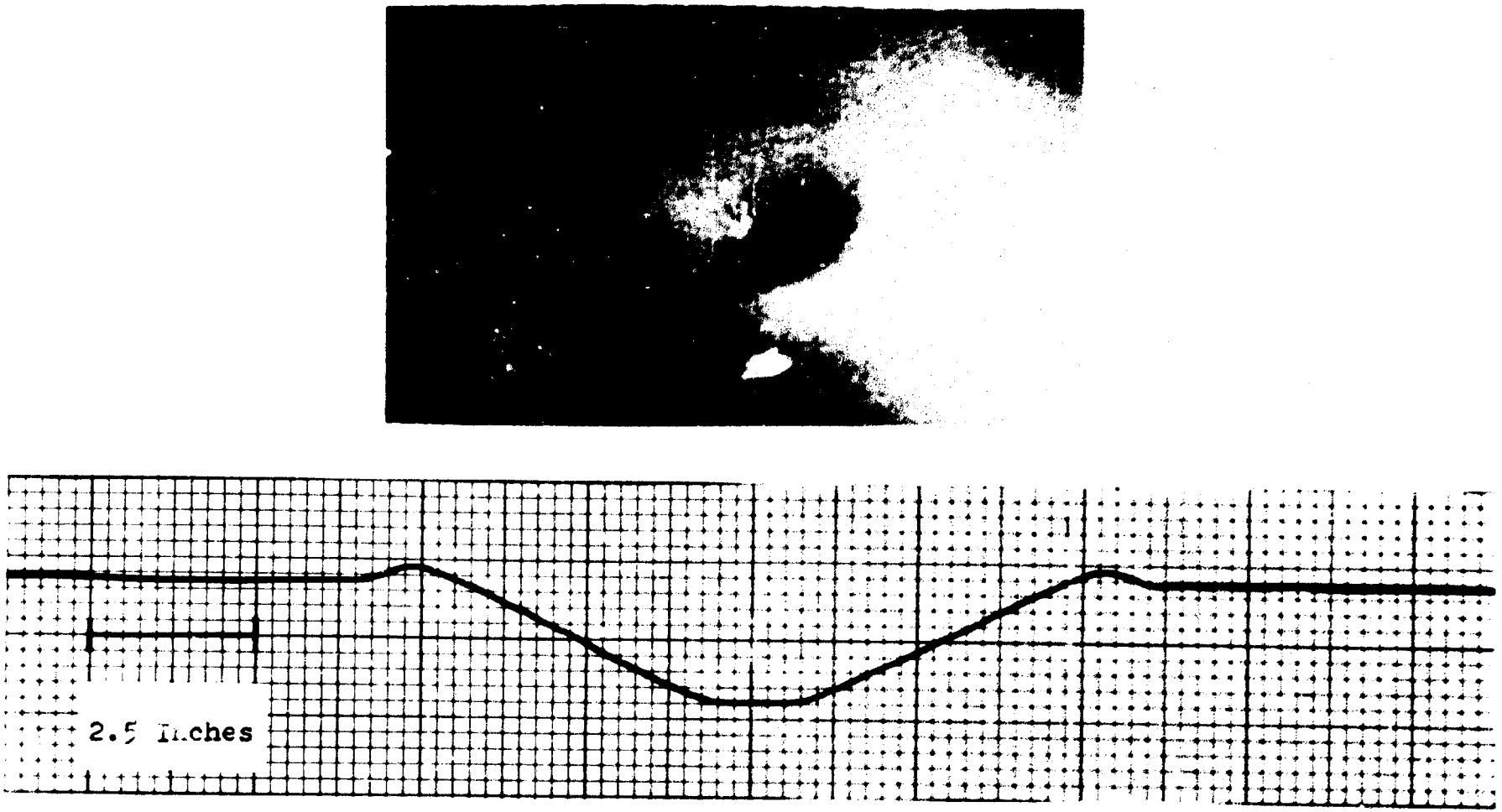

Figure 54

Profile of Crater Formed at 0.0 Inch DOB and 0.98 g

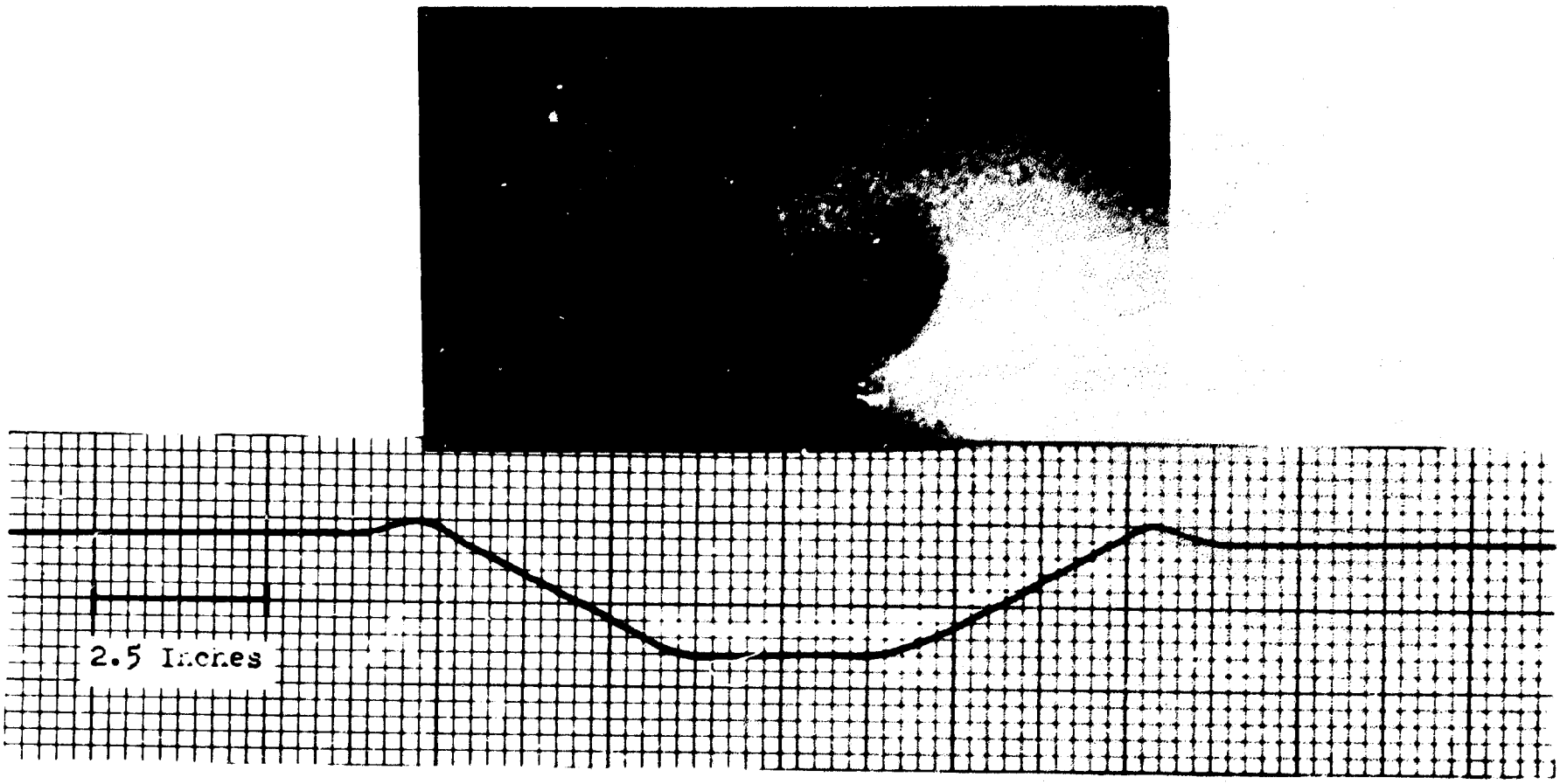

Figure 53

Profile of Crater Formed at 0.0 Inch DOB and 0.17 g

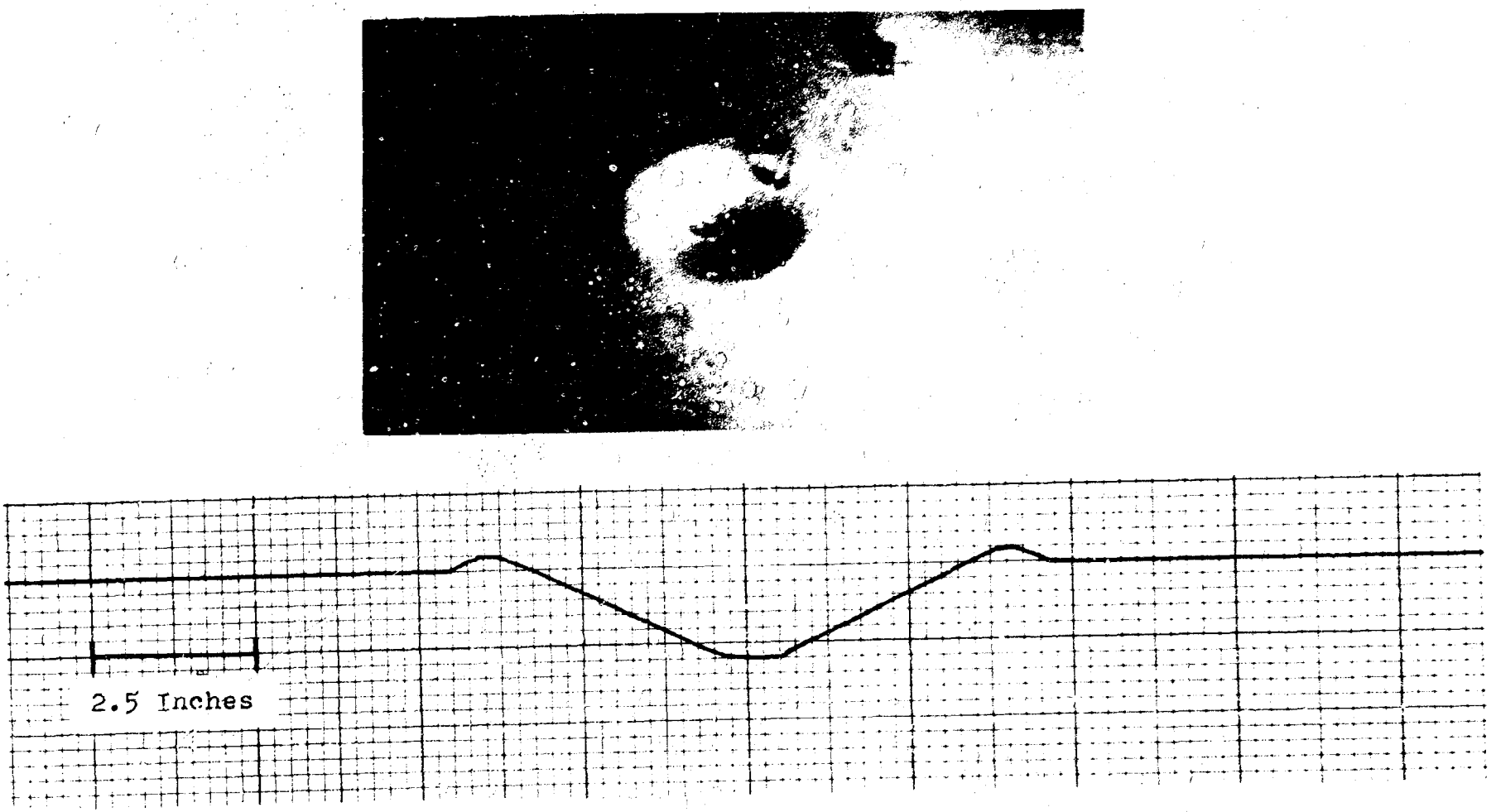

Figure 56

Profile of Crater Formed at 0.0 Inch DOB and 2.5 g

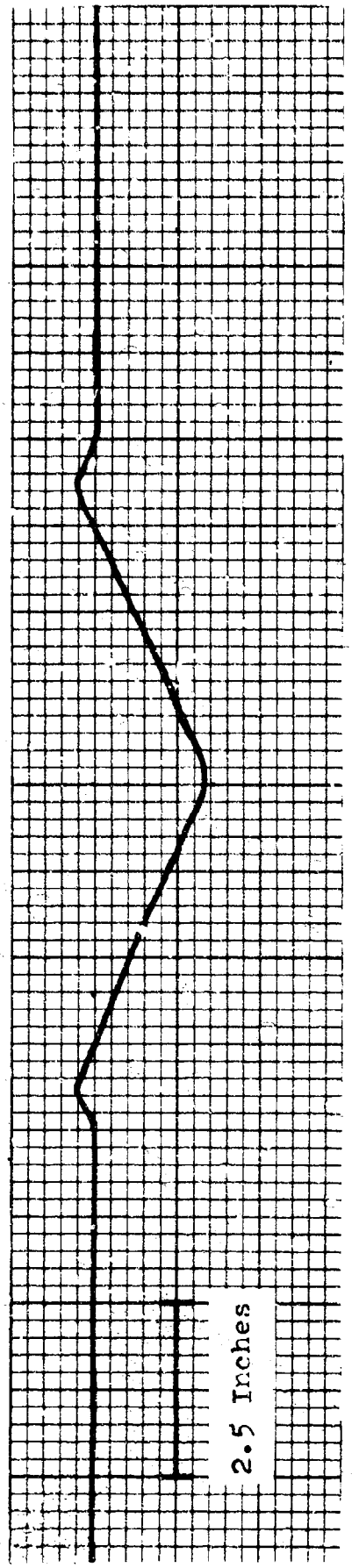

Figure 55

Profile of Crater Formed at 0.0 Inch DOB and 1.0 g

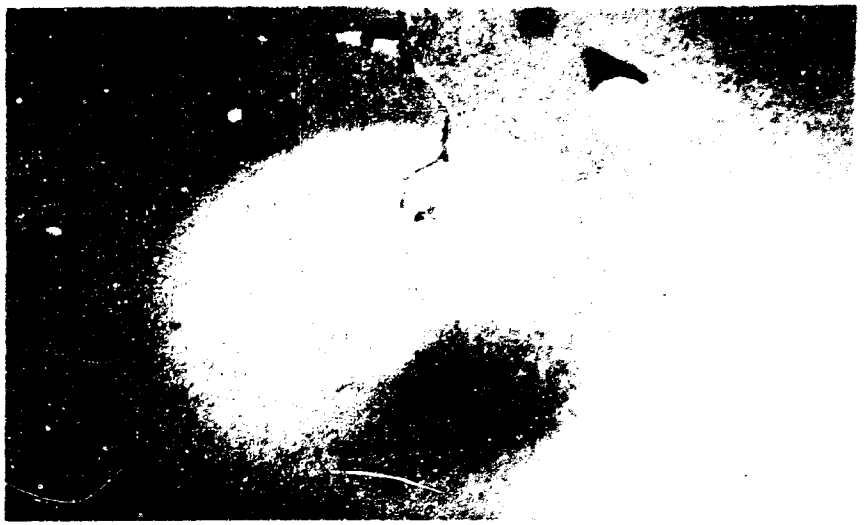

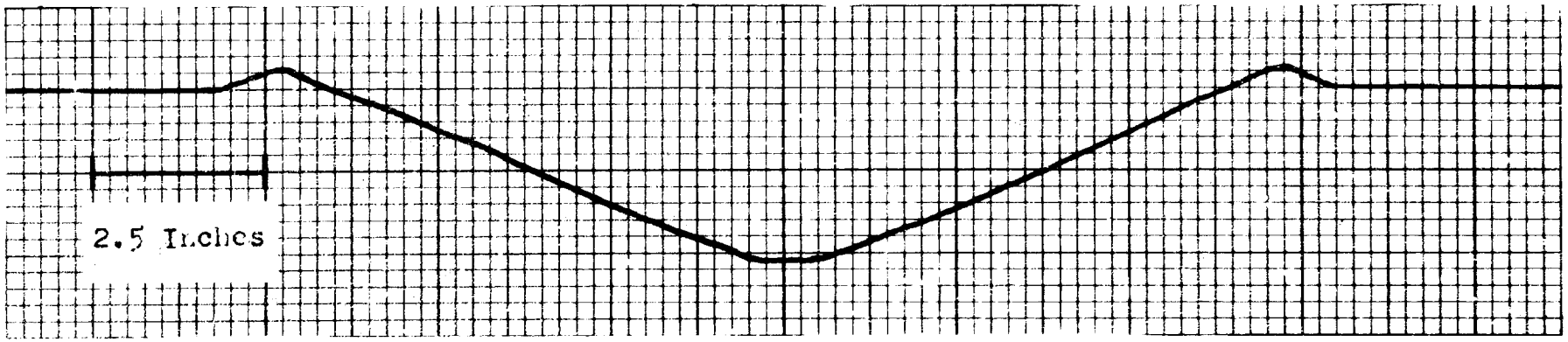

Figure 53

Profile of Crater Formed at 0.5 Inch DOB and 0.3? g

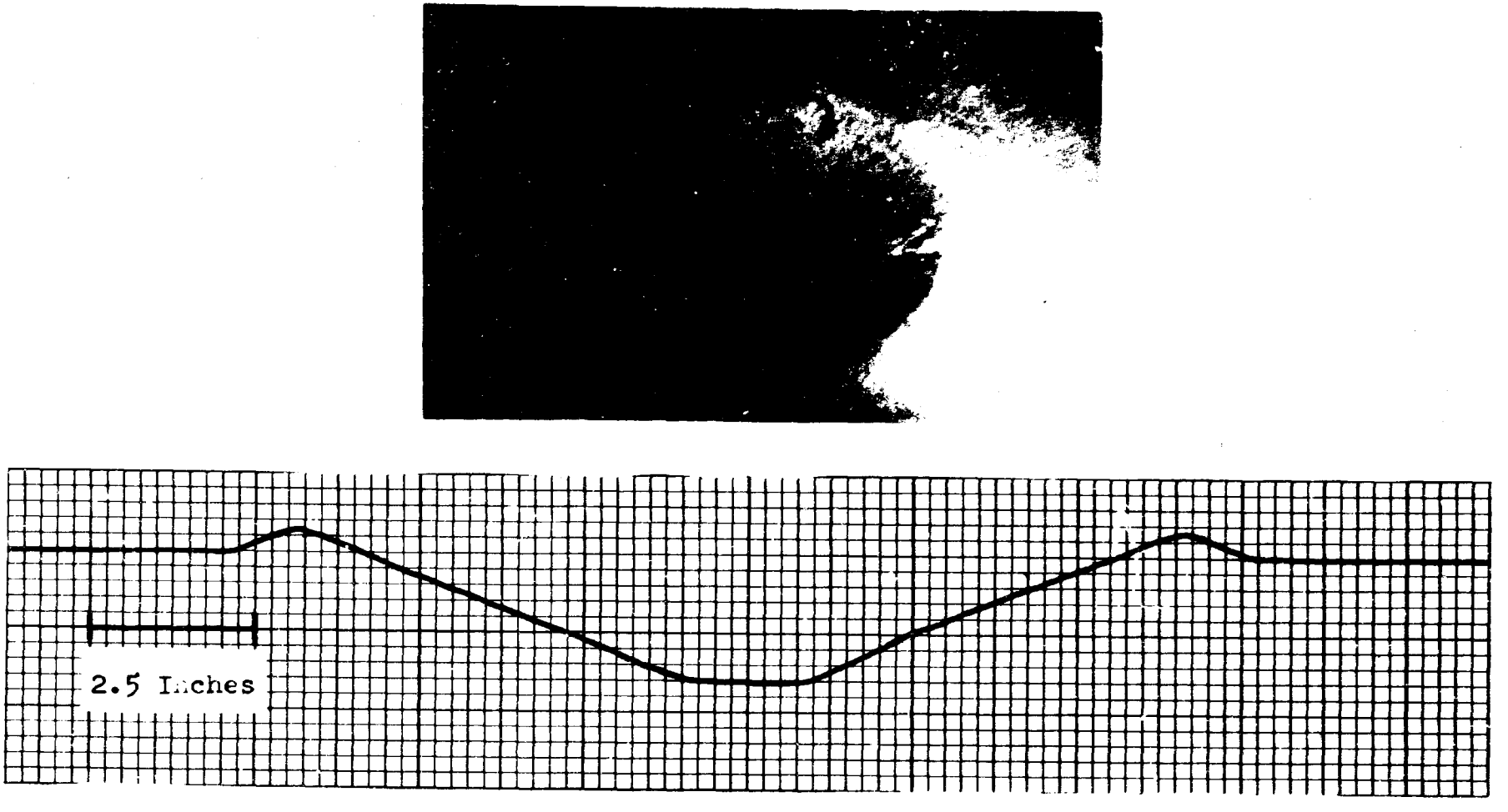

Figure 57

Profile of Crater Formed at 0.5 Inch DOB and 0.17 g

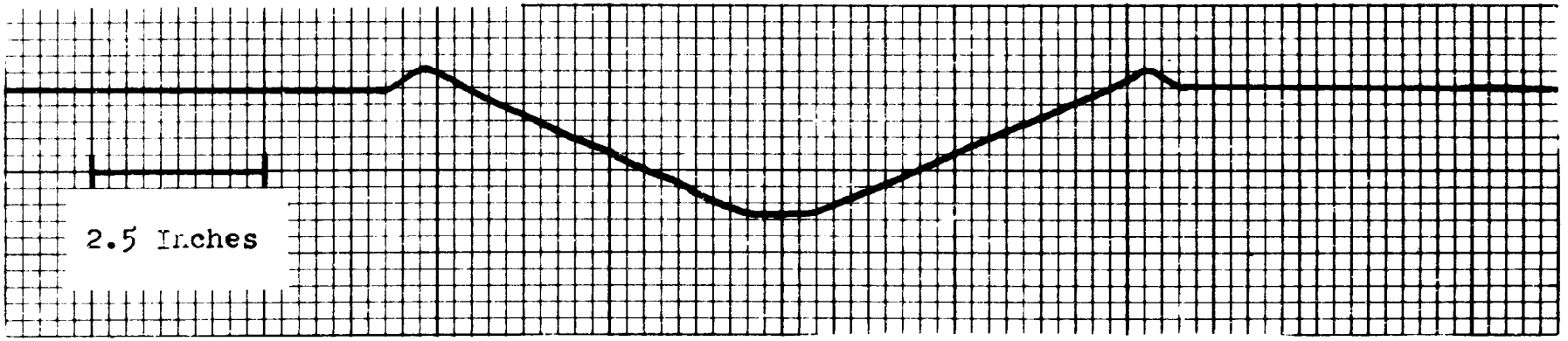

Figure 60

Profile of Crater Formed at 0.5 Inch DOB and 2.5 g

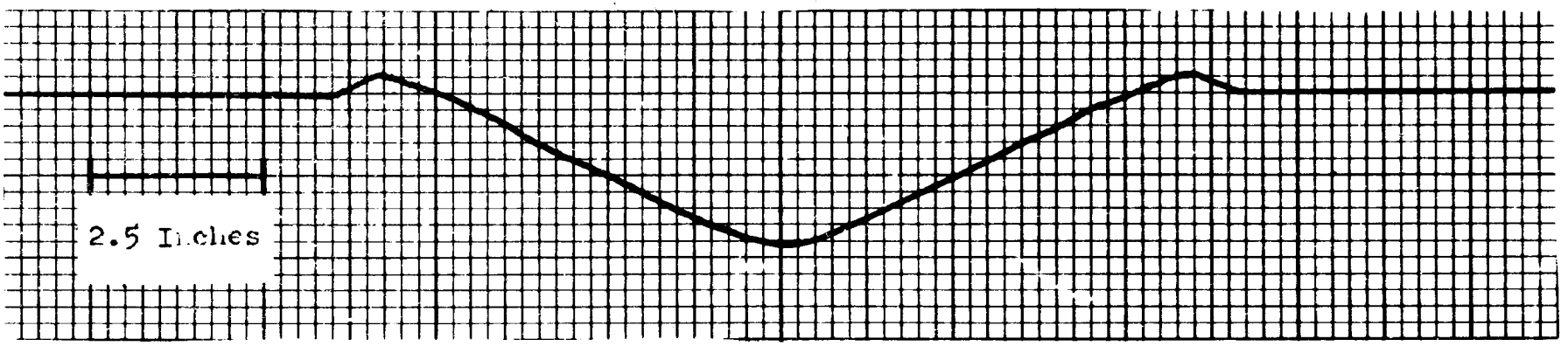

Figure 59

Profile of Crater Formed at 0.5 Inch DOB and 1.0 g

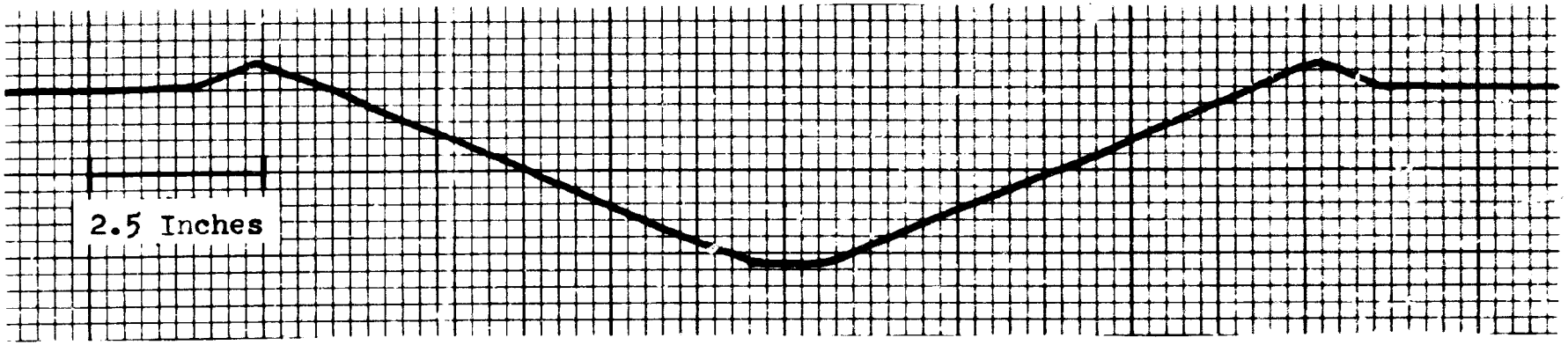

Figure 62

Profile of Crater Formed at 1.0 Inch DOB and 0.33 g

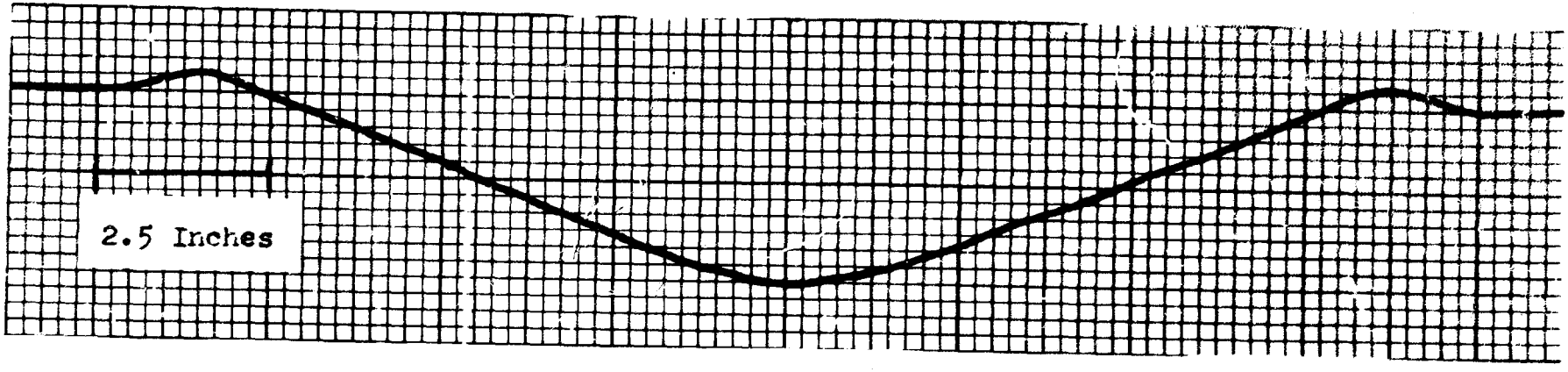

Figure 61

Profile of Crater Formed at 1.0 Inch DOB and 0.17 g

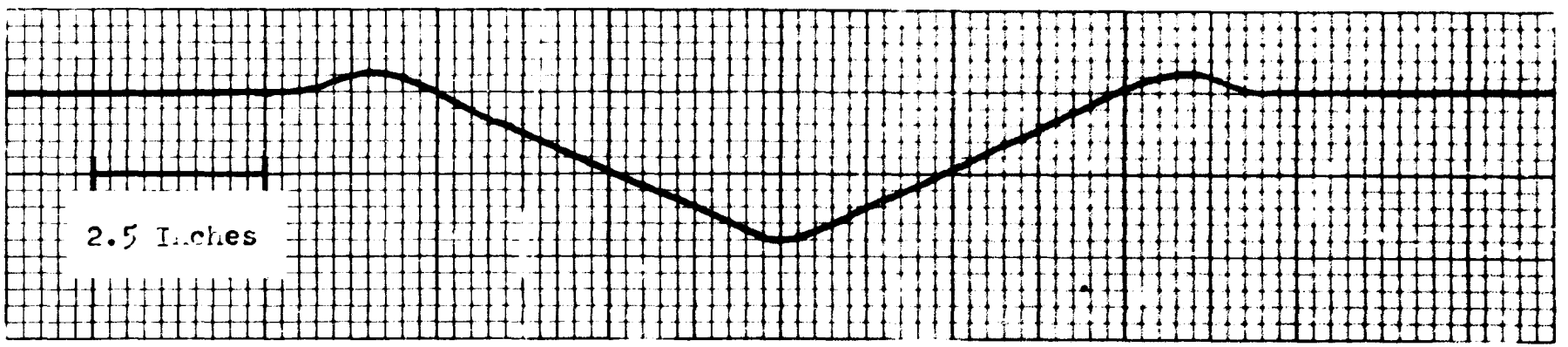

Figure 64

Profile of Crater Formed at 1.0 Inch DOB and 2.5 g

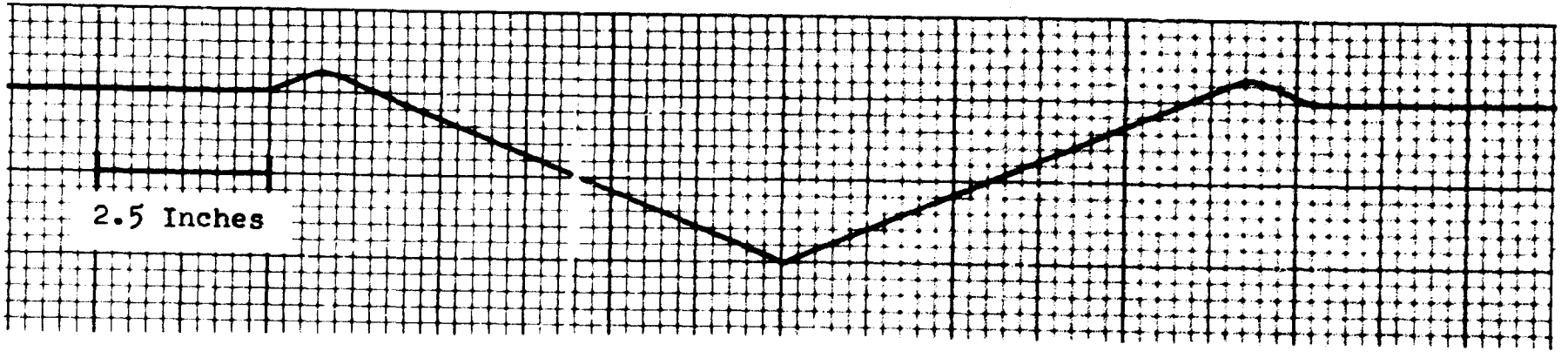

Figure 63

Profile of Crater Formed at 1.0 Inch DOB and 1.0 g

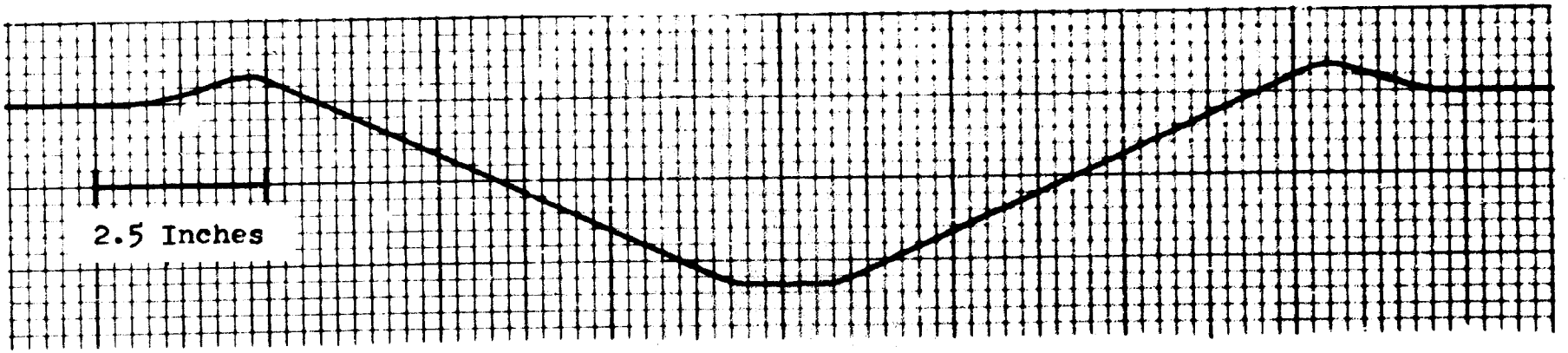

Figure 66

Profile of Crater Formed at 1.5 Inch DOB and 0.38 g

Figure 65

Profile of Crater Formed at 1.5 Inch DOB and 0.17 g

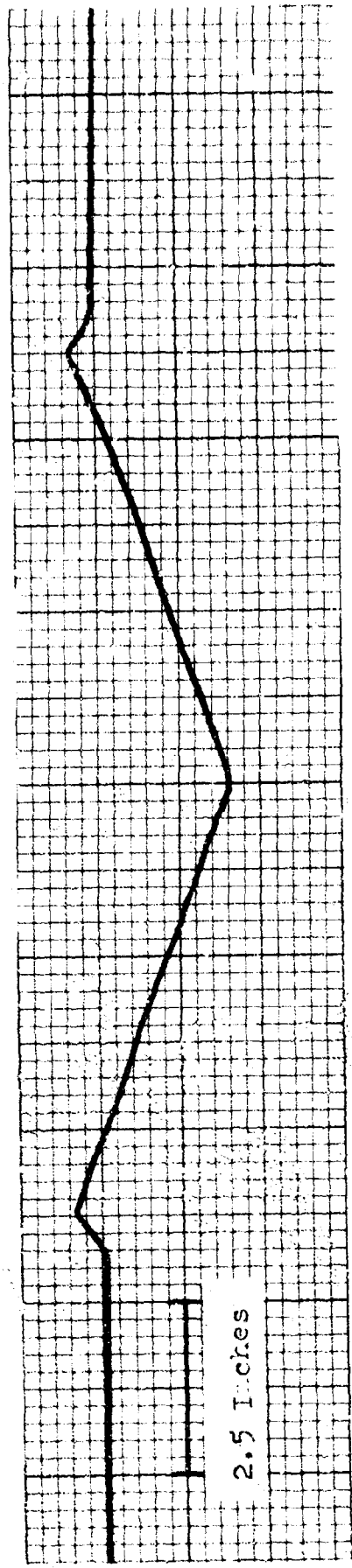

Figure 69

Profile of Crater Formed at 1.5 Inch DOB and 2.5 g

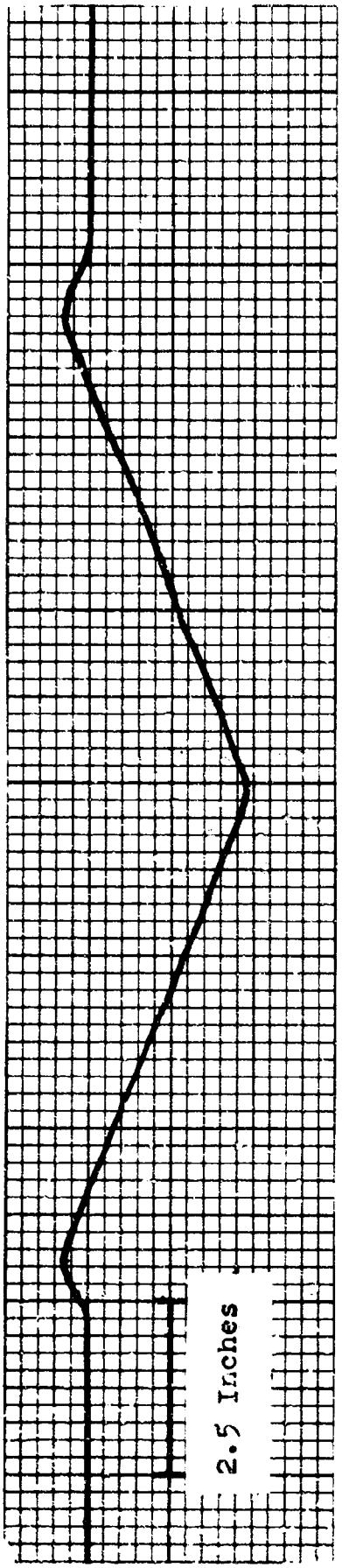

Figure 67

Profile of Crater Formed at 1.5 Inch DOB and 1.0 g

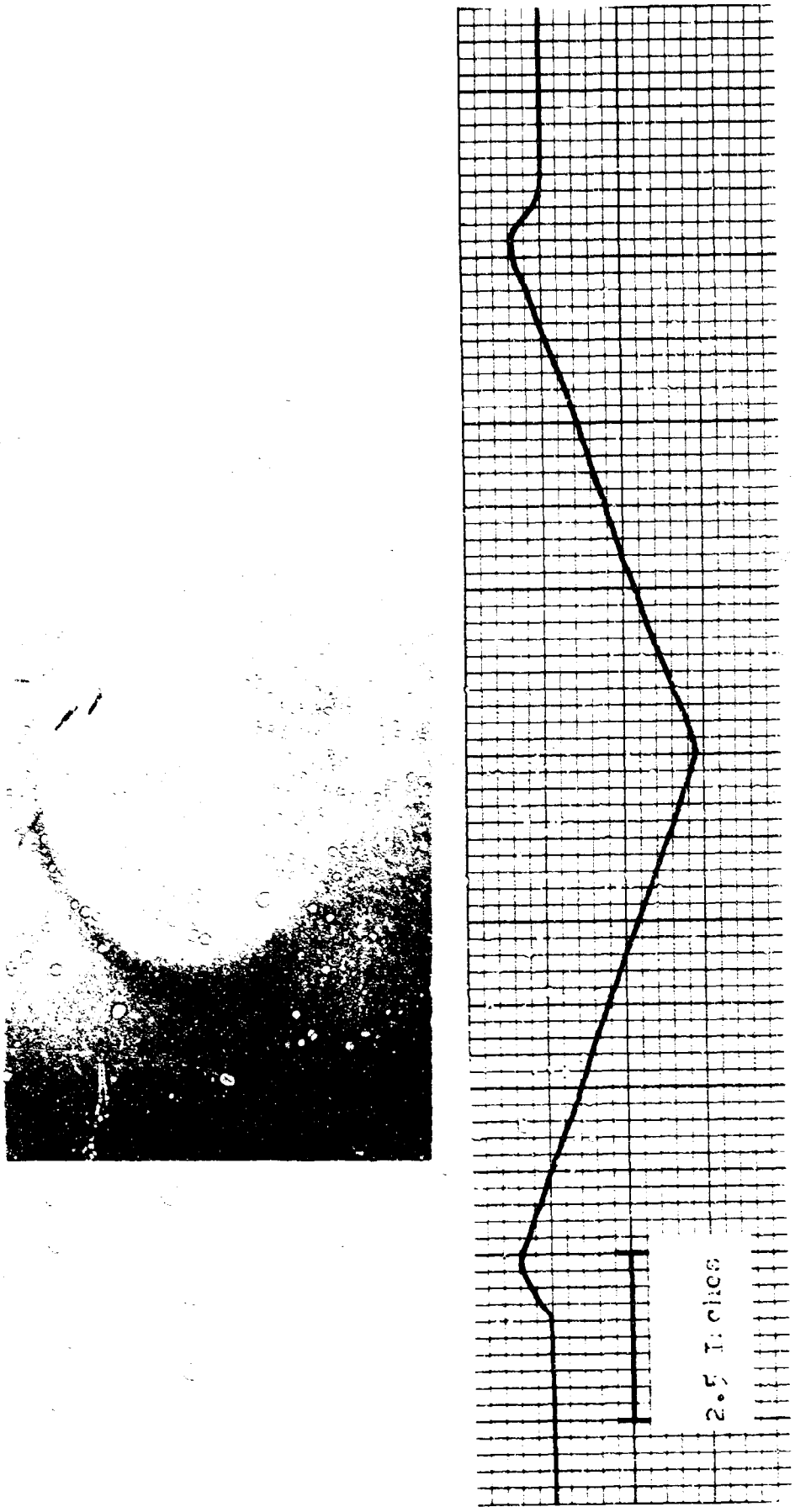

Figure 70

Profile of Crater Formed at 2.0 Inch DOB and 0.33 g

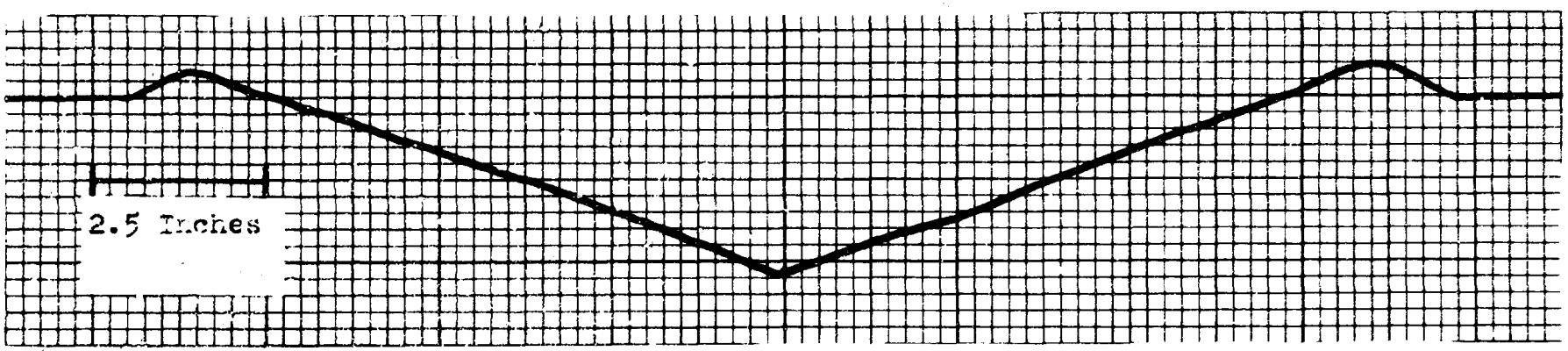

Figure 69

Profile of Crater Formed at 2.0 Inch DOB and 0.17 g

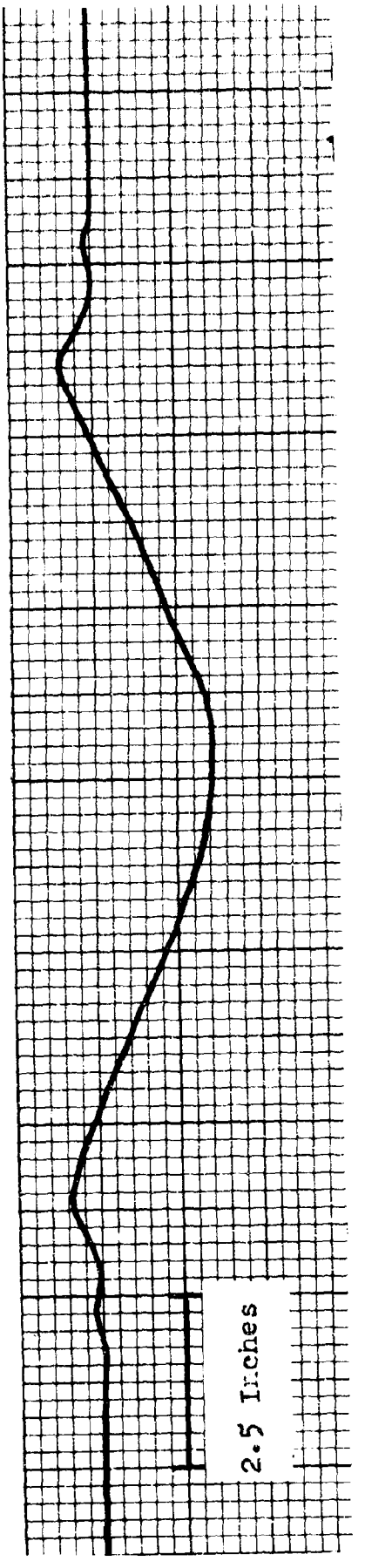

Figure 72

Profile of Crater Formed at 2.0 Inch DOB and 2.5 g

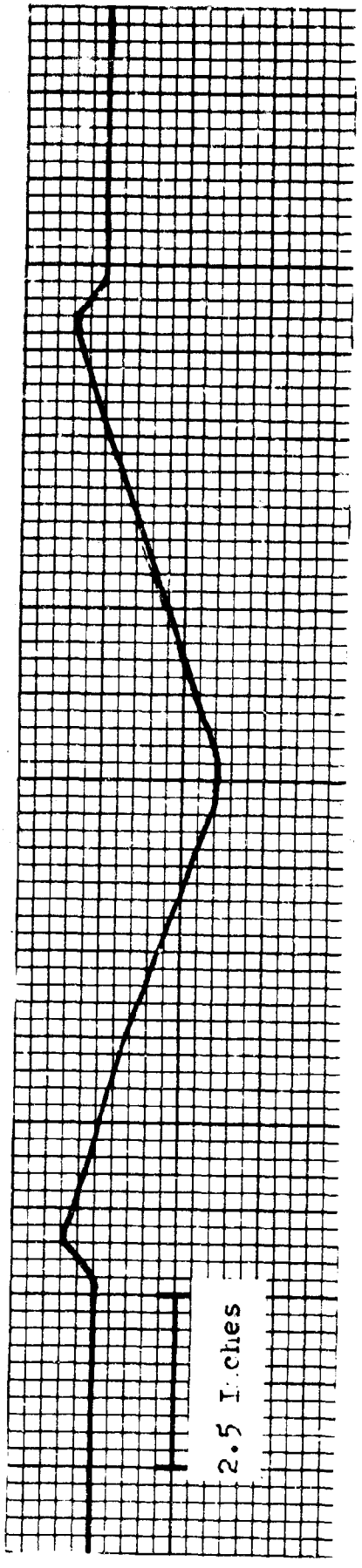

Figure 71

Profile of Crater Formed at 2.0 Inch DOB and 1.0 g

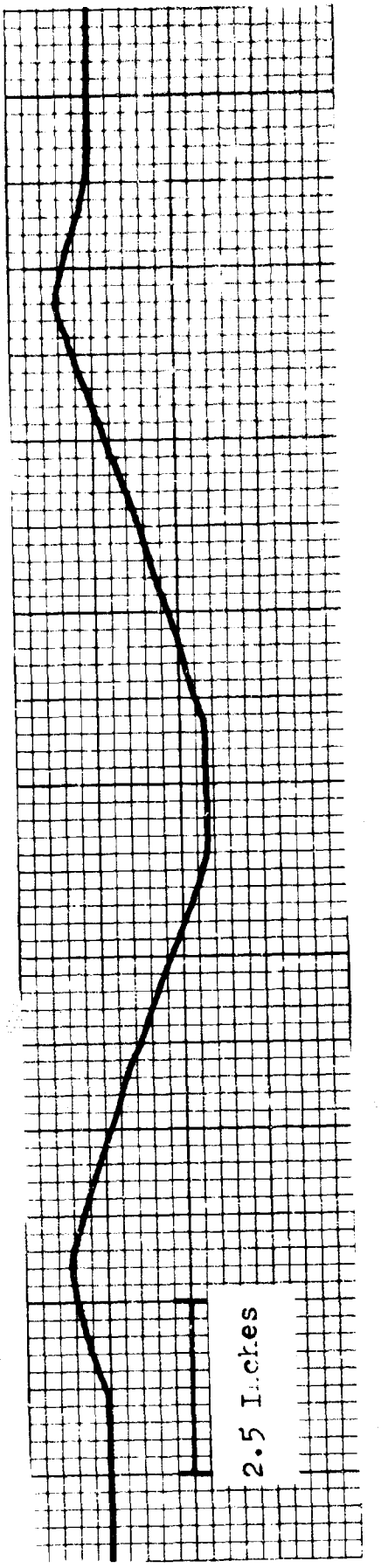

Figure 74

Profile of Crater Formed at 3.0 [illegible] and 0.38 g

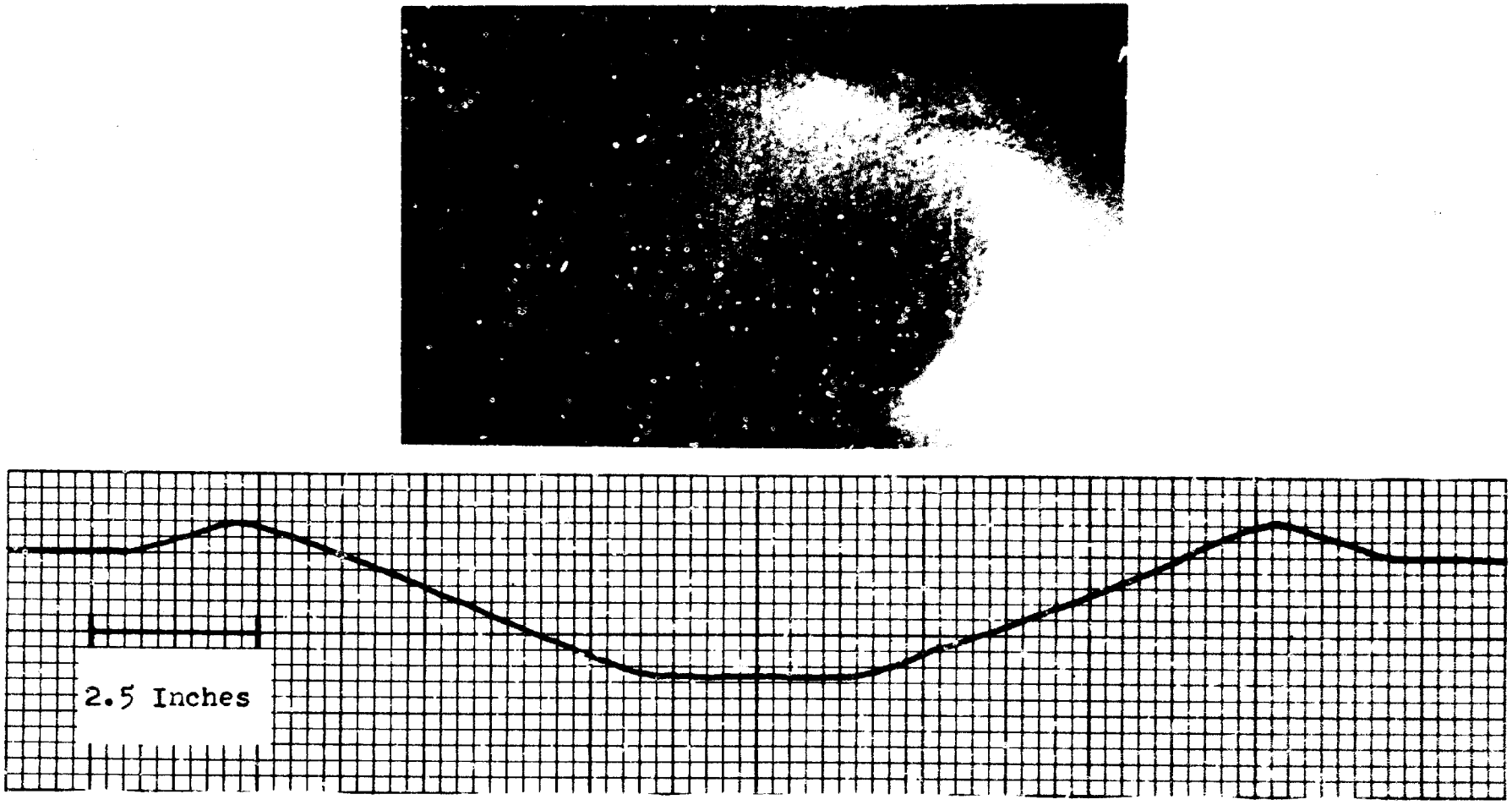

Figure 73

Profile of Crater Formed at 3.0 Inch DOB and 0.17 g

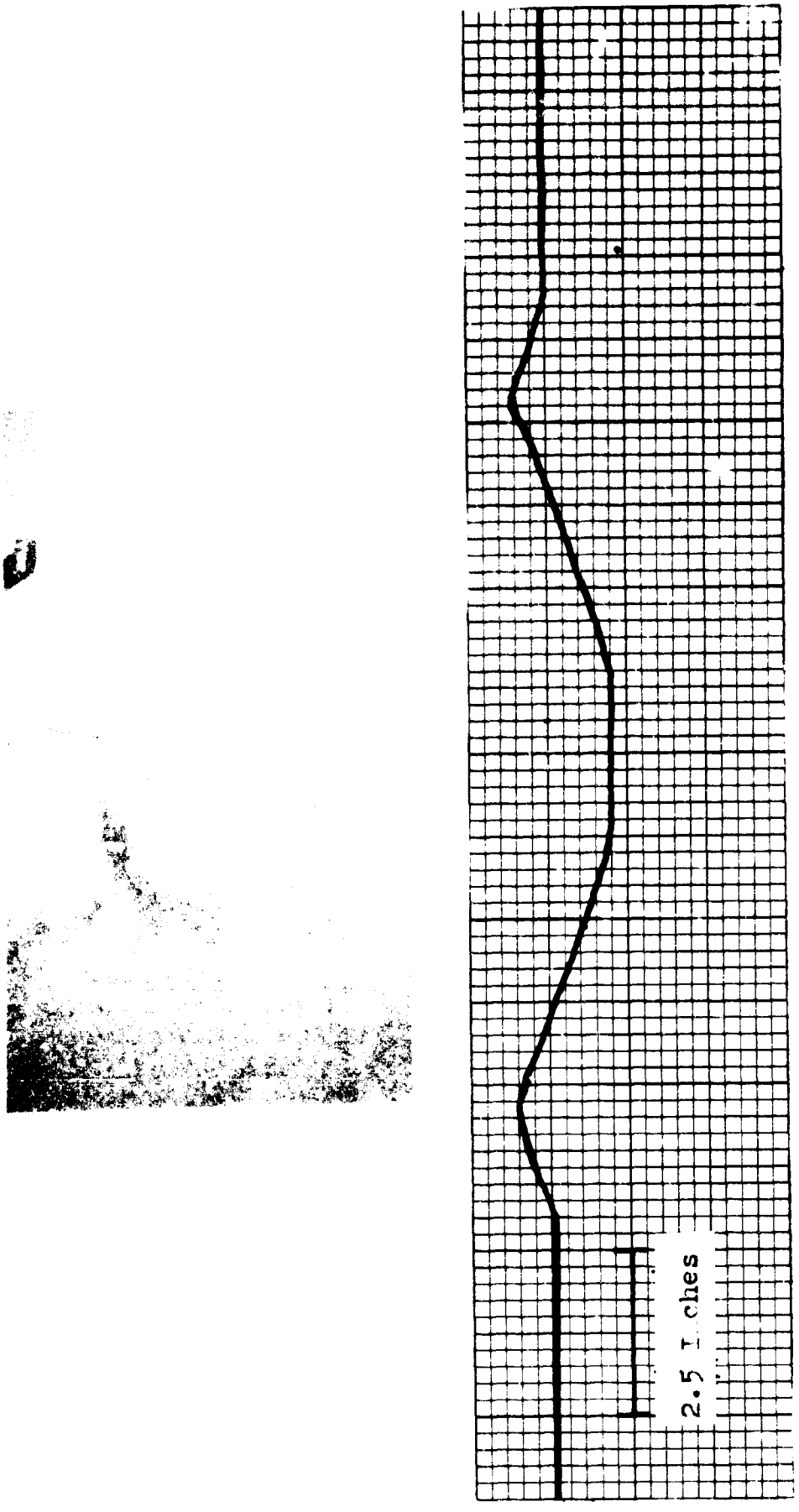

Figure 76

Profile of Crater Formed at 3.0 Inch DOB and 2.5 g

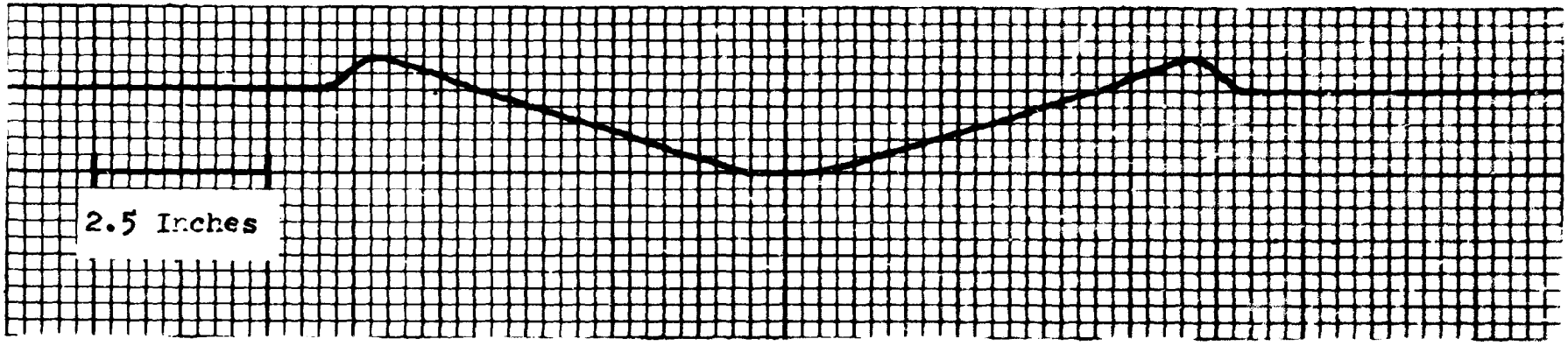

Figure 75

Profile of Crater Formed at 3.0 Inch DOB and 1.0 g

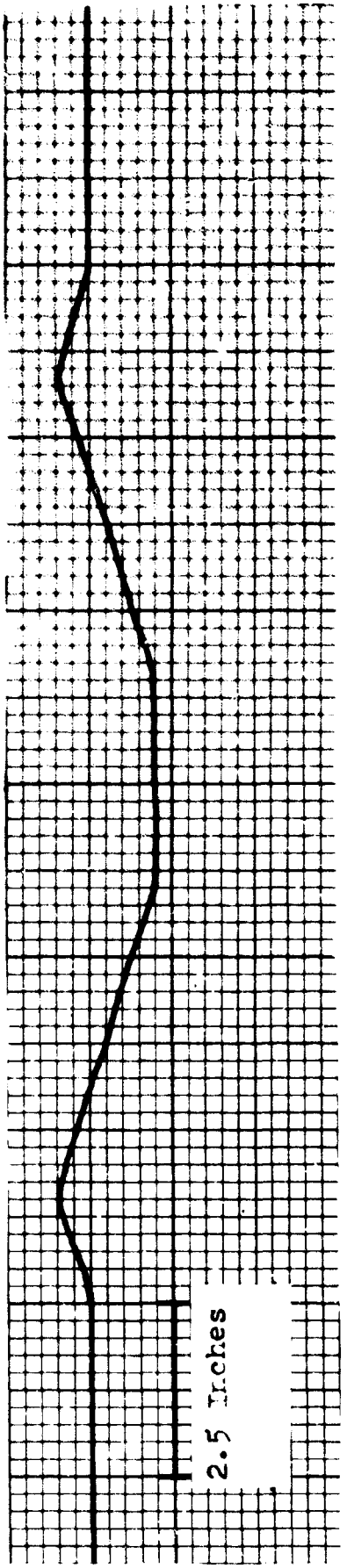

Figure 7°

Profile of Crater Formed at 4.0 Inch DOB and 0.3° g

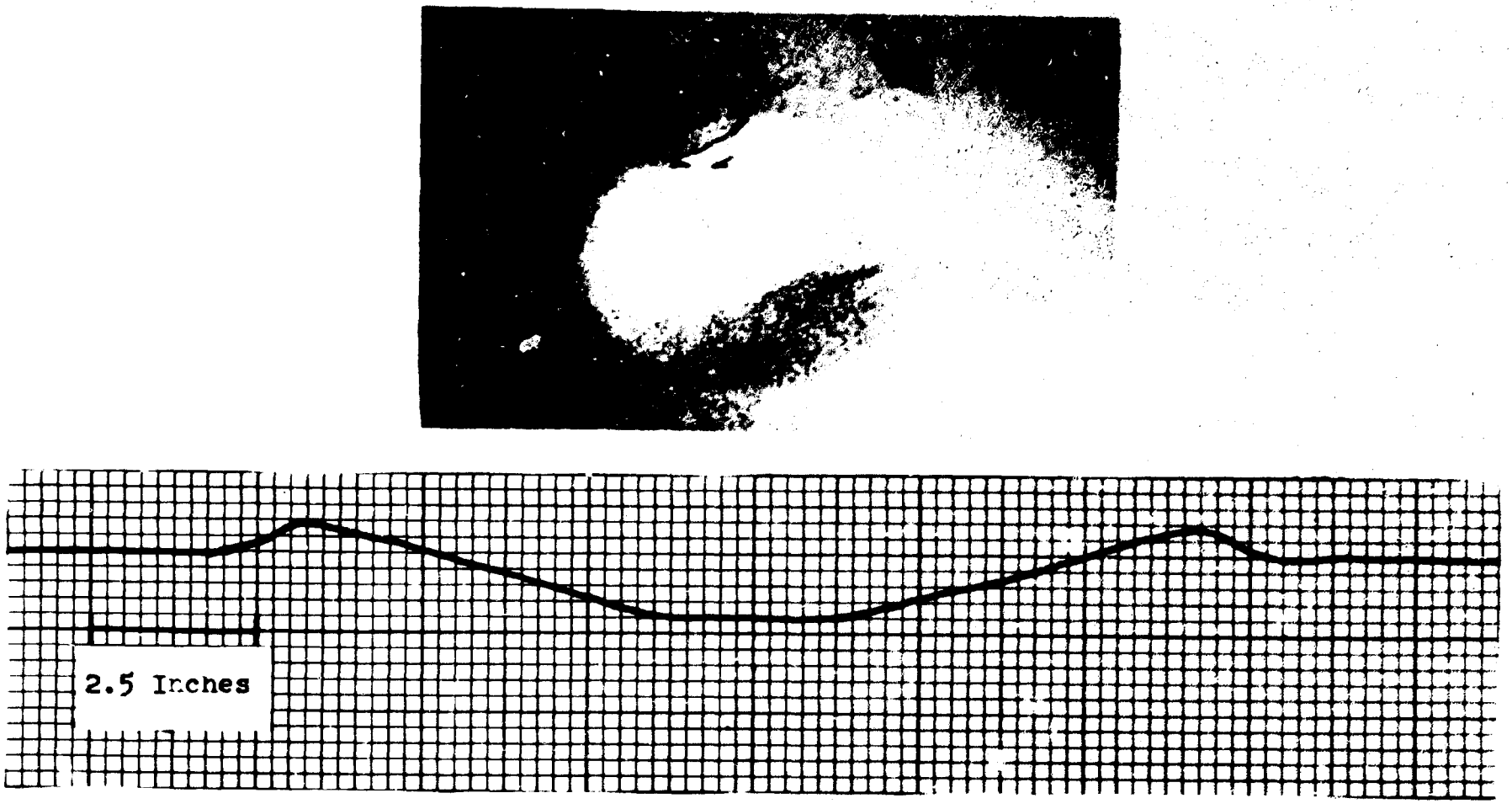

Figure 77

Profile of Crater Formed at 4.0 Inch DOB and 0.17 g

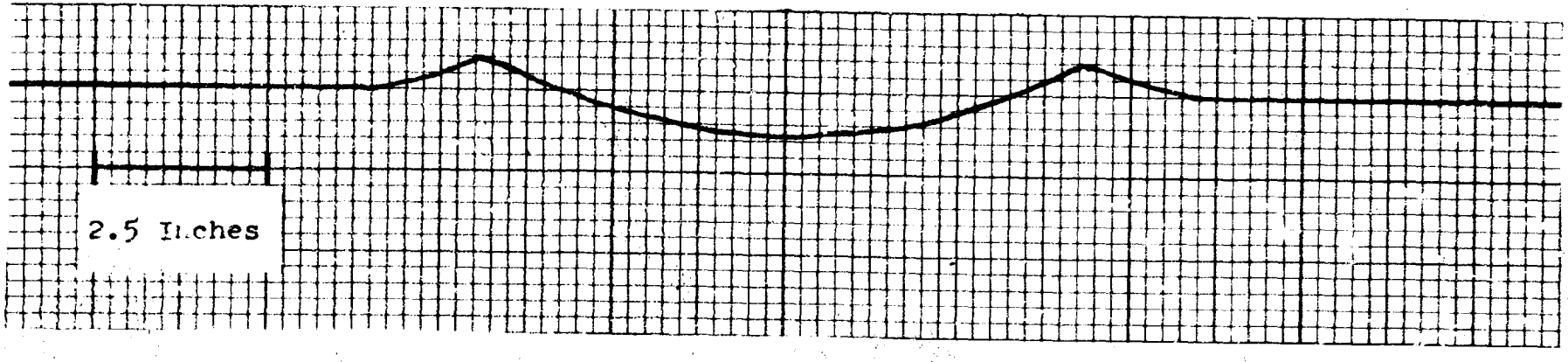

Figure 30

Profile of Crater Formed at 4.0 Inch DOB and 2.5 g

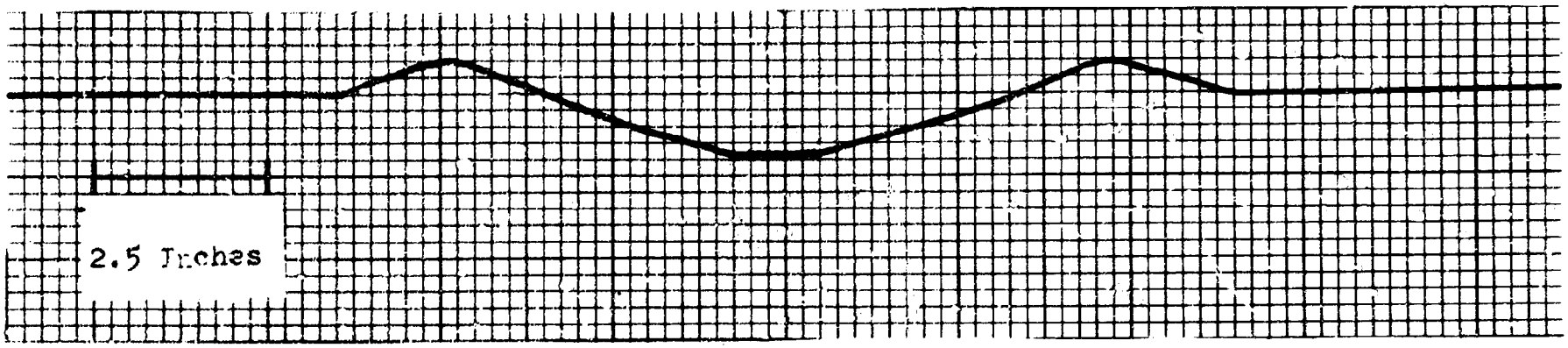

Figure 79

Profile of Crater Formed at 4.0 Inch DOB and 1.0 g

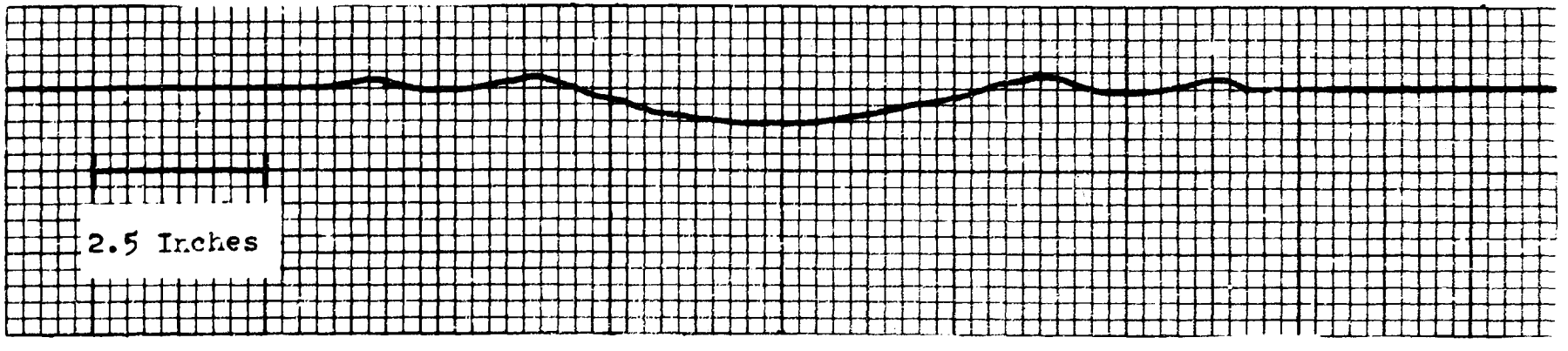

Figure 82

Profile of Crater Formed at 5.0 Inch DOB and 0.38 g

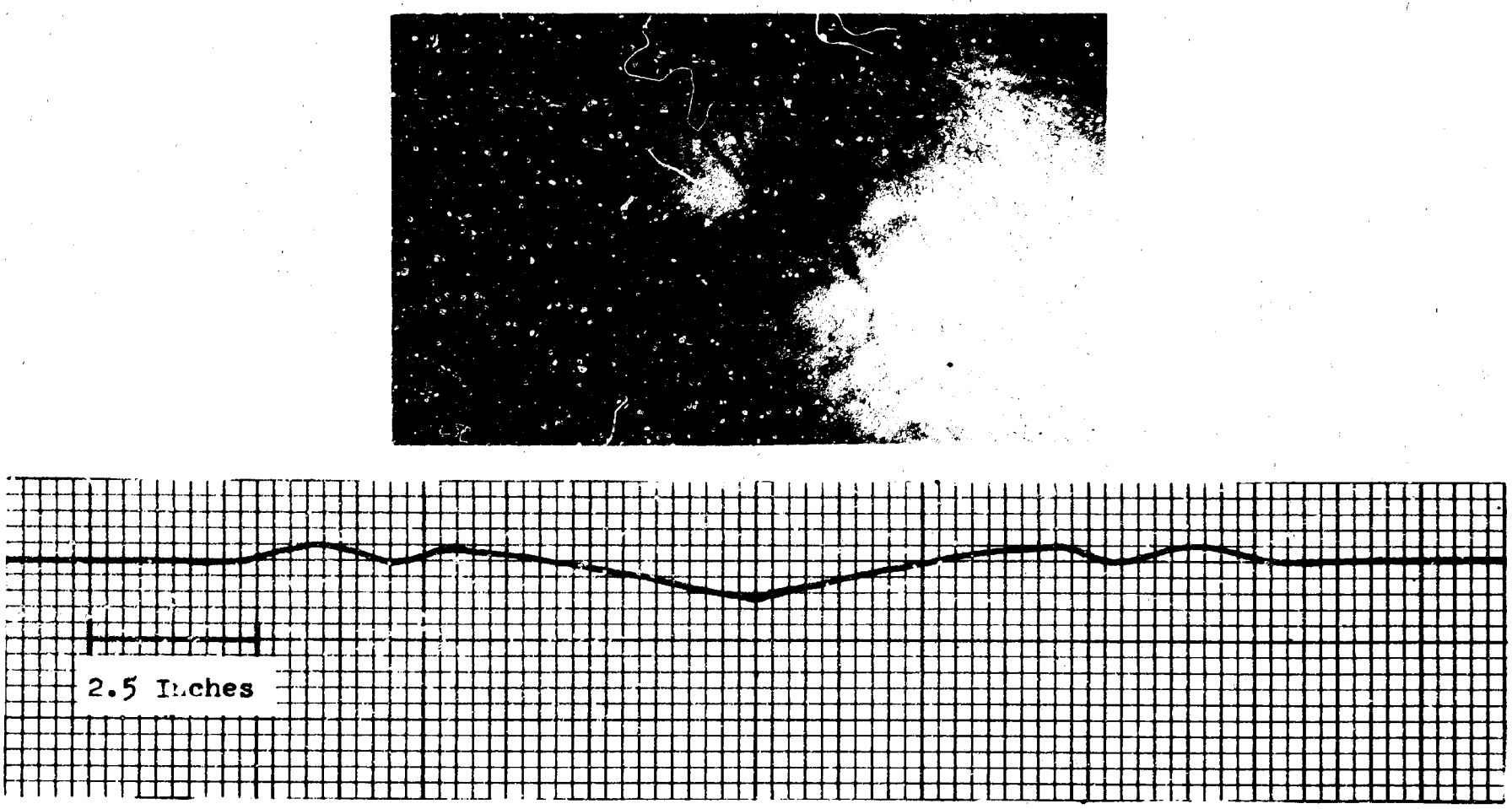

Figure 81

Profile of Crater Formed at 5.0 Inch DOB and 0.17 g

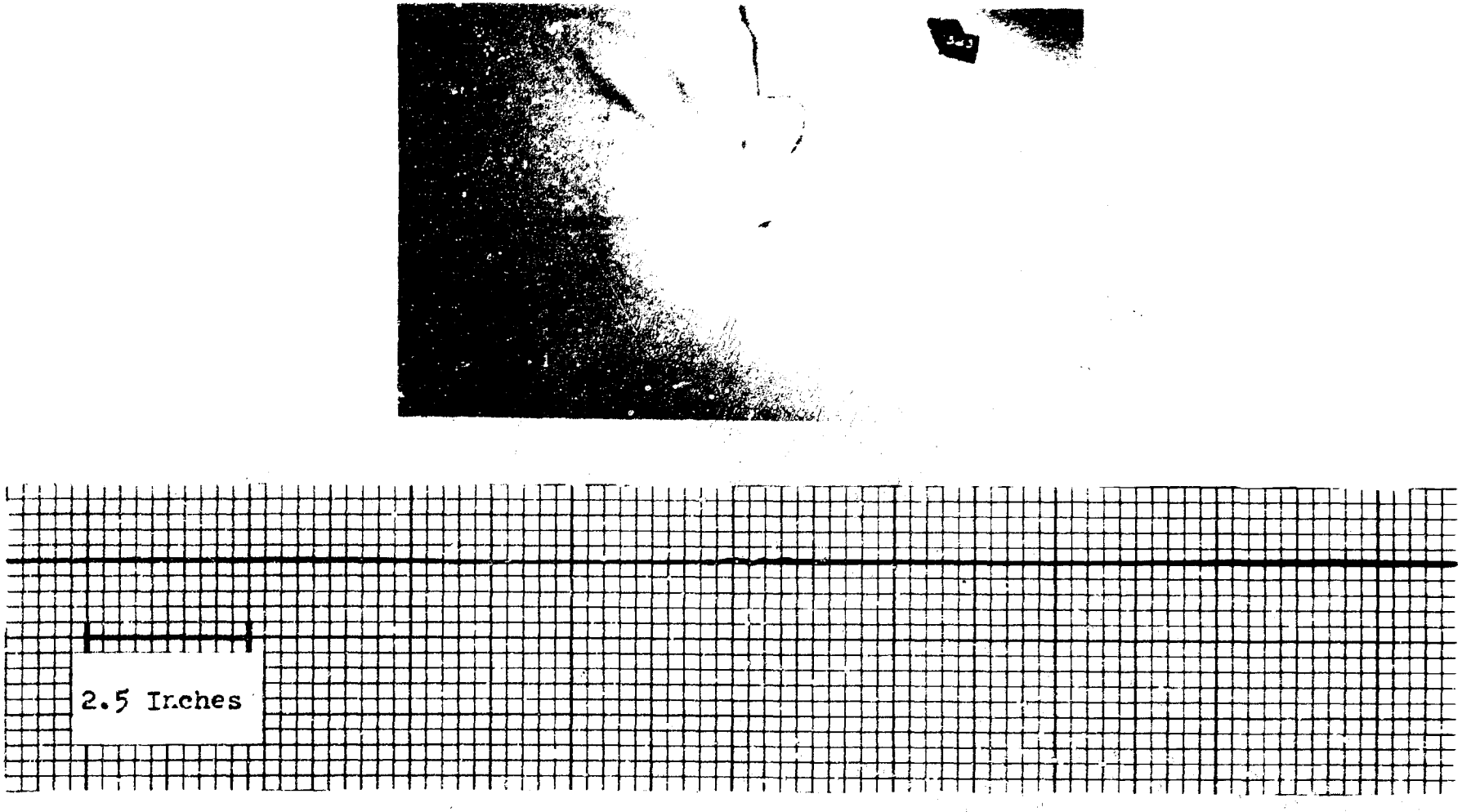

Figure 84

Profile of Crater Formed at 5.0 Inch DOB and 2.5

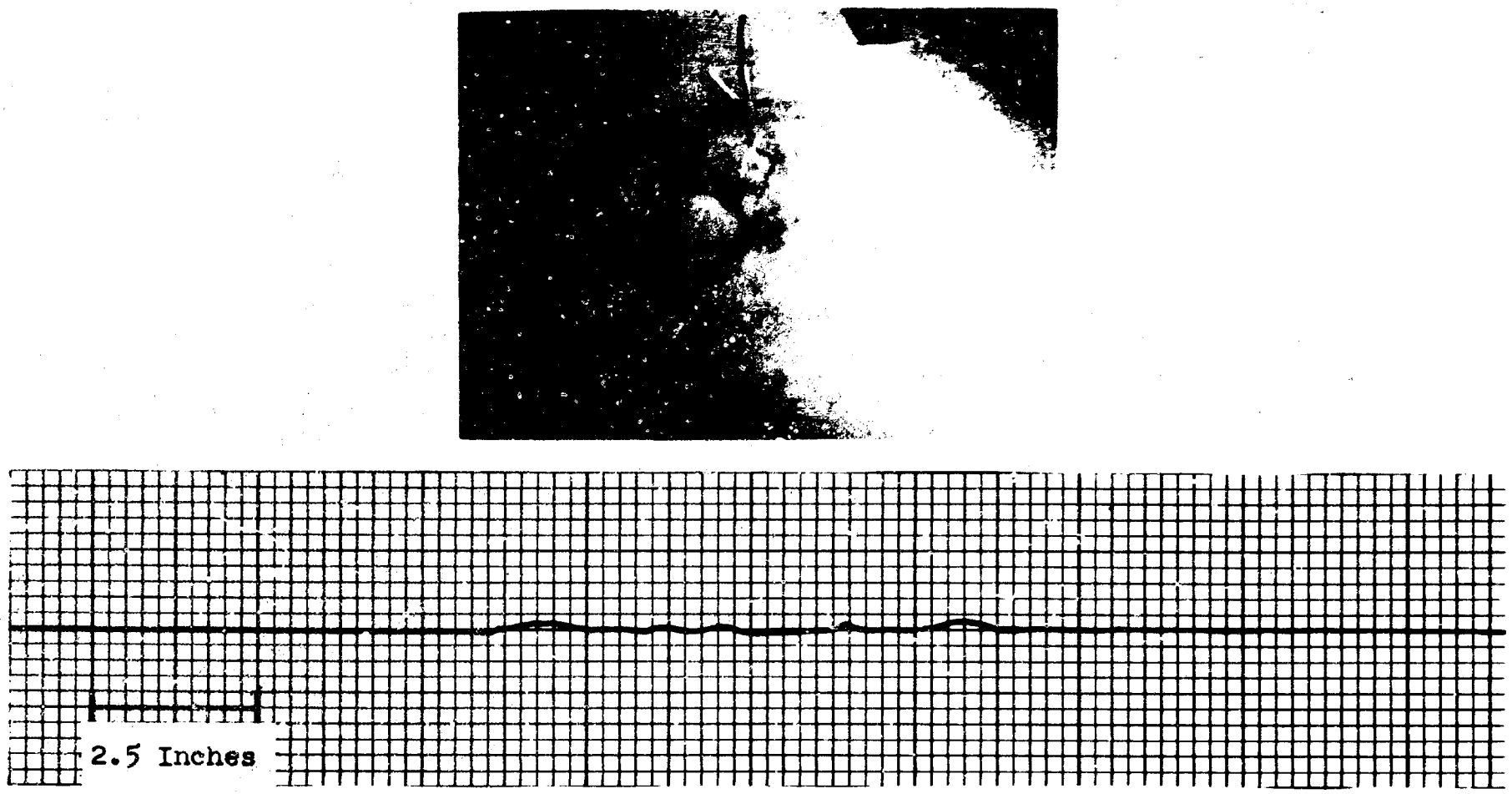

Figure 83

Profile of Crater Formed at 5.0 Inch DOB and 1.0 g

Appendix E

Statistical Analysis and Computations

In this section the statistical tests which were used in analyzing the experimental data are discussed. The Kolmogorov-Smirnov test, which is discussed first, was necessary to determine if the sample data could be assumed to be normally distributed. A normal distribution was necessary as a requirement for using the two-sample t-test to determine if gravity had a significant effect on crater dimensions. The results of these two tests are tabulated in this section. Finally, an explanation is given of the least-squares method used in determining the relationship between crater dimensions and gravity.

Kolmogorov-Smirnov Test

Whenever it is desired to subject data to some type of statistical analysis, one of the first problems is to determine what probability distribution function $F(x)$ the sample cumulative distribution function $S(x)$ approximates. If the assumption is made that $F(x)$ is continuous, a test which may then be used is the Kolmogorov-Smirnov (Ref. 60:50).

In this test, the maximum absolute deviation D_n of the sample $S(x)$ from what is assumed to be the true distribution function $F(x)$ is determined either by tabulating the two functions or by graphical means. A theorem can be proved which states that as long as $F(x)$ is continuous, $S(x)$ will approximate it in the same way. How well $S(x)$

approximates F(x) can be determined by using D_n as a criterion (Ref 60:51). As a consequence, D_n is a random variable which can be used for constructing a confidence band for F(x). In order to use the random variable D_n, it is necessary to know its distribution. This can be worked out for a particular set of n samples and desired level of significance α. The term level of significance or α is defined as the probability of rejecting the stated statistical hypothesis when it should have been accepted. Certain critical values of D_n are tabulated in statistical texts. These critical values are denoted by the symbol

$$t_{\alpha;n}$$

where α = level of significance

n = number of observations in the sample

Therefore, for a given sample of size n and desired level of significance, a value of $t_{\alpha;n}$ can be obtained. For the Kolmogorov-Smirnov Test where D_n is the criterion for the fit of S(x) to F(x), the hypothesis is made that

$$P\ (D_n \geq t_{\alpha;n} \mid F(x) \text{ is the true distribution function of } x) = \alpha$$

where P denotes the probability and all the other terms are as previously defined. Then if

$$D_n \geq t_{\alpha;n}$$

the hypothesis is rejected; if

$$D_n \leq t_{\alpha;n}$$

the hypothesis is accepted (Ref 60:51).

For the crater dimensions obtained during the experimental phase, the hypothesis was made that the sample data approximated a normal or Gaussian distribution. A level of significance of 0.01 was chosen as the minimum level at which the hypothesis would be accepted. Although an α of 0.01 appears to be a weak requirement, the test is so devised that it is easier to reject the hypothesis than to accept it (Ref 60:51). Therefore, the ability to accept the hypothesis at even a 0.01 level of significance is meaningful. As will be shown in the tabulated results of the test, it was possible to accept the hypothesis with an α of 0.20 in the majority of the tests.

To illustrate the preceding technique, a sample calculation is done on the diameters of craters formed under 0.17 g conditions at 1.0 inch DOB. These measurements are

16.250,	17.500,	17.250,	17.000,	18.250
16.250,	17.000,	17.750,	17.500,	17.250

The mean of this data is 17.2 and the variance is 0.348. From this data, the cumulative sample distribution can be tabulated.

For each diameter, it is necessary to compute F(x) by means of the expression

$$F(x) = \int_{-\infty}^{x} \frac{1}{\sqrt{2\pi}} e^{-t^2/2}\, dt \qquad (15)$$

where

$$t = \frac{X - \mu}{\sigma} \tag{16}$$

and X = measured dimension

μ = mean of sample data

σ = standard deviation of sample data

The expression for F(x) has been extensively tabulated. Therefore, by converting each of the sample dimensions to a value of t by means of Eq. (16), the value of F(x) can be obtained from tables. These values along with the cumulative sample distribution S(x) in table form are

Range of x	S(x)	x	F(x)
$x < 16.250$	0.00	15.000	.00
$16.250 \leq x < 17.000$	0.20	16.250	.06
$17.000 \leq x < 17.250$	0.40	17.000	.37
$17.250 \leq x < 17.500$	0.60	17.250	.53
$17.500 \leq x < 17.750$	0.80	17.500	.70
$17.750 \leq x < 18.250$	0.90	17.750	.82
$18.250 \leq x < \infty$	1.00	18.250	.96

Since F(x) is an increasing continuous function and S(x) is an increasing step function, the only differences which must be examined to determine D_n are the differences that occur at the discontinuities in S(x). These differences or deviations are seen in Fig. 85 which shows a plot of F(x) and S(x). These deviations, which can be obtained from the figure or the table, are tabulated below.

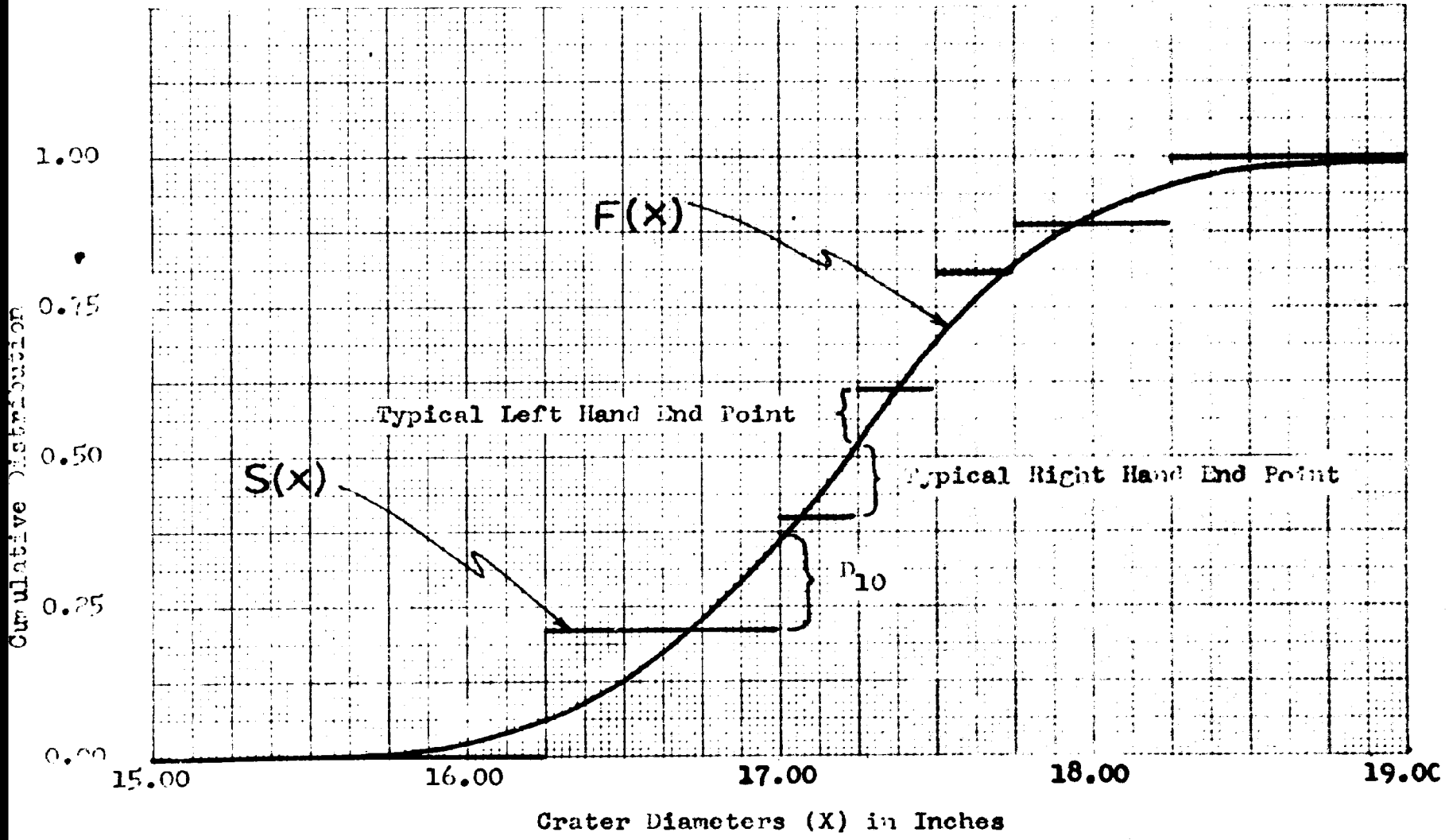

Figure 85

Plot of Sample and Assumed Cumulative Distributions for Kolmogorov-Smirnov Test

Value of X	Left Hand End Point	Right Hand End Point
15.000	.00	.00
16.250	.14	-.06
17.000	.03	-.17
17.250	.07	-.13
17.500	.10	-.10
17.750	.08	-.02
18.250	.06	-.04

Examination of the differences gives the value of

$$D_{10} = \text{Max}\left| S(x) - F(x)\right| = 0.17$$

Referring to a table which lists the values of $t_{\alpha;n}$ where n = 10, it is found that

$$P(D_{10} \geq .323) = 0.20$$

This means that the hypothesis of a normal distribution with mean 17.2 and variance 0.348 for the sample data can be accepted on a significance level of 0.20. The ability to accept on such a high level of significance is a very positive indication that the sample data is normally distributed.

The Kolmogorov-Smirnov Test was performed on all the crater dimensions. In each case, the hypothesis was made that the true distribution of the sample data was the normal distribution. In each test, the highest possible α was used. However, in no instance was an α less than 0.01 considered acceptable. The results of these tests are tabulated in this section. From these tables it can be seen that 63 out of 70 hypotheses were able to be accepted with an α of

0.20. In only one instance did an α of 0.05 have to be used. In no instance did the hypothesis have to be rejected. Therefore, the data is normally distributed.

TABLE VIII

RESULTS OF KOLMOGOROV-SMIRNOV TESTS ON CRATER DIMENSIONS

Diameter

Value of Gravity	DOB in Inches	Deviation of Sample D_n	Critical Value of $t_{\alpha;n}$	Level of Significance α
	0.0	.14	.323	.20
	0.5	.25	.323	.20
	1.0	.17	.323	.20
.17	1.5	.15	.323	.20
	2.0	.21	.323	.20
	3.0	.19	.323	.20
	4.0	.19	.323	.20
	5.0	.18	.359	.20
	0.0	.11	.323	.20
	0.5	.19	.323	.20
	1.0	.17	.323	.20
.38	1.5	.20	.323	.20
	2.0	.17	.339	.20
	3.0	.20	.323	.20
	4.0	.24	.323	.20
	5.0	.27	.447	.20
	0.0	.22	.232	.20
	0.5	.17	.232	.20
	1.0	.14	.232	.20
1.0	1.5	.25	.232	.20
	2.0	.16	.232	.20
	3.0	.13	.232	.20
	4.0	.17	.232	.20
	0.0	.22	.323	.20
	0.5	.25	.323	.20
	1.0	.22	.323	.20
2.5	1.5	.19	.323	.20
	2.0	.32	.323	.20
	3.0	.19	.323	.20
	4.0	.27	.323	.20

TABLE VIII (CONTINUED) RESULTS OF TESTS

Depth

Value of Gravity	DOB in Inches	Deviation of Sample D_n	Critical Value of $t_{\alpha;n}$	Level of Significance α
	0.0	.27	.323	.20
	0.5	.22	.323	.20
	1.0	.21	.323	.20
.17	1.5	.26	.323	.20
	2.0	.29	.323	.20
	3.0	.39	.409	.05
	4.0	.22	.323	.20
	5.0	.20	.339	.20
	0.0	.16	.323	.20
	0.5	.15	.323	.20
	1.0	.21	.323	.20
.38	1.5	.19	.323	.20
	2.0	.17	.339	.20
	3.0	.21	.323	.20
	4.0	.21	.323	.20
	5.0	.64	.669	.01
	0.0	.20	.232	.20
	0.5	.32	.329	.02
	1.0	.25	.265	.10
1.0	1.5	.28	.294	.05
	2.0	.21	.232	.20
	3.0	.17	.232	.20
	4.0	.26	.265	.10
	0.0	.32	.323	.20
	0.5	.24	.323	.20
	1.0	.25	.323	.20
2.5	1.5	.19	.323	.20
	2.0	.24	.323	.20
	3.0	.28	.323	.20
	4.0	.31	.323	.20

TABLE IX

RESULTS OF KOLMOGOROV-SMIRNOV TESTS ON CRATERS USED FOR CALIBRATION PURPOSES

Condition	DOB	Dimension	D_n*	$t_{\alpha;n}$**	α#
13 Inches of Sand	4.0	Diameter	.27	.447	.20
	4.0	Depth	.26	.447	.20
Without Reference Wire	1.0	Diameter	.25	.447	.20
	1.0	Depth	.49	.519	.05
	4.0	Diameter	.40	.447	.20
	4.0	Depth	.26	.447	.20
Aircraft Vibration	1.0	Diameter	.27	.447	.20
	1.0	Depth	.39	.447	.20
	4.0	Diameter	.30	.447	.20
	4.0	Depth	.16	.447	.20

* Deviation of sample
** Critical value of deviation
\# Level of significance

t-Test

In order to justifiably conclude that gravity did or did not affect the crater dimensions, it was decided to resort to a statistical test. The desired test would be one which would compare the mean diameter or depth of craters formed at the same DOB but under different gravity conditions. If the test showed that there was a significant difference between the two means, then it could be stated with a certain probability or level of significance that gravity had an effect on the crater dimension at that DOB. Conversely, if the test resulted in the probability that the means were equal, then gravity did not affect the crater dimensions.

Knowing that the sample data was normally distributed, it was possible to use the two-sample t-test. An advantage of the t-test is that the sample populations may be small. However, in order to use the two-sample t-test, it is necessary to make the assumption that the two distributions being compared have equal standard deviations, i.e., $\sigma_1 = \sigma_2$. Looking at the sample variances, it is seen that in only one instance do the variances differ by more than a factor of ten. Additionally, if the sample sizes of the two populations are not markedly different, then the test is not as sensitive to the assumption that the sample variances are equal (Ref 8:239). Therefore, the use of the t-test is appropriate.

The t-test is derived by means of the likelihood ratio technique which yields a ratio based on the t distribution with $n_1 + n_2 - 2$ degrees of freedom and the statistic

$$t = \frac{x_1 - x_2 - \delta}{\sqrt{\frac{(n_1-1)s_1^2 + (n_2-1)s_2^2}{n_1+n_2-2}}\ \sqrt{\frac{1}{n_1}+\frac{1}{n_2}}} \qquad (17)$$

where x = means of sample data

δ = value by which true means differ

n = sample size

s^2 = variance of sample data

1,2 = subscripts which refer to sample populations being compared

In this test, the common procedure is to state the null hypothesis

$$H_o: \mu_1 - \mu_2 = \delta$$

against one of the alternatives

$$\mu_1 - \mu_2 > \delta;\ \ \mu_1 - \mu_2 < \delta;\ \ \mu_1 - \mu_2 \neq \delta$$

A value of t is then calculated from Eq. (17). This value is compared with the value of the random variable which has the t distribution with $n_1 + n_2 - 2$ degrees of freedom and at a chosen level of significance α . Depending on which alternative was chosen, the magnitude of t_α when compared with the calculated t will determine whether the hypothesis is accepted or rejected.

For this paper, the hypothesis is

$$H_o: \mu_1 - \mu_2 = 0$$

where μ_1 = mean dimension at a given DOB for the lower value of gravity

μ_2 = mean dimension at a given DOB for the higher value of gravity

against the alternative $\mu_1 - \mu_2 > 0$

The maximum acceptable level of significance was 0.10. In the test, if

$$t \geq t_\alpha$$

then the null hypothesis must be rejected. If the hypothesis is rejected, this signifies that gravity did effect the crater dimensions at that DOB. Remembering that α is the probability of rejecting the hypothesis when in fact it should have been accepted, an α = 0.10 indicates that a 0.10 probability is to be allowed in making the improper conclusion that gravity had an effect on the dimensions. However, in every t-test, the lowest α possible was chosen since the lower the value of α, the lower was the probability of making the incorrect conclusion that gravity had an effect on the crater dimensions. To illustrate the technique, a sample calculation is performed.

It is desired to determine if gravity had an effect on the diameter of craters formed under the following conditions:

g	DOB	Mean Diameter	Variance	Sample Size
0.17	4.0	13.550	0.066	10
0.38	4.0	11.900	0.025	10

Based on the tabled data, t is calculated by means of Eq. (17) and is 8.509. Consulting a t-distribution table and noting the value of t for 18 degrees of freedom, one gets

$$t_{.001} = 3.61$$

Therefore, since $t > t_{.001}$, the null hypothesis must be rejected. The conclusion is that there is a difference in the means and that this difference is due to the different gravity fields. Since α = 0.001, there is a 0.001 probability that this conclusion is incorrect.

The results of all the two-sample t-tests are listed in Table X. All possible combinations between craters formed at the same DOB but in different gravity fields are considered.

The two-sample t-test was also used in comparing the means of the craters formed during the calibration phase of the experiment (see Appendix A). For all the t-tests which were done on the calibration data, the hypothesis was

$$H_o: \mu_1 - \mu_2 = 0$$

where μ_1 = mean of one group of sample data

μ_2 = mean of second group of sample data

The alternative was stated as

$$\mu_1 - \mu_2 \neq 0$$

For the calibration comparisons, it was desired that the stated hypothesis be accepted whenever possible. For this reason, the minimum α was chosen to be 0.002. The necessary condition for accepting the hypothesis was

$$t < t_{\alpha/2}$$

The results of the t-tests on the craters formed during the calibration phase show that the hypothesis that the means are equal can be accepted in all cases except two. These two cases are in the comparison of the depths of craters subjected to aircraft vibration. The results of the t-tests are tabulated in Table XI.

Least-Squares Calculations

For the reasons already stated in Section IV, the equation which relates crater dimensions at a given DOB to the gravity field was

TABLE X

RESULTS OF T-TEST ON EFFECT OF
GRAVITY ON CRATER DIMENSIONS

Diameter

DOB	Gravity Field	Gravity Field	Sample t	Tabulated t_α	Level of Significance α
	.17	.38	0.724	1.33	*
	.17	1.00	6.124	3.41	.001
0.0	.17	2.50	6.551	3.61	.001
	.38	1.00	6.189	3.41	.001
	.38	2.50	7.339	3.61	.001
	1.00	2.50	4.244	3.41	.001
	.17	.38	-1.382	1.33	*
	.17	1.00	4.587	3.41	.001
0.5	.17	2.50	21.138	3.61	.001
	.38	1.00	12.435	3.42	.001
	.38	2.50	16.908	3.65	.001
	1.00	2.50	8.306	3.41	.001
	.17	.38	4.511	3.61	.001
	.17	1.00	22.103	3.41	.001
1.0	.17	2.50	24.191	3.61	.001
	.38	1.00	8.220	3.41	.001
	.38	2.50	11.586	3.61	.001
	1.00	2.50	11.360	3.41	.001
	.17	.38	10.506	3.61	.001
	.17	1.00	27.777	3.41	.001
1.5	.17	2.50	27.051	3.61	.001
	.38	1.00	16.598	3.41	.001
	.38	2.50	21.972	3.61	.001
	1.00	2.50	12.914	3.41	.001
	.17	.38	9.958	3.65	.001
	.17	1.00	32.049	3.41	.001
2.0	.17	2.50	35.243	3.61	.001
	.38	1.00	14.937	3.65	.001
	.38	2.50	23.234	3.65	.001
	1.00	2.50	13.217	3.41	.001

TABLE X (CONTINUED) RESULTS OF T-TEST ON GRAVITY

Diameter

DOB	Gravity Field	Gravity Field	Sample t	Tabulated t_{α}	Level of Significance α
	.17	.38	5.989	3.61	.001
	.17	1.00	18.523	3.41	.001
3.0	.17	2.50	23.409	3.61	.001
	.38	1.00	9.493	3.41	.001
	.38	2.50	15.909	3.61	.001
	1.00	2.50	7.292	3.41	.001
	.17	.38	8.509	3.61	.001
	.17	1.00	14.957	3.41	.001
4.0	.17	2.50	16.386	3.61	.001
	.38	1.00	8.696	3.41	.001
	.38	2.50	10.603	3.61	.001
	1.00	2.50	5.914	3.41	.001
5.0	.17	.38	2.388	2.20	.025

Depth

	.17	.38	-0.850	1.33	*
	.17	1.00	0.748	1.33	*
0.0	.17	2.50	3.688	3.61	.001
	.38	1.00	2.266	2.05	.025
	.38	2.50	3.699	3.61	.001
	1.00	2.50	4.314	3.41	.001
	.17	.38	-5.16	3.65	*
	.17	1.00	-2.965	2.77	*
0.5	.17	2.50	8.962	3.61	.001
	.38	1.00	5.847	3.42	.001
	.38	2.50	7.979	3.65	.001
	1.00	2.50	6.028	3.41	.001
	.17	.38	0.651	1.33	*
	.17	1.00	2.291	2.06	.025
1.0	.17	2.50	3.642	3.61	.001
	.38	1.00	1.355	1.31	.10
	.38	2.50	2.510	2.10	.025
	1.00	2.50	5.997	3.41	.001

TABLE X (CONTINUED) RESULTS OF T-TEST ON GRAVITY

Depth

DOB	Gravity Field	Gravity Field	Sample t	Tabulated t_α	Level of Significance α
	.17	.38	0.435	1.33	*
	.17	1.00	6.532	3.41	.001
1.5	.17	2.50	9.407	3.61	.001
	.38	1.00	6.740	3.41	.001
	.38	2.50	10.775	3.61	.001
	1.00	2.50	7.472	3.41	.001
	.17	.38	1.567	1.33	.10
	.17	1.00	6.928	3.41	.001
2.0	.17	2.50	8.881	3.61	.001
	.38	1.00	8.897	3.65	.001
	.38	2.50	9.636	3.65	.001
	1.00	2.50	4.493	3.41	.001
	.17	.38	2.044	1.73	.05
	.17	1.00	6.313	3.41	.001
3.0	.17	2.50	8.068	3.61	.001
	.38	1.00	3.720	3.41	.001
	.38	2.50	5.458	3.61	.001
	1.00	2.50	3.831	3.41	.001
	.17	.38	0.912	1.33	*
	.17	1.00	2.798	2.79	.005
4.0	.17	2.50	5.152	3.61	.001
	.38	1.00	2.028	1.70	.05
	.38	2.50	4.208	3.61	.001
	1.00	2.50	4.789	3.41	.001
5.0	.17	.38	0.409	1.33	*

* Hypothesis that means are equal was accepted

TABLE XI

RESULTS OF T-TEST ON CRATERS FORMED
DURING CALIBRATION PHASE OF EXPERIMENT

DOB	Dimension	Sample t	Tabulated t_{α}	Level of Significance α
		Depth of Sand		
	Diameter	.742	.86	.40
4.0	Depth	.085	.26	.80
		Effect of Reference Wire		
1.0	Diameter	.399	.53	.60
1.0	Depth	1.071	1.32	.20
4.0	Diameter	.246	.26	.80
4.0	Depth	.085	.26	.80
		Effect of Aircraft Vibration		
1.0	Diameter	.035	.26	.80
1.0	Depth	3.873	*	*
4.0	Diameter	1.798	2.07	.05
4.0	Depth	4.482	*	*

* Hypothesis that means are the same cannot be accepted

assumed to be

$$D = Ae^{-gB} \tag{18}$$

where D = dimension of the crater

A = dimension at zero gravity

g = acceleration due to gravity

B = measure of gravity effectiveness

The method of least-squares was used to find the values of A and B which would best fit the experimental data. This meant that it was necessary to find the minimum value of

$$D^* = \sum_{i=1}^{4} \left[D_i - Ae^{-g_i^B} \right]^2 \tag{19}$$

where D^* = least-squares deviation

Taking the partial derivative of Eq. (19) with respect to A and B and setting the result equal to zero gives the expressions

$$\frac{\partial D^*}{\partial A} = - \sum_{i=1}^{4} 2 \left[D_i - Ae^{-g_i^B} \right] \left[e^{-g_i^B} \right] = 0 \tag{20}$$

$$\frac{\partial D^*}{\partial B} = \sum_{i=1}^{4} 2 \left[D_i - Ae^{-g_i^B} \right] \left[e^{-g_i^B} \right] \left[g_i^B \right] \left[\ln g_i \right] = 0 \tag{21}$$

Instead of solving these equations simultaneously, it was decided to solve for A in terms of B from Eq. (20). Then, by assuming a value for

B, a value for A could be obtained. The expression for A was found to be

$$A = \frac{\sum_{i=1}^{4} D_i \, e^{-g_i^B}}{\sum_{i=1}^{4} e^{-(2g_i)^B}} \qquad (22)$$

Knowing A and B allowed the deviation to be calculated by means of Eq. (19). By repeating the process for various values of B until a minimum value of the deviation was found, it was possible to obtain the value of A and B which best fit the given data. This iterative process was done on the 1620 computer. The results are tabulated in Section V.